ROTATING FLOWS IN ACOUSTICALLY UNSTABLE ROCKET MOTORS

Thesis by

Gary A. Flandro

In Partial Fulfillment of the Requirements

For the Degree of

Doctor of Philosophy

California Institute of Technology

Pasadena, California

1967

(Submitted March 1, 1967)

ACKNOWLEDGMENTS

The writer gratefully acknowledges the assistance offered by members of the faculty in Aeronautics and Jet Propulsion in the completion of this study.

Particular appreciation is due Professors F. E. Marble and F. E. C. Culick for their patience and for numerous suggestions without which insight into the problem could not have been achieved. Special thanks are also due Professors Rannie and Zukoski for their participation in several helpful discussions.

The author wishes to express his sincere appreciation to the Institute for financial assistance in the form of scholarships and teaching assistantships, and to the National Aeronautics and Space Administration for a fellowship held during the 1965-1966 academic year.

Thanks are due Mrs. Robert Duffy for her fine efforts in typing and proofreading the final manuscript.

ABSTRACT

One of the most interesting manifestations of acoustic combustion instability in solid propellant rocket motors is the formation of strong vortices in the combustion chamber. A single vortex filament stretching along the motor axis from the head-end has been observed in several experiments in association with gas oscillations in the frequently occurring traveling tangential mode of instability. These flows are sometimes accompanied by a quite noticeable axial torque on the motor itself, and this effect has given rise to flight performance difficulties in a number of instances. Previous theoretical studies of the vortex generation effect have been inadequate in several respects. The present work is an attempt to place the theory on a more firm base and to clarify the connection between traveling wave motions and the generation of vortices and torques.

It is readily shown that traveling waves transport momentum, and in the case of traveling tangential waves in a cylindrical combustion chamber this represents a steady axial component of angular momentum in the gas. This observation gives rise to a simple conceptual model of the vortex generation effect. Thus the presence of a steady mass flux about the axis implies the existence of a layer of vorticity at the chamber walls which may be represented by a vortex sheet composed of axially oriented bound vortex filaments. In the three-dimensional case these vortices are shed either at the end of propellant grain or at the periphery of the nozzle; the other ends of the filaments traverse the fore-end closure to the center and are combined and shed in an intense vortex filament along the symmetry axis of the motor.

Due to the production of gas at the chamber wall, tangential forces at the wall are produced by the interaction of this mean flow with the bound vortices. Angular momentum arguments must be used in this conceptual mechanism to estimate the strength of the axial vortex filament, and it is readily shown that the sense of the vortex must be opposite to the direction of travel of the waves. The direction and magnitude of the torque on the motor depend on the mean flow Mach number at the wall and must be established by calculation of the wall shear stresses.

The detailed calculations are guided by the mechanism just outlined. All physical features of the problem which appear to be significant are simulated mathematically. In particular, the effects of the three-dimensional mean flow pattern in the chamber and the pressure-sensitive combustion region at the burning surface are represented. Also considered are the effects of freedom of motion of the rocket motor in the plane normal to the symmetry axis. Both inviscid and viscous theories are developed using multi-parameter asymptotic perturbation expansion techniques. It is proved that traveling tangential waves are subject to amplification under conditions existing in typical solid propellant rockets, and that a steady transport of gas about the chamber axis accompanies this motion as a second-order perturbation. The equations of motion admit of only a vortex-like steady second-order azimuthal solution. This must be superimposed on the acoustic wave motions in such a way that angular momentum is conserved (due consideration being given to body forces on the gas and tangential forces at the wall). Thus the net pattern of steady circumfer-

ential mass flux at a given motor cross-section consists of a drift of fluid in the direction of the wave adjacent to the wall with a rapid transition to an oppositely spinning vortex flow as the longitudinal axis is approached. Introduction of the viscous corrections gives rise to a boundary condition which sets the vortex strength, and a formal connection with the classical acoustic streaming effect is established. Since momentum is dissipated in the shear region at the wall, a torque appears on the chamber itself. This roll moment is opposite in sense to the wave travel during amplification of the acoustic waves, and numerical calculations give torque magnitudes which are in agreement with experimental data from several sources.

TABLE OF CONTENTS

LIST OF FIGURES

I. INTRODUCTION

In their pioneering report on combustion instability in solid propellant rockets, Boys and Schofield (1) concluded that the secondary pressure peaks and grain erosion characteristic of unstable burning are due "... to some abnormal flow or oscillation... as if the gas were swirling with a high velocity." The succeeding 25 years have produced an abundance of experimental evidence showing that unstable combustion in certain geometrical situations is often accompanied by such vortical flows. It is the purpose of this work to clarify the connection between acoustic combustion instability and the generation of swirling flow phenomena.

An interesting manifestation which often accompanies vortex flows is the generation of moments about the axis of symmetry of the rocket motor. This has led to flight performance difficulties in a number of cases. The roll torque effect was first observed in flight tests of the Sergeant missile system (2, 3, 4). Telemetry records indicated that the attitude control system was opposing large (100 to 500 ft-lb) roll moments during the first few seconds of motor operation. A connection with combustion instability was indicated, since these occurrences coincided with periods of intense motor induced vibration. This connection was subsequently verified in specially instrumented static motor firings. Typical roll moment time-histories for the Sergeant motor are shown in Figure 1. The presence of swirling flow in the exhaust gases was demonstrated by placing instrumented vanes within the nozzle flow. Figure 2 shows the side-force time-history on such a vane.

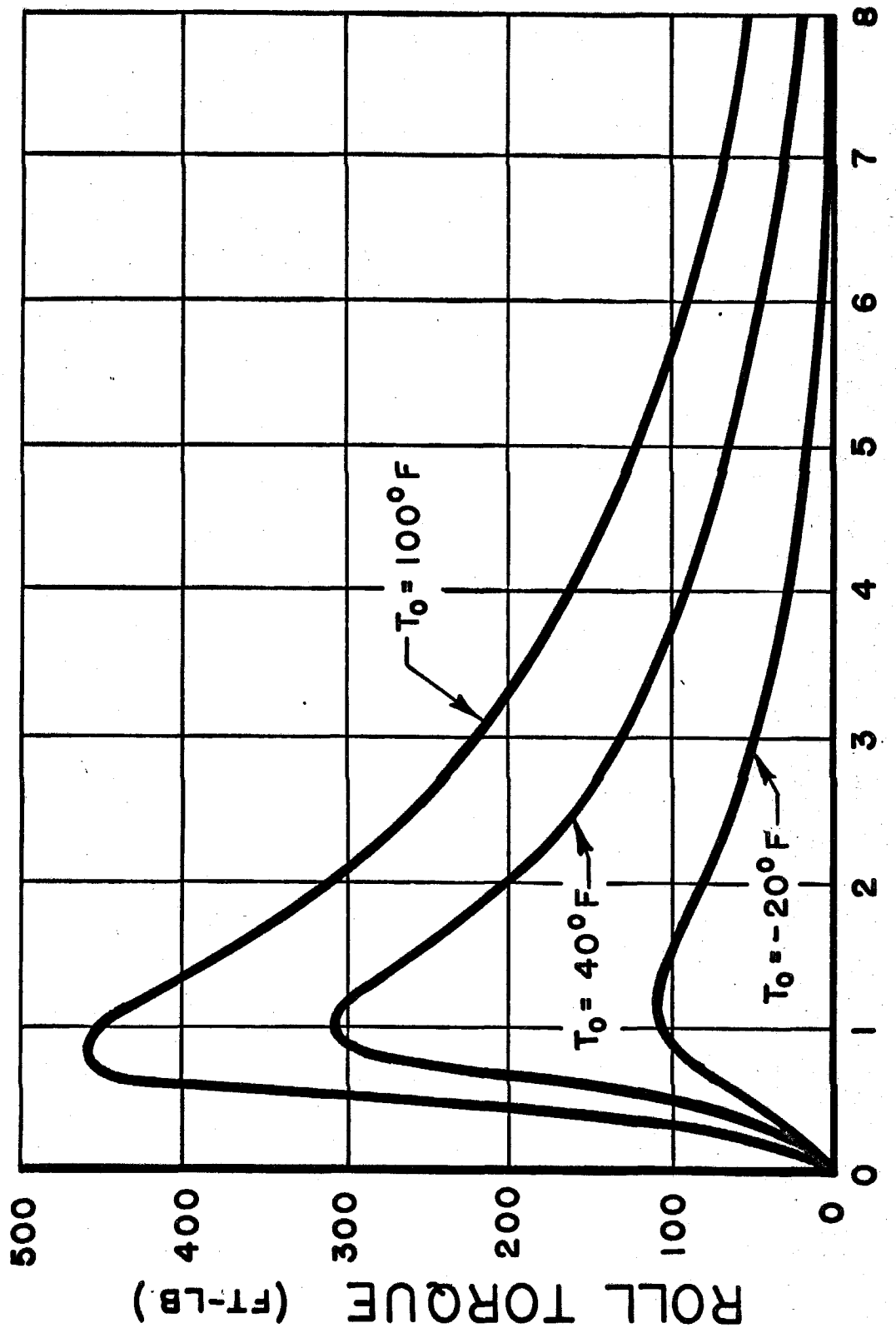

Fig. 1. Roll Moment Time History for Several Initial Propellant Temperatures

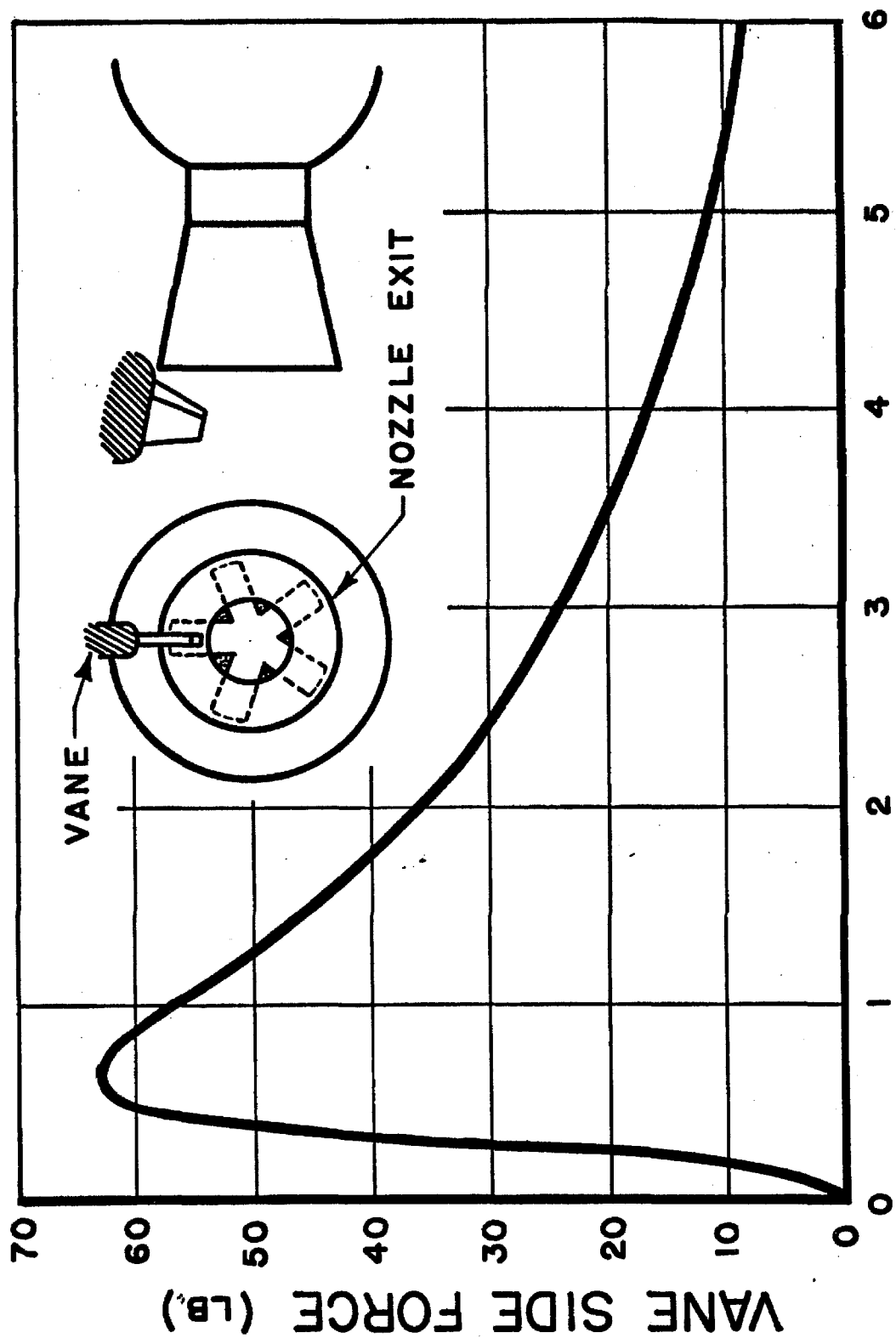

Fig. 2. Demonstration of Presence of Swirling Flow in Exhaust Gases (Sergeant)

A spectacular demonstration of the phenomenon was provided in the first flight test of the Scout space probe launching system. Shortly after ignition of the third stage (Antares) motor, roll perturbations of uncontrollable magnitude appeared which resulted in guidance failure (5). Proof of the correlation of the roll torque effect with the very marked unstable burning characteristics of the rocket was provided by static firings carried out with the motor supported in low-friction mountings.

A third example of the roll torque effect was reported by Landsbaum and Spaid (6) who found that small instability research motors with a cylindrical internal burning grain configuration tended to rotate in their mountings during periods of severe combustion instability.

Effects such as these should have been anticipated on the basis of previous experimental studies of unstable solid rockets. For example, rotating flows were observed in both cylindrical and star-perforated grains by Green (7, 8) who utilized high-speed motion pictures taken through transparent fore-end closures. According to Green, "several of the films revealed brief intervals when vortex motion of the gases was visible; sometimes the vortex would fill the entire cavity (in the tubular charge), sometimes only localized motion was suggested (as in the arms of the star-shaped cavity)." Figure 3 illustrates the flow patterns suggested by these experiments. A similar experimental study was carried out recently by Swithenbank and Sotter (9) which indicated that the flow perturbations depend strongly on the mode of oscillation present. The transverse modes produced

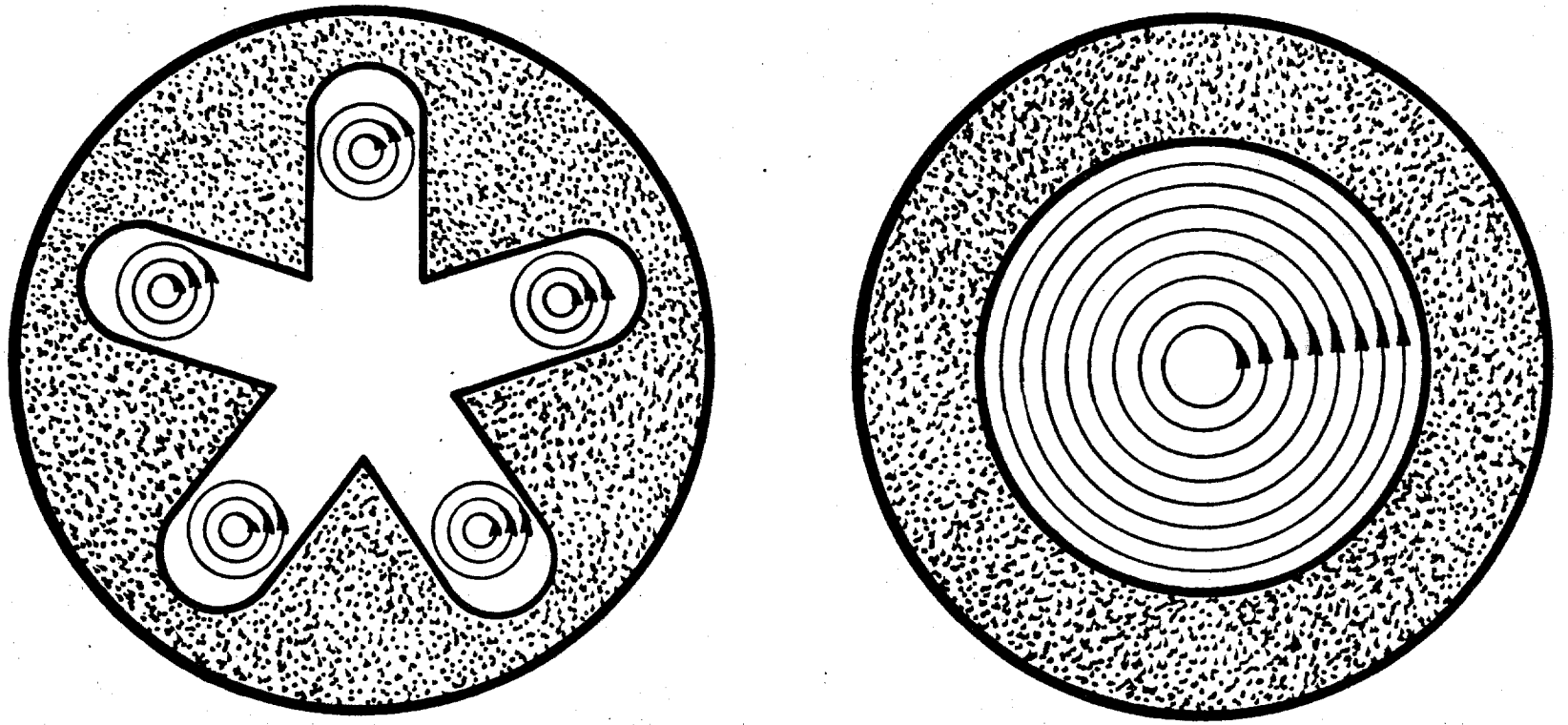

Fig. 3. Vortex Flow Patterns Suggested by Experimental Observations

sets of cellular rotating flows somewhat reminiscent of Taylor vortices, while a single strong axial vortex accompanied the traveling form of the first tangential mode.

Attempts to develop a theoretical description of the vortex generation effect have been made previously by the present author (3, 4) and by Swithenbank, Sotter and others (9, 10, 11) at the University of Sheffield (England). These have all leaned heavily on the acoustic streaming theory of Maslen and Moore (12), and while they do contain some elements of the true picture, they suffer from several errors in the latter work and from certain important misinterpretations and omissions. Acoustic streaming theory does seem to answer the principal questions concerning formation of the cellular vortices arising with standing acoustic oscillations. The much more important case, however, is that involving traveling waves, a single axial vortex, and roll torque on the motor. This case is not well represented by acoustic streaming theory alone. The main objections to the previous theories are: 1) the significance of angular momentum transport about the chamber axis by the traveling wave motions has been ignored; 2) the effects of the mean flow field have not been represented in calculations dealing with either the inviscid or the high shear regions of the chamber; 3) the influence of the pressure sensitive combustion region which drives the gas oscillations themselves has not been properly accounted for; 4) the results of the viscous calculations and their significance in regard to the whole flow field have been misinterpreted in certain respects.

The present work is an attempt to produce a theoretical

description of the three-dimensional flow field in an unstable solid propellant rocket. On the basis of the experimental observations, emphasis is placed on traveling transverse wave motions in a tubular propellant grain burning at the inner surface. All physical features of the problem which appear to be significant are simulated mathematically, appropriate simple models being used where necessary to represent complex phenomena. In particular, the combustion region at the burning propellant surface is represented by a model which gives it the characteristics which are exhibited experimentally and avoids an extremely detailed description of the combustion dynamics.

On the other hand, several features which have not been assessed before were included. For example, it seems apparent that freedom of motion of the rocket in the plane normal to its axis of symmetry might have an important effect on the internal flow field. The motor moves (the often observed vibrations accompanying combustion instability) in response to the oscillating pressures in the combustion chamber, and it is of considerable interest to determine how this motion affects the character of the flow.

Angular momentum considerations provide a mechanism for the vortex generation effect which guides the theoretical work. It is appropriate at this point to describe this mechanism before the detailed supporting calculations themselves are undertaken. Figure 4(a) illustrates the type of transverse wave motions most often observed in acoustically unstable solid propellant rockets. The instantaneous velocity distribution is shown for the lowest order traveling tangential mode, and the rotation of the velocity nodes about the chamber axis is

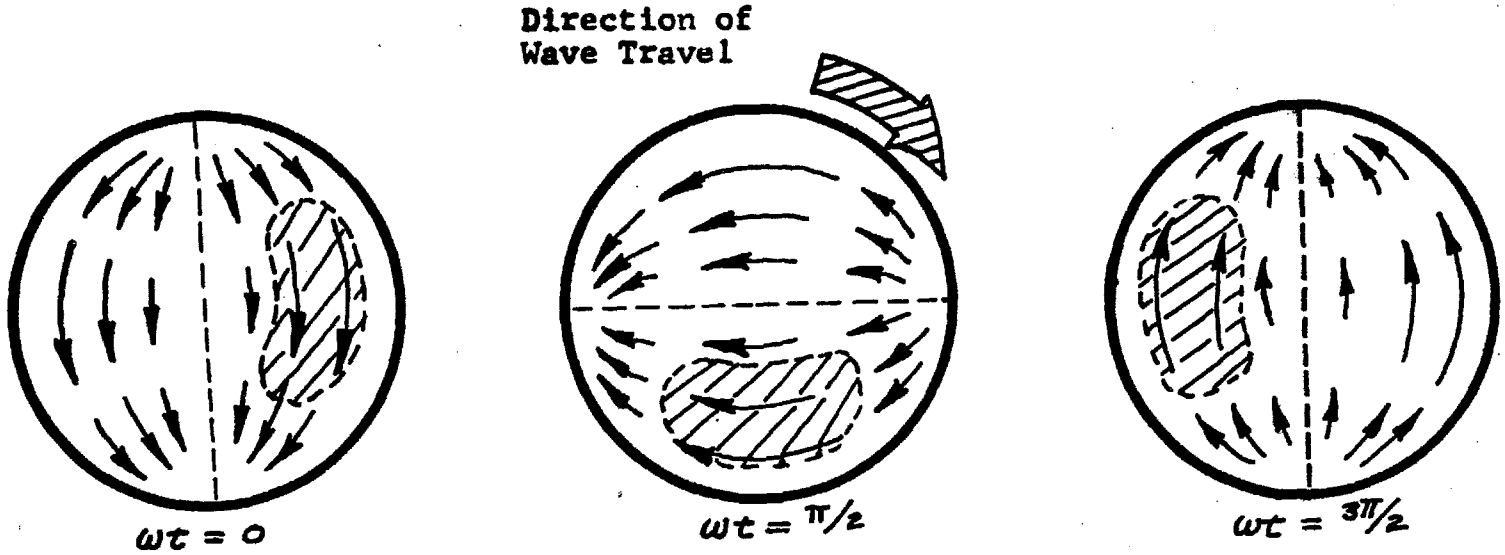

Fig. 4(a). Instantaneous wave velocity distributions for first traveling tangential mode for several times.

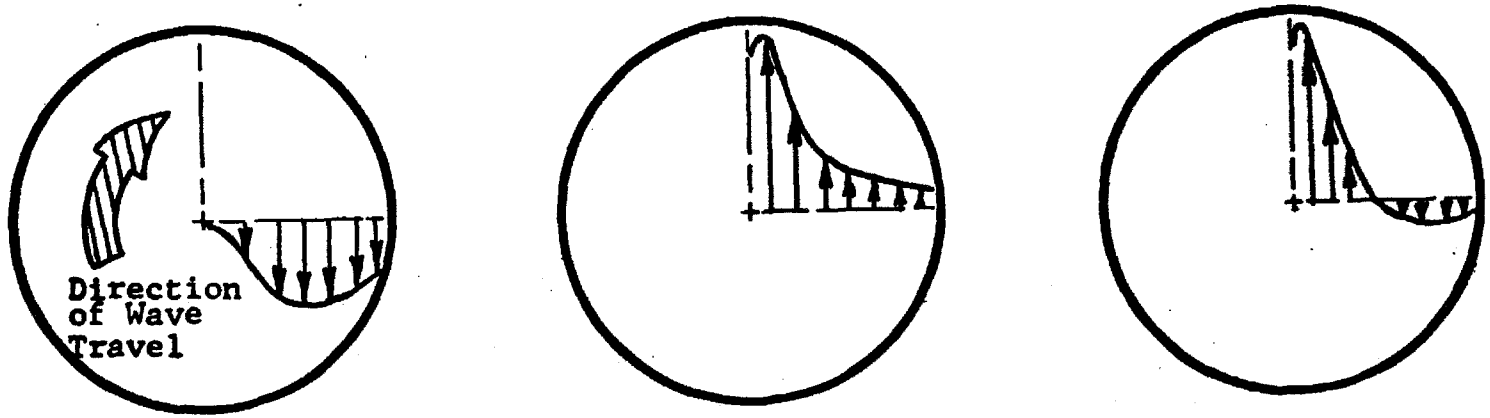

Distribution of mass transported by wave

Distribution of mass flux due to secondary flow

Combined steady mass flux profile

Fig. 4(b). Steady net circumferential mass flux profiles.

indicated. One complete revolution of the nodes corresponds to one cycle of oscillation. The superimposed shaded areas in the sketches represent the high density region of the wave. The motion is analagous to free surface sloshing of a liquid about the axis of a cylindrical container. It is obvious that momentum is transported by any traveling wave, and in the present case there results a net angular momentum about the axis of the chamber in the direction of nodal travel. We must inquire as to the source of this angular momentum and seek the answers to the following related questions: 1) how are the waves (and the angular momentum indicated by their presence) driven to higher amplitude in an unstable situation; 2) what interaction forces on the surfaces of the combustion chamber may accompany the traveling wave motions, and what relationship do they have to the driving mechanism; 3) what relationship is implied between the wave motions themselves and experimentally observed secondary flows (vortices) which also involve angular momentum? It is tempting to answer the first two questions simultaneously by claiming that tangential forces acting at the wall produce both the angular momentum in the gas and a reaction on the wall leading to the observed torque effects. Thus, during wave amplification, there would result: 1) a net increase in angular momentum in the gases within the chamber; 2) a loss of angular momentum from the system due to flux through the nozzle; and 3) a moment about the axis in a direction opposite to the nodal travel of the waves. This model may be appropriate,for instance,in the case in which the traveling waves are driven intentionally by circumferential

gas injection at the wall* (9, 10), but it certainly does not work properly in the more interesting and more frequently encountered case in which the waves grow spontaneously from small random perturbations. In fact, if the gas is non-viscous and if the burning surface is assumed smooth and undistorted, then no tangential wall forces can exist in the closed system. Even if account is taken of frictional effects, it is difficult to explain how forces due to dissipation of momentum could act to drive momentum into the wave. The correct answer to the question seems to lie in the possibility of a superimposed steady** secondary flow. This flow must spin in a direction opposite the wave travel such that an appropriate law of conservation of angular momentum is not violated. The situation is illustrated in Figure 4(b). The radial distribution of mass flux carried by the wave is shown in the first sketch. To account for both changes in amplitude of the motion within the chamber and the flux of angular momentum through the nozzle without postulating unjustifiable tangential forces at the wall, we must superimpose a secondary flow opposite to the wave travel as shown in the center sketch. The net distribution of steady mass flux about the axis is illustrated in the last drawing. Note that the radial

---

* The model is in fact only partially correct for this case, since only part of the momentum carried by the injectant goes into the driving of the waves. Some momentum is transported with the mean flow and a vortex is produced in the manner of the Ranque-Hilch effect. This vortex is in the direction of injection and thus also has the same direction as the nodal travel.

** The word "steady" will be used throughout this report to refer to non-oscillatory phenomena. However, the steady quantities may vary exponentially with time.

distribution of the secondary flow is dictated by the equations of motion of the gas. Thus, while there is no net time rate of change (including flux through the nozzle) of angular momentum and no forces on the system, there may be a net steady mass flux at a given point in the chamber.

There exists an interesting analogy with subsonic wing theory which may help to clarify the above reasoning. To achieve analytically a flow pattern about an airfoil which resembles that observed experimentally, it is necessary to apply auxiliary conditions which lie beyond the hydrodynamic theory itself. Thus, a net circulation (generated by an imaginary bound vortex) is superimposed to properly locate the rear stagnation point at the trailing edge. In the present problem we may imagine a large number of bound vortices of infinitesimal strength in the walls of the chamber as illustrated in Figure 5. Thus, the wall may be replaced in effect by a superposed cylindrical vortex sheet and a sheet of sources to account for the mean flow. Inclusion of a few of the three-dimensional aspects of the problem will give some insight into the type of secondary flow which would be generated within the chamber. First note that the cylindrical vortex sheet must be shed at the sharp edge of the chamber (corresponding to the aft edge of the propellant grain or the nozzle exit in the actual case). Hence a line integral around the exhaust plume would yield a net vorticity equal to the sum of that represented by the bound vortices. This situation cannot be allowed, and we must trace the opposite ends of the bound vortex filaments in order that the Helmholtz vortex theorems not be violated. The filaments may lie in a radial pattern

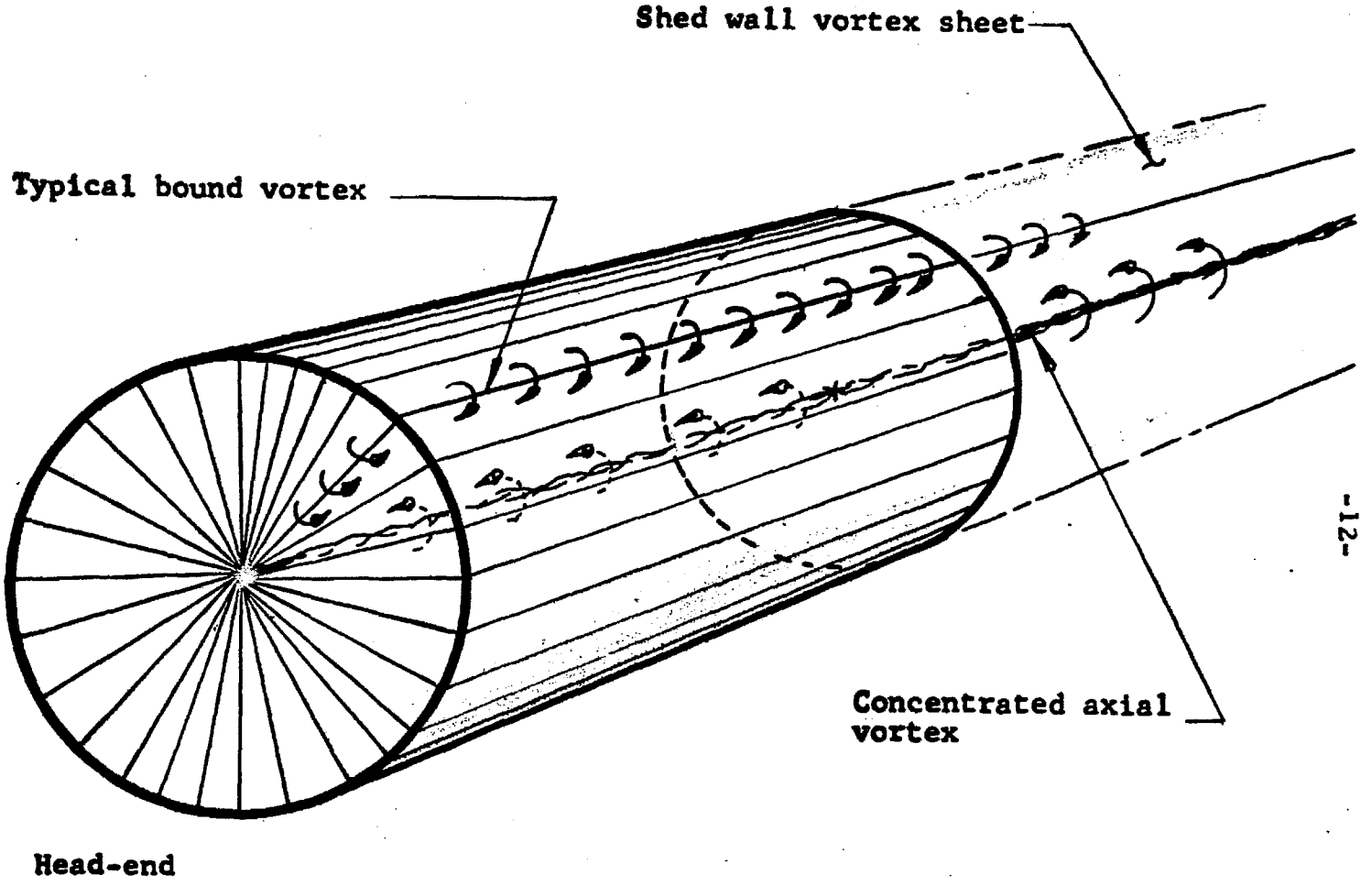

Fig. 5. Replacement of combustion chamber walls by a vortex sheet.

along the head-end closure as illustrated in Figure 5, or they may spiral in some complicated way toward the chamber axis. In either case, symmetry arguments can be used to show that all of the filaments must meet at the axis, and at this point they must leave the solid and be shed in an intense vortex filament coincident with the motor axis. This vortex with those shed from the edge of the nozzle constitute an exact analog to the shed wing-tip vortices in the three-dimensional wing problem. We are thus led to expect that the superimposed secondary flow pattern postulated above must have the form of a potential vortex, at least under steady-state conditions. This model seems to agree in all important respects with the observations already discussed. In the airfoil problem, viscous effects must ultimately be used to justify the Kutta condition at the trailing edge. It will be proven by detailed calculations in a later section that the effects of viscosity at the chamber wall impose a similar requirement on the flow in the chamber. That is, a steady secondary flow opposite in direction to the wave must exist to satisfy the no-slip boundary condition at the gas - solid interface. This is the classical "acoustic streaming" effect, and it produces a vortex flow which properly balances the angular momentum carried by the waves themselves. Shearing stresses at the walls, head-end, and in the nozzle give rise to a steady moment on the motor. Since a very complicated momentum balance is involved, the direction of the torque in relation to the direction of wave travel cannot be specified without making the detailed calculations of these stresses.

The above mechanism for formation of vortices in unstable

rocket motors guides the analysis to follow. The presentation divides itself naturally into three main parts. In the first, the mathematical formulation for the entire problem is set forth. Basic assumptions, equations of motion, and boundary conditions are discussed, and a strategy for solution of the problem by asymptotic expansion techniques is laid out. The second part consists of an inviscid approximation to the solution. The first task is to prove that the traveling tangential waves,whose importance in the generation of vortical flows has already been demonstrated, are indeed subject to amplification under conditions existing in typical motors. The influence of motion of the motor in response to the oscillating internal flow field is assessed and the main result is found to be a stabilizing influence on the wave motions. Solutions are carried out to higher order, and it is demonstrated that a steady vortex-like secondary flow with sense opposite that of the nodal travel of the waves must accompany the gas oscillations. The vortex strength is computed somewhat arbitrarily in the inviscid case by requiring that the shearing stress be zero at the wall. In the last section, some real fluid effects are introduced, and the viscous corrections near the chamber walls are investigated in detail using boundary layer theory. Damping of the wave motion by viscous shear is assessed. Second-order boundary layer calculations show that a steady secondary flow opposite to the wave travel direction must be superimposed to satisfy the no-slip wall boundary condition. This is the classical "acoustic streaming" effect, and it provides the information necessary for estimation of the strength of the axial vortex. The influence of combustion and boundary layer "blowing" by the

mean flow on these effects is investigated in detail. The steady shearing stress at the wall is calculated, and the magnitude of the roll torque on the motor is established. Finally, some numerical calculations are made and the results are compared to data from experimental studies.

II. MATHEMATICAL MODEL

This section is a summary of the equations, boundary conditions, and assumptions which form the basis for the analysis of the various aspects of the flow field in an unstably operating rocket motor.

1. Assumptions

An internally burning, cylindrically perforated propellant geometry is assumed. The propellant and other solid portions of the system are taken to be rigid, but will be allowed to move in response to the pressure and momentum forces generated at the propellant - gas interface. Only motions in a plane normal to the motor axis are to be considered.

The region of principal concern consists of that part of the combustion gas bounded by the cylindrical propellant grain, the head-end closure and the nozzle entrance plane. Details of the flow through the nozzle itself will not be considered here. An inviscid fluid will be assumed at first; later, both viscosity and heat conduction effects will be added. Variation of the viscosity coefficient with temperature fluctuations will also be accounted for.

The combustion process is assumed to be concentrated at the inner surface of the cylinder. The physical character of the combustion zone which is of importance in this study will be simulated by specifying a boundary condition at its outer surface which matches the behavior exhibited experimentally. Both the effects of regression of the burning surface and the change of system mass as the propellant is consumed can be safely neglected, since the characteristic times associated with these effects are long compared to the period typical of

the gas oscillations and to the characteristic amplification time for acoustic waves.

2. Equations of Motion

The motion of a viscous, compressible, heat conducting gas relative to coordinates accelerating with respect to the inertial system but not rotating relative to it is governed by

$$\frac{\partial \rho}{\partial t} + \nabla \cdot (\rho \underline{u}) = 0 \tag{2.1}$$

$$\rho \frac{D\underline{u}}{Dt} + \frac{\nabla P}{\gamma} = \underline{\mathfrak{F}} + \\ + \delta^2 \{\mu[\nabla^2 \underline{u} + \nabla(\nabla \cdot \underline{u}] + \nabla[\underline{u} \cdot \nabla \mu - \tfrac{2}{3}\mu \nabla \cdot \underline{u}] + (\nabla \mu \cdot \nabla)\underline{u} - (\underline{u} \cdot \nabla)\nabla \mu\} \tag{2.2}$$

$$\rho \frac{DT}{Dt} - \frac{(\gamma-1)}{\gamma} \frac{DP}{Dt} = \frac{\delta^2}{\sigma} \nabla \cdot (\mu \nabla T) + (\gamma-1)\delta^2 \mu \cdot \\ \cdot \{\nabla^2(\underline{u} \cdot \underline{u}) - (\nabla \times \underline{u}) \cdot (\nabla \times \underline{u}) - 2\underline{u} \cdot (\nabla^2 \underline{u}) - \tfrac{2}{3}(\nabla \cdot \underline{u})^2\} \tag{2.3}$$

$$P = \rho T \tag{2.4}$$

where $\underline{\mathfrak{F}}$ is the body force acting on a unit volume element of the combustion gases due to the acceleration of the system. The equations are written in terms of the dimensionless variables:

$$P = P'/P_o \qquad \underline{r} = r'/R$$

$$\rho = \rho'/\rho_o \qquad t = (a_o/R)t'$$

$$\underline{u} = \underline{u}'/a_o \qquad \mu = \mu'/\mu_o$$

$$T = T'/T_o \qquad m = m'/\rho_o R^3$$

where R = chamber radius, a_o = average speed of sound. Dimensional quantities are denoted by primes and subscript o indicates the average values of the principal thermodynamic variables (dimensional) in the absence of wave motion. σ is the Prandtl number

$$\sigma \equiv \frac{C_p \mu_o}{k} \tag{2.5}$$

where C_p = specific heat at constant pressure and k = thermal conductivity of the gas. Both are assumed constant throughout the flow. δ is the inverse square root of a Reynolds number based on the chamber radius and the average speed of propagation of small disturbances

$$\delta \equiv \left[\frac{\mu_o}{\rho_o a_o R}\right]^{\frac{1}{2}} . \tag{2.6}$$

The body force is

$$\underline{\mathfrak{F}} = -\rho \frac{d^2 \underline{s}}{dt^2} \tag{2.7}$$

where $\underline{s}$ denotes the position of the moving origin relative to the inertial system as illustrated in Figure 6. The acceleration is determined from a relation of the form

$$\frac{d^2 \underline{s}}{dt^2} = \lambda \underline{Q} \left(\underline{s}, \frac{d\underline{s}}{dt}, t\right) , \tag{2.8}$$

where the vector function $\underline{Q}$ reflects the integrated effect of the surface tractions acting on the propellant grain and the mechanical constraints between the moving motor and its mounting. The scaling parameter λ is the inverse of the dimensionless chamber mass

$$\lambda \equiv 1/m \tag{2.9}$$

and is therefore proportional to the ratio of the mass of gas contained within the chamber at a given instant to the chamber mass itself.

3. Perturbation Expansions

In order to solve the equations of motion, we must utilize the

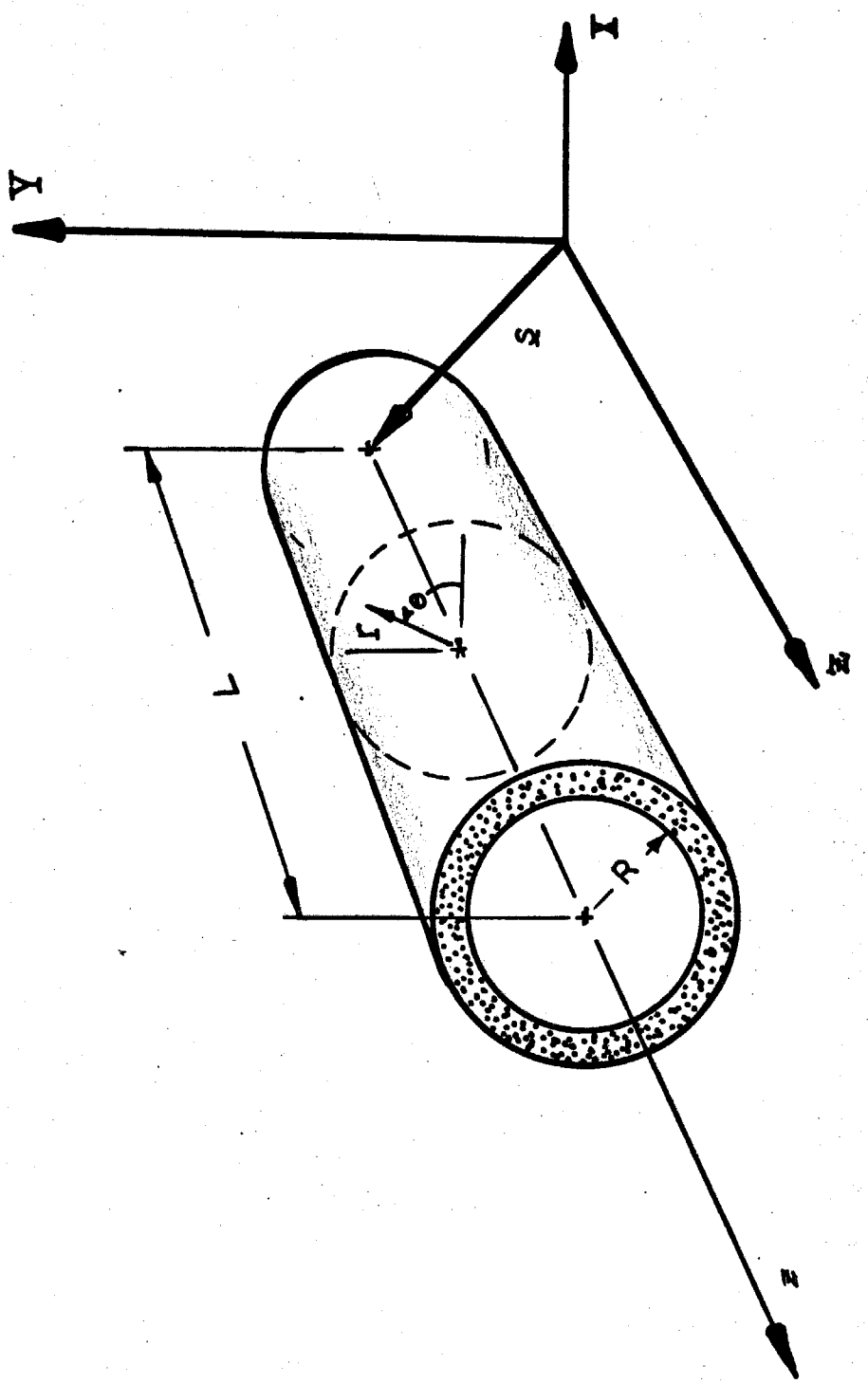

Fig. 6. Coordinate System

following observation: the phenomena of importance must grow from disturbances which are at first small. The strategy is thus to analyze the motion as though it were a small perturbation to the equilibrium flow pattern with the hope that the results thus obtained will yield insight into related phenomena at higher amplitudes. Introduce a scaling parameter ϵ, which is proportional to the average Mach number of the disturbance, and another small parameter ν which represents the relative importance of the mean flow of combustion gases through the chamber. ν is taken for later convenience to equal the mean flow Mach number at the burning surface:

$$\nu \equiv \left(\frac{u'}{a_o}\right)_{r=1} . \tag{3.1}$$

The mean flow field within the chamber is represented by

$$(\underline{u})_{\text{mean flow}} = \nu \underline{U} \tag{3.2}$$

where $\underline{U}$ reflects the geometrical qualities of the mean flow. The validity of the perturbation method depends on proper relationships between the small parameters based on suitable limit processes (15). Since acoustic conditions are assumed (that is, $\epsilon \ll 1$), it is necessary to relate ϵ and ν as follows

$$\lim_{\epsilon, \nu \to 0} \left(\frac{\epsilon}{\nu}\right) = 0 . \tag{3.3}$$

That is, $(\epsilon/\nu) = O(\epsilon)$. Other relationships between small quantities which will be of some importance in what follows are

$$(\nu/\delta) = O(1) \tag{3.4}$$

and

$$(\lambda/\nu) = O(1) . \tag{3.5}$$

Justification for these will be given in more detailed discussions later. The physical significance of the small parameters will also receive more attention at appropriate points in the development.

The following perturbation expansions are employed:

$$\begin{aligned} P &= 1 + \epsilon P^{(1)} + \epsilon^2 P^{(2)} + \dots \\ \rho &= 1 + \epsilon \rho^{(1)} + \epsilon^2 \rho^{(2)} + \dots \\ T &= 1 + \epsilon T^{(1)} + \epsilon^2 T^{(2)} + \dots \\ \mu &= 1 + \left(\frac{\partial \mu}{\partial T}\right)[\epsilon T^{(1)} + \epsilon^2 T^{(2)} + \dots] \\ \underline{u} &= \nu \underline{U} + \epsilon \underline{u}^{(1)} + \epsilon^2 \underline{u}^{(2)} + \dots \\ \mathfrak{F} &= \epsilon \underline{\mathfrak{F}}^{(1)} + \epsilon^2 \underline{\mathfrak{F}}^{(2)} + \dots \end{aligned} \tag{3.6}$$

where μ has been assumed to be a linear function of temperature over the range of interest. $\frac{\partial \mu}{\partial T}$ is assumed constant throughout the region.

Several double expansions will be necessary. In particular, higher-order corrections in ν will be required eventually. Thus,

$$\begin{aligned} P^{(1)} &= P^{(10)} + \nu P^{(11)} + \nu^2 P^{(12)} + \dots \\ \underline{u}^{(1)} &= \underline{u}^{(10)} + \nu \underline{u}^{(11)} + \nu^2 \underline{u}^{(12)} + \dots \end{aligned} \tag{3.7}$$

and so on.

4. Boundary Conditions

Since the combustion process takes place in a very thin lamina of fluid with thickness δ_f in the range

$$10^{-3} < \delta_f < 10^{-1}$$

at the wall of the chamber, it is possible to represent the effects of combustion as a boundary condition on the flow at the interface. This is accomplished by introducing an admittance function A such that

$$\hat{n} \cdot \underline{\tilde{u}} = -\nu \left(\frac{\tilde{P}}{\gamma}\right) A \qquad \text{at } r = 1 \tag{4.1}$$

where $\tilde{\underline{u}}$ and $\tilde{P}$ are the (complex) velocity and pressure fluctuations at the wall. $\hat{n}$ is an outward pointing unit vector normal to the chamber wall at the point in question, and γ, the ratio of specific heats, is inserted for later convenience. Now, since A is taken to be a complex number,

$$A = A^{(r)} + iA^{(i)} , \qquad (4.2)$$

it is seen that the response of the burning surface to the pressure fluctuations is a normal oscillating gas influx which may be out of phase with the pressure. The admittance function is discussed in detail in references (16 - 19) from both the theoretical and experimental points of view. Since only transverse wave motions will be considered in what follows, boundary conditions at the head-end and nozzle entrance planes are of no consequence, as proven by Culick (16).

For the viscous flow computations, the boundary condition for gas motions parallel to the wall is the usual no-slip condition. The normal component will be forced to satisfy the same condition as expressed by (4.1) but at a distance of order δ_f from the wall.

III. INVISCID THEORY

If it is assumed that the effects of viscosity are confined to thin layers at the boundaries of the chamber and perhaps to a region near the chamber axis under certain conditions, then the frictional terms may be dropped from equations (2. 2) and (2. 3). Solutions to the resulting simplified problem will provide considerable insight into the situation and facilitate later development of the viscous corrections.

An important task is to demonstrate that such wave motions can indeed be amplified in an internally burning solid rocket with the simple geometry we have assumed. This part of the analysis will be carried out using methods suggested by Professor F. E. C. Culick, and are similar in most respects to those employed in his study of standing wave combustion instability (16). The principal departures involve use of complex eigenfunctions which are suitable for description of traveling waves and inclusion of the effects of motion of the rocket. Also, the solutions are extended to higher order in both of the principal scaling parameters ϵ and ν in order to study certain nonlinear aspects of the wave motion.

5. First-Order Calculations

Dropping the viscous terms from the equations of motion (2. 1 - 2. 4) and eliminating the temperature by combining the resulting state and energy equations yields the set

$$\frac{\partial P}{\partial t} + \gamma P \nabla \cdot \underline{u} = - \underline{u} \cdot \nabla P \tag{5. 1}$$

$$\rho \frac{D\underline{u}}{Dt} + \frac{\nabla P}{\gamma} = \underline{\mathcal{F}} \tag{5. 2}$$

which governs the principal variables P and $\underline{u}$. In accordance with the mathematical strategy laid out in the last section, we expand (5.1) and (5.2) using integral powers of ϵ as an asymptotic sequence:

Order ϵ:

$$\frac{\partial P^{(1)}}{\partial t} + \gamma \nabla \cdot \underline{u}^{(1)} = - \nu [\underline{U} \cdot \nabla P^{(1)}] \tag{5.3}$$

$$\frac{\partial \underline{u}^{(1)}}{\partial t} + \frac{\nabla P^{(1)}}{\gamma} = - \nu [\underline{U} \cdot \nabla \underline{u}^{(1)} + \underline{u}^{(1)} \cdot \nabla \underline{U}] + \underline{\mathcal{F}}^{(1)} \tag{5.4}$$

Order ϵ^2:

$$\frac{\partial P^{(2)}}{\partial t} + \gamma \nabla \cdot \underline{u}^{(2)} = - \gamma P^{(1)} \nabla \underline{u}^{(1)} - \underline{u}^{(1)} \cdot \nabla P^{(1)} - \nu [\underline{U} \cdot \nabla P^{(2)}] \tag{5.5}$$

$$\frac{\partial \underline{u}^{(2)}}{\partial t} + \frac{\nabla P^{(2)}}{\gamma} = - \rho^{(1)} \frac{\partial \underline{u}^{(1)}}{\partial t} - \underline{u}^{(1)} \cdot \nabla \underline{u}^{(1)} - \nu [(\underline{u}^{(2)} \cdot \nabla \underline{U} + \underline{U} \cdot \nabla \underline{u}^{(2)}) + \rho^{(1)} (\underline{u}^{(1)} \cdot \nabla \underline{U} + \underline{U} \cdot \nabla \underline{u}^{(1)})] + \underline{\mathcal{F}}^{(2)} \tag{5.6}$$

where $\underline{U}$ has been assumed steady and solenoidal. A useful approximation to the mean flow for a cylindrical combustion chamber is

$$\underline{U} = - r \hat{e}_r + 2 z \hat{e}_z \tag{5.7}$$

which will be used ultimately in the numerical calculations. This representation is easily seen to be a solution of Laplace's equation, and is thus also irrotational. It departs from reality by exhibiting an axial flow component at the wall. This is of little consequence in the present development, since tangential gas motions will receive the most attention. Culick has shown that forcing the mean flow to behave according to a boundary condition more representative of the actual situation (that is, that the flow be exactly normal at the wall) gives rise to a rotational mean flow with transport of an azimuthal component of vorticity along the streamlines (20). Since only axial vorticity

is of primary interest here, effects of this type are assumed negligible.

First-Order Boundary Value Problem. The wave equation for the pressure fluctuations is derived by subtracting the divergence of the momentum equation (5.4) from the time derivative of the pressure equation (5.3):

$$\frac{\partial^2 P^{(1)}}{\partial t^2} - \nabla^2 P^{(1)} = -\gamma \nabla \cdot \underline{\mathfrak{F}} + \nu [\gamma \nabla \cdot (\underline{U} \cdot \nabla \underline{u}^{(1)} + \underline{u}^{(1)} \cdot \nabla \underline{U}) - \frac{\partial}{\partial t} (\underline{U} \cdot \nabla P^{(1)})] . \quad (5.8)$$

In anticipation of oscillations, it is convenient to assume that all dependent variables exhibit exponential time dependence:

$$\begin{aligned} P^{(1)} &= \gamma p^{(1)} e^{iKt} \\ \underline{u}^{(1)} &= \underline{q}^{(1)} e^{iKt} \\ \underline{\mathfrak{F}}^{(1)} &= \lambda \underline{f}^{(1)} e^{iKt} \end{aligned} \quad (5.9)$$

where K is the complex frequency

$$K \equiv \Omega + i\Lambda \quad (5.10)$$

and the amplitudes $p^{(1)}$, $\underline{q}^{(1)}$, and $\underline{f}^{(1)}$ may be complex. Thus, (5.8) may be written in the form of the non-homogeneous Helmholtz equation:

$$\nabla^2 p^{(1)} + K p^{(1)} = \nu g^{(1)} \quad (5.11)$$

where

$$g^{(1)} = \{iK(\underline{U} \cdot \nabla p^{(1)}) - \nabla \cdot (\underline{U} \cdot \nabla \underline{q}^{(1)} + \underline{q}^{(1)} \cdot \nabla \underline{U}) + (\frac{\lambda}{\nu}) \nabla \cdot \underline{f}^{(1)}\} \quad (5.12)$$

The boundary condition on $p^{(1)}$ can be found by combining the definition for the admittance function (4.1) with the momentum equation in the form of a condition on the component of the pressure gradient normal to the wall:

$$\hat{n}\cdot\nabla p^{(1)} = \hat{n}\cdot\left[-iK\underline{q}^{(1)}-\nu(\underline{U}\cdot\nabla\underline{q}^{(1)}+\underline{q}^{(1)}\cdot\nabla\underline{U})+\lambda\underline{f}^{(1)}\right].$$

Using (4. 1),

$$\hat{n}\cdot\underline{q}^{(1)} = \begin{cases} -\nu A p^{(1)} & \text{on the burning surface} \\ 0 & \text{at the head-end} \end{cases}$$

Thus, the boundary conditions can be expressed in the form

$$\hat{n}\cdot\nabla p^{(1)} = -\nu h^{(1)} \tag{5. 13}$$

where

$$h^{(1)} = \left\{-iKAp^{(1)}+\hat{n}\cdot\left[\underline{U}\cdot\nabla\underline{q}^{(1)}+\underline{q}^{(1)}\cdot\nabla\underline{U}-(\lambda/\nu)\underline{f}^{(1)}\right]\right\}_{r=1} \tag{5. 14}$$

on the burning surface.

Solution by Green's Function Method. Equations (5. 11) and (5. 13) constitute a boundary value problem in which solutions of a non-homogeneous wave equation are sought which satisfy a non-homogeneous Neumann boundary condition. The solution is facilitated by use of the Green's function.

The fundamental solution (Green's function) for the Helmholtz equation satisfies the system

$$(\nabla^2+K)G(\underline{r}|\underline{r}_o) = \delta(\underline{r}-\underline{r}_o) \tag{5. 15}$$

$$\hat{n}\cdot\nabla G(\underline{r}|\underline{r}_o) = 0 \quad \text{for} \quad \underline{r} = \underline{r}^s \tag{5. 16}$$

where $\underline{r}^s$ is a vector defining position of points on the bounding surface and $\delta(\underline{r}-\underline{r}_o)$ is the Dirac delta function. Multiplying (5. 11) by $G(\underline{r}|\underline{r}_o)$ and (5. 15) by $p^{(1)}$ and combining the results yields

$$G\nabla^2 p^{(1)} - p^{(1)}\nabla^2 G = \nu(Gg^{(1)}) - p^{(1)}\delta(\underline{r}-\underline{r}_o) .$$

Integration of this result over the volume of the combustion chamber gives

$$\int_V [G(\underline{r}|\underline{r}_o)\nabla^2 p^{(1)} - p^{(1)}\nabla^2 G(\underline{r}|\underline{r}_o)]dV =$$

$$= \nu \int_V G(\underline{r}|\underline{r}_o) g^{(1)} dV - \int_V p^{(1)} \delta(\underline{r}-\underline{r}_o) dV \ .$$

The last integral in this expression is just $p^{(1)}$ evaluated at $\underline{r} = \underline{r}_o$. Application of the symmetry property

$$G(\underline{r}|\underline{r}_o) = [G(\underline{r}_o|\underline{r})]^*$$

gives an expression for $p^{(1)}$ in terms of G^*:

$$p^{(1)}(\underline{r}) = \nu \int_V G^*(\underline{r}|\underline{r}_o) g_o^{(1)} dV_o - \int_V [G^*(\underline{r}|\underline{r}_o)\nabla^2 p^{(1)} - p^{(1)}\nabla^2 G^*(\underline{r}|\underline{r}_o)]dV_o \ .$$

Employing Green's theorem, the latter volume integral can be transformed to a surface integral

$$\int_V (G^*\nabla^2 p^{(1)} - p^{(1)}\nabla^2 G^*)dV = \int_S (G^*\nabla p^{(1)} - p^{(1)}\nabla G^*)\cdot \hat{n}\, dS \ ,$$

but

$$\hat{n}\cdot\nabla p^{(1)} = -\nu h^{(1)}$$

and

$$\hat{n}\cdot\nabla G^* = 0$$

over the boundary surface. Thus,

$$p^{(1)}(\underline{r}) = \nu \int_V G^*(\underline{r}|\underline{r}_o) g_o^{(1)} dV_o + \nu \int_S G^*(\underline{r}|\underline{r}_o^s) h_o^{(1)} dS_o \ , \qquad (5.17)$$

where the superscript s again refers to values at points on the bounding surface. The Green's function is conveniently expressed as a linear combination of the eigenfunctions of the unperturbed wave equation:

$$G^*(\underline{r}|\underline{r}_o) = \sum_\alpha A_\alpha \psi_\alpha(\underline{r}) \qquad (5.18)$$

where the eigenfunction $\psi_\alpha(\underline{r})$ satisfies the boundary value problem

$$\begin{cases} (\nabla^2 + K_\alpha^2)\psi_\alpha(\underline{r}) = 0 & (5.19) \\ \hat{n}\cdot\nabla\psi_\alpha = 0 \qquad \text{on the boundary} & (5.20) \end{cases}$$

and the amplitudes A_α remain to be computed. α represents the three-tuple (ℓ, m, n) which identifies the mode of wave motion. For the cylindrical geometry assumed, the eigenfunctions for traveling waves are best expressed in complex form as

$$\psi_\alpha = J_m(k_{mn}r)e^{\pm im\theta}\cos(k_\ell z) \qquad (5.21)$$

where the upper sign in the exponential corresponds to clockwise traveling waves; the negative sign refers to counterclockwise waves. The angular speed of wave travel is $\mp(K/m)$. To satisfy condition (5.20) at the boundary of the cylindrical region, it is necessary that

$$k_\ell = \frac{\ell\pi R}{L} \qquad \ell = 0, 1, 2, \ldots$$

and that k_{mn} be the root of

$$\frac{d}{dr} J_m(k_{mn}r) = 0 \qquad (5.22)$$

at $r = 1$. It is also clear from (5.19) that the eigenvalues are

$$K_\alpha^2 = k_\ell^2 + k_{mn}^2 .$$

Since ψ_α must be periodic in angle θ, it is necessary that $m = 0, 1, 2, \ldots$.

The eigenfunctions must also be orthogonal, that is,

$$(\psi_\alpha, \psi_\beta) \equiv \int_V \psi_\alpha^* \psi_\beta dV = 0 \quad \text{for } \alpha \neq \beta \qquad (5.23)$$

and

$$(\psi_\alpha, \psi_\alpha) \equiv \int_V \psi_\alpha^* \psi_\alpha dV = E_\alpha^2 \qquad (5.24)$$

where E_α is the normalizing constant for mode α, and * denotes the complex conjugate.

Substituting the expansion (5.18) into the differential equation (5.15) for G yields

$$(\nabla^2 + K^2)\sum_\alpha A_\alpha \psi_\alpha(\underline{r}) = \delta(\underline{r}-\underline{r}_o)$$

or

$$\sum_\alpha A_\alpha(\nabla^2\psi_\alpha + K\psi_\alpha) = \delta(\underline{r}-\underline{r}_o)$$

but $\nabla^2\psi_\alpha = -K_\alpha^2\psi_\alpha$ from (5.19). Thus,

$$\sum_\alpha A_\alpha \psi_\alpha(K^2-K_\alpha^2) = \delta(\underline{r}-\underline{r}_o) \quad . \tag{5.25}$$

The coefficients A_α can now be determined by manipulating this expression. By definition of the delta function,

$$\int_V \psi_\beta^*(\underline{r})\delta(\underline{r}-\underline{r}_o)dV = \psi_\beta^*(\underline{r}_o)$$

for all β. Thus, multiplying (5.25) by $\sum_\beta \psi_\beta^*(\underline{r})$ and integrating over the region,

$$\sum_\beta \psi_\beta^*(\underline{r}_o) = \int_V \sum_\beta \psi_\beta^*(\underline{r}) \left[\sum_\alpha A_\alpha\psi_\alpha(K^2-K_\alpha^2)\right]dV \quad .$$

Utilizing the orthogonality properties (5.23) and (5.24), only those terms on the right of the last expression for which $\alpha = \beta$ are non-zero. Therefore

$$\sum_\alpha \psi_\alpha^*(\underline{r}_o) = \sum_\alpha A_\alpha(K^2-K_\alpha^2)\int_V \psi_\alpha^*\psi_\alpha dV$$

or

$$\psi_\alpha^*(\underline{r}_o) = A_\alpha(K^2-K_\alpha^2)E_\alpha^2 \quad .$$

Thus the coefficients in the Green's function expansion are

$$A_\alpha = \frac{\psi_\alpha^*(\underline{r}_o)}{E_\alpha^2(K^2-K_\alpha^2)} \tag{5.26}$$

and the Green's function can be written in series form as

$$G(\underline{r}|\underline{r}_o) = \left\{ \sum_\alpha \frac{\psi_\alpha(\underline{r})\psi_\alpha^*(\underline{r}_o)}{E_\alpha^2(K^2-K_\alpha^2)} \right\}^* \tag{5.27}$$

The normalization constant is found by inserting the eigenfunctions (5.21) into (5.24). Thus

$$\begin{aligned} E_\alpha^2 &= \int_V \psi_\alpha^* \psi_\alpha \, dV \\ &= \int_0^{L/R} \int_0^{2\pi} \int_0^1 r\,dr\,d\theta\,dz \left[J_m^2(k_{mn}r)\cos^2(k_\ell z) \right] \\ &= \frac{L\pi}{2R}\left(1 + \frac{\sin 2\pi\ell}{2\pi\ell}\right) \begin{cases} J_o^2(k_{on}) + J_1^2(k_{on}) & m = 0 \\ J_m^2(k_{mn})\left(1 - \dfrac{m^2}{k_{mn}^2}\right) & m \neq 0 \end{cases} \end{aligned} \tag{5.28}$$

Solution to Zeroth Order in ν. The form of the wave equation governing the behavior of $p^{(1)}$

$$\nabla^2 p^{(1)} + K^2 p^{(1)} = \nu g^{(1)}$$

and the boundary condition

$$\hat{n} \cdot \nabla p^{(1)} = -\nu h^{(1)}$$

suggest that $p^{(1)}$ can be represented as a perturbation expansion with integral powers of ν as the asymptotic sequence. Thus we put

$$p^{(1)} = p^{(10)} + \nu p^{(11)} + \nu^2 p^{(12)} + \ldots$$

where the first element of the superscript refers to the order of the

solution in ϵ; the second element refers to the order of the term in ν. Inserting the expansion into the differential equation and boundary conditions, and collecting terms of like order in ν,

Order (0):

$$\left[\begin{array}{l} \nabla^2 p^{(10)} + K^2 p^{(10)} = 0 \\ \hat{n} \cdot \nabla p^{(10)} = 0 \quad \text{at the boundary} \end{array}\right] \tag{5.29}$$

Order (ν):

$$\left[\begin{array}{l} \nabla^2 p^{(11)} + K^2 p^{(11)} = g^{(10)} \\ \hat{n} \cdot \nabla p^{(11)} = -h^{(10)} \end{array}\right] \tag{5.30}$$

and so on. Since $g^{(1)}$ and $h^{(1)}$ are functions of $p^{(1)}$, they have also been expanded

$$g^{(1)} = g^{(10)} + \nu g^{(11)} + \ldots$$
$$h^{(1)} = h^{(10)} + \nu h^{(11)} + \ldots$$

Note that (5.29) is formally identical to the boundary value problem expressed by (5.19) and (5.20). This simply demonstrates that the solution as it is unfolding is a perturbation on the classical acoustic solution. Thus $p^{(10)} \equiv \psi_\alpha$ and it is proper to write

$$p^{(1)} = \psi_\alpha + O(\nu) . \tag{5.31}$$

This form is also justified experimentally, as it is often noticed that the pressure fluctuations in unstable rocket motors are identifiable in the majority of cases with classical acoustic modes of the burning cavity. Now, the solution for $p^{(1)}$ was found in terms of the Green's function to be

$$p^{(1)} = \nu \int_V G^*(\underline{r}|\underline{r}_o) g_o^{(1)} dV_o + \nu \int_S G^*(\underline{r}|\underline{r}_o^s) h_o^{(1)} dS_o$$

where

$$G^*(\underline{r}|\underline{r}_o) = \sum_{\alpha} \frac{\psi_\alpha^*(\underline{r}_o)\psi_\alpha(\underline{r})}{E_\alpha^2(K^2-K_\alpha^2)} \quad .$$

Thus

$$p^{(1)} = \nu \int_V g_o^{(1)} \sum_{\alpha} \frac{\psi_\alpha^*(\underline{r}_o)\psi_\alpha(\underline{r})}{E_\alpha^2(K^2-K_\alpha^2)} dV_o + \nu \int_S h_o^{(1)} \sum_{\alpha} \frac{\psi_\alpha^*(\underline{r}_o)\psi_\alpha(\underline{r})}{E_\alpha^2(K^2-K_\alpha^2)} dS_o$$

$$= \nu \sum_{\alpha} \frac{\psi_\alpha(\underline{r})}{E_\alpha^2(K^2-K_\alpha^2)} \left\{ \int_V g^{(1)} \psi_\alpha^*(\underline{r}) dV + \int_S h^{(1)} \psi_\alpha^*(\underline{r}) dS \right\} \qquad (5.32)$$

where the dummy subscript o has been dropped since it is no longer necessary to distinguish field-point and source-point terms in the integrals. Investigating a particular mode of oscillation, say, $\alpha = N$,

$$p^{(1)} = \psi_N(\underline{r}) \left\{ \frac{\nu}{E_N^2(K^2-K_N^2)} \left[\int_V g^{(1)} \psi_N^* dV + \int_S h^{(1)} \psi_N^* dS \right] \right\} +$$

$$+ \nu \sum_{\alpha \neq N} \frac{\psi_\alpha(\underline{r})}{E_\alpha^2(K^2-K_\alpha^2)} \left[\int_V g^{(1)} \psi_\alpha^* dV + \int_S h^{(1)} \psi_\alpha^* dS \right] \quad .$$

Thus, the required form of equation (5.31) is achieved only if

$$\frac{\nu}{E_N^2(K^2-K_N^2)} \left[\int_V g^{(1)} \psi_N^* dV + \int_S h^{(1)} \psi_N^* dS \right] = 1 \quad .$$

Satisfaction of this condition provides an equation for the eigenvalue K:

$$K^2 = K_N^2 + \frac{\nu}{E_N^2} \left[\int_V g^{(1)} \psi_N^* dV + \int_S h^{(1)} \psi_N^* dS \right] \quad . \qquad (5.33)$$

Remember that

$$K \equiv \Omega + i\Lambda$$

where Ω represents the frequency of the fluctuations and Λ reflects their rate of growth. In view of the form of (5.33), it is natural to

put

$$\Omega = \Omega^{(10)} + \nu\Omega^{(11)} + \ldots$$
$$\Lambda = \Lambda^{(10)} + \nu\Lambda^{(11)} + \ldots \qquad (5.34)$$

Expanding (5.33) in a Taylor series, we find

$$K = K_N + \frac{\nu}{2K_N E_N^2}\left[\int_V g^{(1)}\psi_N^* dV + \int_S h^{(1)}\psi_N^* dS\right] + O(\nu^2)$$

and it is apparent that K has no imaginary part of order unity. Thus

$$\Lambda^{(10)} = 0$$
$$\Omega^{(10)} = K_N \; . \qquad (5.35)$$

Also,

$$\Omega^{(11)} = \frac{1}{2K_N E_N^2}\,\Re\left[\int_V g^{(10)}\psi_N^* dV + \int_S h^{(10)}\psi_N^* dS\right]$$
$$\Lambda^{(11)} = \frac{1}{2K_N E_N^2}\,\Im\left[\int_V g^{(10)}\psi_N^* dV + \int_S h^{(10)}\psi_N^* dS\right] \qquad (5.36)$$

Equation (5.35) shows that the frequency of the oscillations is the same as the acoustic frequency to zeroth order in the mean-flow Mach number ν in accord with the oft-mentioned experimental observation. The growth rate Λ will be discussed later when all components of the integrals in (5.36) have been collected.

The First-Order Velocity Field. The solution for the amplitude $\underline{q}^{(1)}$ (time-independent part) of the velocity field vector is easily deduced from the momentum equation (5.4) written in the form

$$iK\underline{q}^{(1)} + \nabla p^{(1)} = -\nu[\underline{U}\cdot\nabla\underline{q}^{(1)} + \underline{q}^{(1)}\cdot\nabla\underline{U} - (\lambda/\nu)\underline{f}^{(1)}] \; .$$

Thus

$$\underline{q}^{(1)} = \frac{i}{K}\{\nabla p^{(1)} + \nu(\underline{U}\cdot\nabla\underline{q}^{(1)} + \underline{q}^{(1)}\cdot\nabla\underline{U} - (\lambda/\nu)\underline{f}^{(1)})\} \; . \qquad (5.37)$$

Now, using (5.34),

$$K = \Omega^{(10)} + \nu[\Omega^{(11)} + i\Lambda^{(11)}] + O(\nu^2) \tag{5.38}$$

and

$$\frac{1}{K} = \frac{1}{K_N} - \frac{\nu}{K_N^2}[\Omega^{(11)} + i\Lambda^{(11)}] + O(\nu^2) \ .$$

Expanding $\underline{q}^{(1)}$ in powers of ν,

$$\underline{q}^{(1)} = \underline{q}^{(10)} + \nu\underline{q}^{(11)} + \ldots \tag{5.39}$$

we find immediately

$$\underline{q}^{(10)} = \frac{i\nabla p^{(10)}}{K_N} \tag{5.40}$$

$$q^{(11)} = \frac{i}{K_N}\left\{-\frac{\nabla p^{(10)}}{K_N}[\Omega^{(11)}+i\Lambda^{(11)}] + \nabla p^{(11)} + \right.$$

$$\left. + [\underline{U}\cdot\nabla\underline{q}^{(10)} + \underline{q}^{(10)}\cdot\nabla\underline{U} + (\lambda/\nu)\underline{f}^{(10)}]\right\} \tag{5.41}$$

and so on. Note that the body force amplitude has also been represented by an expansion in ν.

Summary of Results to Zeroth Order in ν. Before further progress can be made, assessment of the body force term $\underline{f}^{(1)}$ must be completed. Let us now summarize the results to zeroth order in ν. In what follows, only transverse modes will be of interest. Thus, $\ell = 0$ and consequently $k_\ell = 0$. Therefore,

$$K_N = k_{mn}$$

and the complex amplitudes are

$$p^{(10)} = J_m(k_{mn}r)e^{\pm im\theta} \tag{5.42}$$

$$\underline{q}^{(10)} = \frac{i}{k_{mn}}\left[\frac{d}{dr}J_m(k_{mn}r)e^{\pm im\theta}\hat{e}_r \pm im\frac{J_m(k_{mn}r)}{r}e^{\pm im\theta}\hat{e}_\theta\right] \tag{5.43}$$

where $\hat{e}_r$ and $\hat{e}_\theta$ are unit vectors in the radial and circumferential directions respectively. The first-order pressure and velocity fluctuations are, to zeroth order in ν:

$$P^{(10)} = \gamma J_m(k_{mn}r)e^{-\nu\Lambda^{(11)}t}\cos(k_{mn}t \pm m\theta) \qquad (5.44)$$

$$\underline{u}^{(10)} = \left[-\frac{1}{k_{mn}}\frac{d}{dr}J_m(k_{mn}r)\sin(k_{mn}t \pm m\theta)\right]e^{-\nu\Lambda^{(11)}t}\hat{e}_r + \mp\left[\left(\frac{m}{k_{mn}}\right)\frac{J_m(k_{mn}r)}{r}\cos(k_{mn}t \pm m\theta)\right]e^{-\nu\Lambda^{(11)}t}\hat{e}_\theta \qquad (5.45)$$

These are, of course, the well-known acoustic solutions for transverse traveling waves in a closed circular cylinder, and represent a "sloshing" motion of the fluid in which the pressure nodes travel around the circumference of the chamber at angular rate k_{mn}. Considerable effort has been expended in securing these solutions which could have been deduced immediately from the formulation of equations (5.19) and (5.20) in the style of classical acoustics. However, three important things have been accomplished in the process: 1) an expression for the growth rate of the waves has been found which will allow an assessment of the stability of interesting modes; 2) machinery has been set up which will facilitate carrying out the solutions to higher order; and 3) terms have been included which will make it possible to explore the effects of body forces due to motor acceleration and also, later, to assess the effects of viscosity on the wave motion. It is in the higher-order, non-linear corrections that the phenomena of interest in the present study seem likely to appear.

6. Angular Momentum Considerations

It is an observed fact (cf. references 21 and 22) that traveling waves are accompanied by a steady secondary flow of fluid which is generally in the direction of travel of the wave if other perturbing effects are of no consequence. In the present case, this secondary mass flux represents the presence of angular momentum in the fluid relative to the moving coordinate system fixed to the motor. No forces have appeared in the formulation thus far which could account for this seemingly anomalous situation, and it is certainly not obvious how the waves, and consequently the angular momentum, can increase in intensity under these conditions. Subsequent efforts will be guided by an understanding of the balances of angular momentum involved.

The mass flow at a point fixed to the (moving) chamber coordinate system is

$$\underline{m} \equiv \rho \underline{u} \tag{6.1}$$

where, in the case of acoustic waves, the density variations and pressure fluctuations are related by the isentropic law:

$$P = \rho^{\gamma}$$

which is, in expanded form,

$$(1 + \epsilon P^{(1)} + \dots) = (1 + \epsilon \rho^{(1)} + \dots)^{\gamma}$$
$$= 1 + \epsilon (\gamma \rho^{(1)}) + O(\epsilon^2) \ .$$

Thus,

$$\rho^{(1)} = \frac{P^{(1)}}{\gamma} \tag{6.2}$$

and so on. Writing the mass flow as a perturbation series,

$$\underline{\mathbb{m}} = (1+\epsilon\rho^{(1)}+\dots)(\nu\underline{U}+\epsilon\underline{u}^{(1)}+\dots)$$

$$= \nu\underline{U}+\epsilon(\underline{u}^{(1)}+\nu\rho^{(1)}\underline{U})+\epsilon^2(\nu\rho^{(2)}\underline{U}+\rho^{(1)}\underline{u}^{(1)}+\underline{u}^{(2)})+O(\epsilon^3) \quad . \qquad (6.3)$$

The first term is of course just the steady zeroth-order mean flow through the motor. The order ϵ term contains two fluctuating components representing momentum flux (purely oscillatory) due to the wave and the correction to the zeroth-order mass flux due to the density fluctuations. The order ϵ^2 term contains correction terms analogous to those just mentioned (which cannot be discussed until the solution is extended to second order) and the interesting term

$$\rho^{(1)}\,\underline{u}^{(1)} \quad .$$

Ignoring the other components of the second order expression for the moment, we note that

$$\underline{\mathbb{m}}^{(2)} = \rho^{(1)}\underline{u}^{(1)} + \text{other terms} \qquad (6.4)$$

has a non-oscillating part, that is

$$\left\langle \rho^{(1)}\underline{u}^{(1)} \right\rangle = \left\langle \frac{P^{(1)}}{\gamma}\,\underline{u}^{(1)} \right\rangle \neq 0 \quad .$$

Using (5.44) and (5.45), we find, to zeroth order in ν:

$$\frac{P^{(10)}}{\gamma}\underline{u}^{(10)} = \frac{J_m(k_{mn}r)}{k_{mn}}\begin{cases} \left[-\frac{d}{dr}J_m(k_{mn}r)\sin(k_{mn}t\pm m\theta)\cos(k_{mn}t\pm m\theta)\right]\hat{e}_r \\ \mp\left[m\,\frac{J_m(k_{mn}r)}{r}\cos^2(k_{mn}t\pm m\theta)\right]\hat{e}_\theta \end{cases} \qquad (6.5)$$

and

$$\left\langle \rho^{(10)}\underline{u}^{(10)} \right\rangle = \mp\left[\frac{mJ_m^2(k_{mn}r)}{2k_{mn}r}\right]\hat{e}_\theta \quad , \qquad (6.6)$$

which shows that the wave carries a steady, second-order momentum flux component in its direction of travel (the upper sign, again,

corresponding to a clockwise traveling wave). The radial distribution of this mass flux is plotted in Figure 7 for the first tangential mode. The point of maximum mass transport is located about a fourth of the chamber radius from the wall for this mode.

The last result implies that there is a net steady, second-order angular momentum about the cylinder axis. Due to the mean flow, there is also evidently a net efflux of angular momentum from the system which is of order $(\nu\epsilon^2)$. This, in turn, implies that whatever drives the waves must also act on the gas in such a way as to account for the increase in angular momentum as the wave intensity builds up and to balance the loss of angular momentum which flows from the system with the mean flow. It is instructive to examine the situation in the large by application of the momentum theorem to the entire mass of fluid contained within the combustion chamber at a given instant. Thus,

$$\underline{M} = \frac{\partial}{\partial t}\int_V (\underline{r}\times\rho\underline{u})dV + \int_S (\underline{r}\times\rho\underline{u})(\underline{u}\cdot\hat{n})dS \qquad (6.7)$$

relates the summation of all external moments (including those due to body forces resulting from acceleration of the system) to the rate of change of angular momentum within the chamber and the net efflux of angular momentum through the boundary. Expanding as usual, the angular momentum balance to various levels of approximation is

Order ϵ:

$$\underline{M}^{(1)} = \frac{\partial}{\partial t}\int_V \underline{r}\times\underline{u}^{(1)}dV + \nu\left\{\frac{\partial}{\partial t}\int_V \underline{r}\times\rho^{(1)}\underline{U}dV + \int_S \underline{r}\times[(\underline{U}\cdot\hat{n})\underline{u}^{(1)} + \underline{U}(\underline{u}^{(1)}\cdot\hat{n})]dS\right\}$$

$$+ O(\nu^2) \qquad (6.8)$$

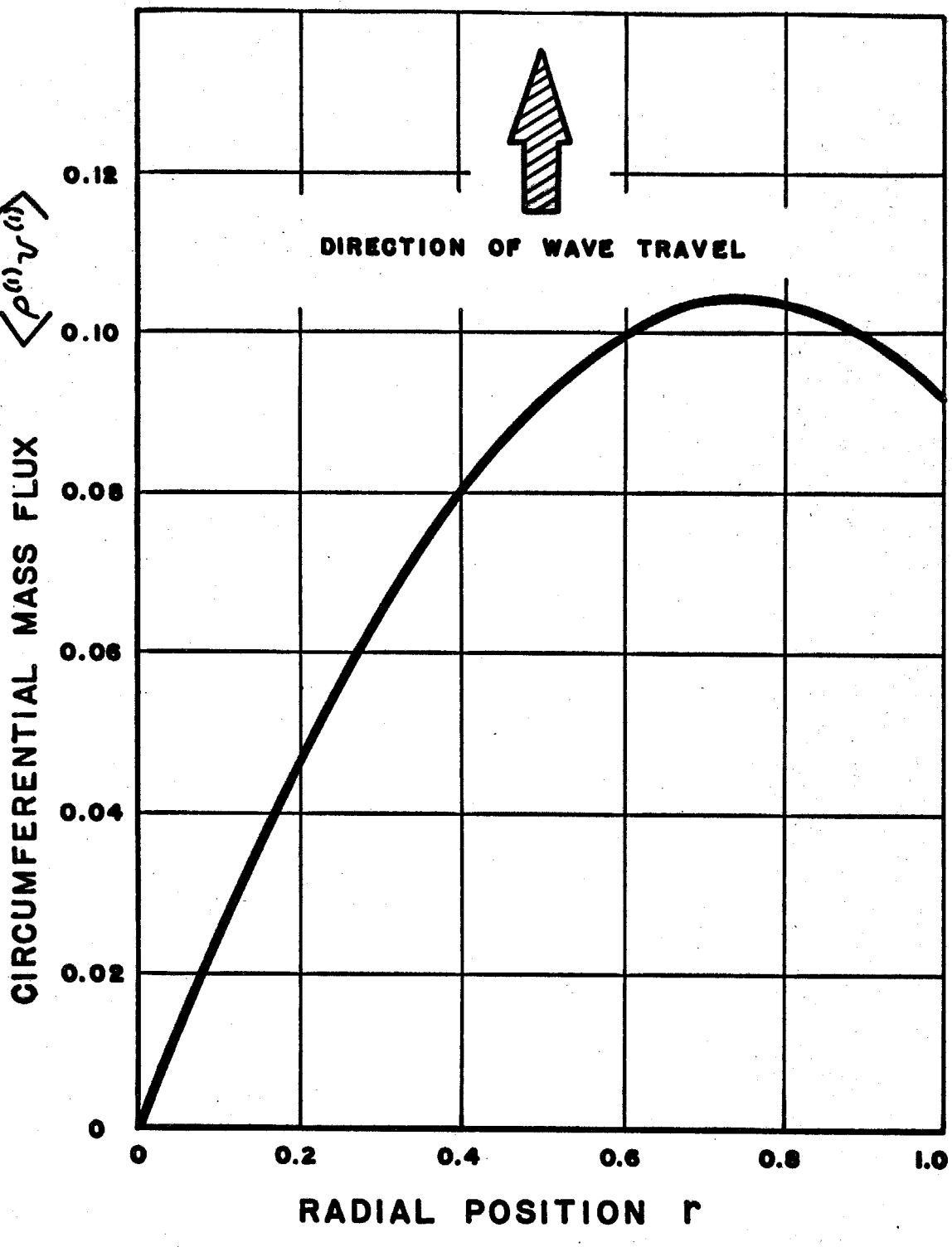

Fig. 7. Steady Momentum Flux Carried by Traveling Wave (First Transverse Mode).

Order ϵ^2:

$$\underline{M}^{(2)} = \frac{\partial}{\partial t}\int_V \underline{r}\times[\underline{u}^{(1)}\rho^{(1)}+\underline{u}^{(2)}]dV + \int_S (\underline{u}^{(1)}\cdot\hat{n})\,\underline{r}\times\underline{u}^{(1)}dS$$

$$+\nu\left\{\begin{array}{l}\dfrac{\partial}{\partial t}\displaystyle\int_V \underline{r}\times(\rho^{(2)}\underline{U})dV \\ +\displaystyle\int_S \underline{r}\times\{\underline{U}\cdot\hat{n}(\rho^{(1)}\underline{u}^{(1)}+\underline{u}^{(2)})+\underline{U}[\rho^{(1)}(\underline{u}^{(1)}\cdot\hat{n})+(\underline{u}^{(2)}\cdot\hat{n})]\}dS\end{array}\right.$$

$$+ O(\nu^2)\ . \qquad (6.9)$$

Examining the axial component of (6.9), the axial moment of all externally applied forces is

$$M_z^{(2)} = \frac{\partial}{\partial t}\int_V r(\rho^{(1)}v^{(1)}+v^{(2)})dV + \int_S rv^{(1)}(\underline{u}^{(1)}\cdot\hat{n})dS$$

$$+\nu\int_S (\underline{U}\cdot\hat{n})r(\rho^{(1)}v^{(1)}+v^{(2)})dS + O(\nu^2) \qquad (6.10)$$

where

$$\underline{u}^{(1)} = u^{(1)}\hat{e}_r + v^{(1)}\hat{e}_\theta + w^{(1)}\hat{e}_z$$

$$\underline{M}^{(1)} = M_r^{(1)}\hat{e}_r + M_\theta^{(1)}\hat{e}_\theta + M_z^{(1)}\hat{e}_z$$

and so on. Note that, for tangential modes of oscillation, $w^{(1)} \equiv 0$ and

$$\underline{u}^{(1)}\cdot\hat{n} = \left\{\begin{array}{lll} 0 & \text{at nozzle entrance plane} & (z = L) \\ 0 & \text{at the head-end} & (z = 0) \\ \Re[-\nu A p^{(1)} e^{iKt}] & \text{at the wall} & (r = 1)\end{array}\right.$$

Also,

$$\underline{U}\cdot\hat{n} = \begin{cases} 2L/R & \text{at the nozzle entrance plane} \\ 0 & \text{at the head-end} \\ -1 & \text{at the wall} \end{cases}$$

Thus,

$$M_z^{(2)} = \frac{L}{R}\frac{\partial}{\partial t}\int_0^{2\pi} d\theta \int_0^1 r^2(\rho^{(1)}v^{(1)}+v^{(2)})dr +$$

$$+\nu\left\{\begin{array}{l} -\frac{L}{R}\int_0^{2\pi}(v^{(1)}A^{(r)}\rho^{(1)})_{r=1}d\theta - \frac{L}{R}\int_0^{2\pi}(\rho^{(1)}v^{(1)}+v^{(2)})_{r=1}d\theta \\ +2\frac{L}{R}\int_0^{2\pi}d\theta\int_0^1 r^2(\rho^{(1)}v^{(1)}+v^{(2)})dr \end{array}\right.$$

$$+ O(\nu^2) .$$

We are most interested in the non-oscillatory part of (6. 10). Evaluating the integrals for this case, keeping in mind that the total axial angular momentum within the chamber at any instant is

$$H^{(2)} = \int_V r(\rho^{(1)}v^{(1)}, v^{(2)})dV \qquad (6.12)$$

we find, for the steady part,

$$\left\langle M_z^{(2)}\right\rangle = \pm\left(\frac{L\pi}{k_{10}R}\right)\nu J_1^2(k_{10})\left[(1+A^{(r)})+\left(\frac{k_{10}^2-1}{k_{10}^2}\right)(\Lambda^{(11)}-1)\right]$$

$$+\left\langle\frac{\partial}{\partial t}\int_V rv^{(2)}dV + \nu\int_S(\underline{U}\cdot\hat{n})rv^{(2)}dS\right\rangle \qquad (6.13)$$

where evaluation has been carried out for the first traveling (0, 1, 0) mode. Evaluation of the terms involving the second-order circumferential velocity will be carried out later. Assume for the moment

that $v^{(2)}$ is zero. (In actuality, the two integral terms will cancel exactly, since they represent the integral form of the momentum equation which must be satisfied by $v^{(2)}$.) Note that the total steady moment on the gas $\langle M_z^{(2)} \rangle$ is zero for a unique value of the growth rate constant. Thus, $\langle M_z^{(2)} \rangle = 0$ if

$$\Lambda^{(11)} = -\frac{1}{(k_{10}^2 - 1)} [1 + k_{10}^2 A^{(r)}] \quad . \tag{6.14}$$

Under the conditions we have proposed, this result must be interpreted as follows: angular momentum is carried into the system from the burning surface by the mean flow at a rate which balances the loss of angular momentum from the system through the nozzle and the gain due to amplification of the waves. No moments act on the system, yet the magnitude of the angular momentum increases (as do the losses in the system) at a rate proportional to

$$e^{-2\nu\Lambda^{(11)}t}$$

where $\Lambda^{(11)}$ is that value given by (6.14). It will perhaps not be surprising to discover later that $\Lambda^{(11)}$ as computed from equation (5.36) is precisely that given by (6.14).

We can proceed no further with the inspection of the steady second-order momentum balance as expressed by (6.13) without computing $\langle \underline{M} \rangle$ and $\underline{u}^{(2)}$; further comments will be forthcoming when these things have been accomplished. The first task will be to examine the body moments which result from motion of the combustion chamber. The question of stability will then be investigated. Corrections to the acoustic solutions of first-order in the wall Mach

number will then be computed. These will be used in determining the characteristics of the second-order flow field insofar as this is possible within the framework of the inviscid model.

7. Effects Due to Motion of the Chamber

It is well known that angular momentum can be generated in a confined fluid by a properly programmed motion of the container. This is in the spirit of the "cocktail glass vortex" which is probably observed even more frequently than the famous "bathtub vortex", and was the subject of a delightful paper by Crow (23). The same problem has also arisen in connection with sloshing of liquid propellants in cylindrical fuel tanks, and there has been considerable confusion in the literature concerning these effects (cf. references 24 and 25).

The connection between cocktail glasses and rocket motors may not be completely clear at the outset. The analogy is this: the combustion chamber moves in response to the momentum effects and integrated pressure forces at its inner boundary. The motions thus produced feed back into the gas motion via the body-force terms in the equations of motion. A related problem which is highly interesting is the effect of oscillatory elastic deformation of the propellant itself, but incorporation of such complications in the present model must be postponed for later consideration.*

---

* Some work, which is not directly applicable to the problem as set forth here, has been reported in references (26) and (27), and deals with some of the consequences of a flexible propellant grain.

It was shown in a previous section that the non-homogeneous terms of order ν in the equations governing the motion of the combustion gases (equations (5. 11) and (5. 13)) contain terms proportional to the body force $\underline{\mathfrak{F}}$. Therefore, before higher-order approximations can be carried out, these terms must be evaluated. This can be accomplished by use of the first-order solutions found already.

The body force $\underline{\mathfrak{F}}$ appears in the equations as a result of writing the equations of motion of the gas in terms of coordinates which move with the rocket motor and its attachments. As mentioned before, we are concerned with that part of the motion of the rocket in a plane perpendicular to the axis of symmetry; axial effects are therefore neglected. Motions of this type result from the forces at the combustion chamber wall, and in accordance with the inviscid approximations employed in the present section, we take these forces to be normal to the wall. A consequence of this assumption is the considerable simplification that the moving coordinates accelerate with respect to inertial space without rotation. As before, the body force is

$$\underline{\mathfrak{F}} = - \rho \frac{d^2 \underline{s}}{dt^2} \tag{7. 1}$$

where $d^2\underline{s}/dt^2$ represents the acceleration of the moving coordinates relative to the inertial ones, and is governed by the differential equation

$$\frac{d^2 \underline{s}}{dt^2} = \lambda \underline{Q}(\underline{s}, \frac{d\underline{s}}{dt}, t)$$

where $\lambda = m^{-1}$ and the vector function $\underline{Q}$ depends on the mechanical

constraints between the motor and its mountings. The two limiting cases are: 1) free motion in which $\underline{Q}$ represents the force of interaction between the combustion gases and the chamber walls; and 2) fixed case in which the system is rigidly mounted, the propellant is regarded as rigid, and therefore $d^2\underline{s}/dt^2 \equiv 0$. As implied above, intermediate cases are of potential importance, since there is evidence that the motions of the propellant grain in an elastic sense may also play a role in the instability problem. Instead of attempting to analyze this very complicated situation in which elastic or plastic wave motions in the propellant must be matched to the gas fluctuations on one boundary and to a thin elastic shell (the motor case) on another with additional complicated mechanical constraints, a greatly simplified model is considered here. The propellant grain and the other solid components of the rocket motor and its attachments are taken as rigid bodies, but the mounting in which the system operates (simulation of static test situation) is represented by a set of idealized springs and dampers.

Wall Forces. The combustion chamber is assumed to move in response to the interaction forces at the gas - solid interface. It is also assumed that the surface force $d\underline{F}$ at any point on the interface is normal to the surface and consists of: 1) pressure forces and 2) momentum forces due to expulsion of mass resulting from combustion. $d\underline{F}$ is easily evaluated by application of the momentum theorem to a small volume element at the burning surface. Figure 8 shows the element and its free-body diagram.

The momentum theorem states

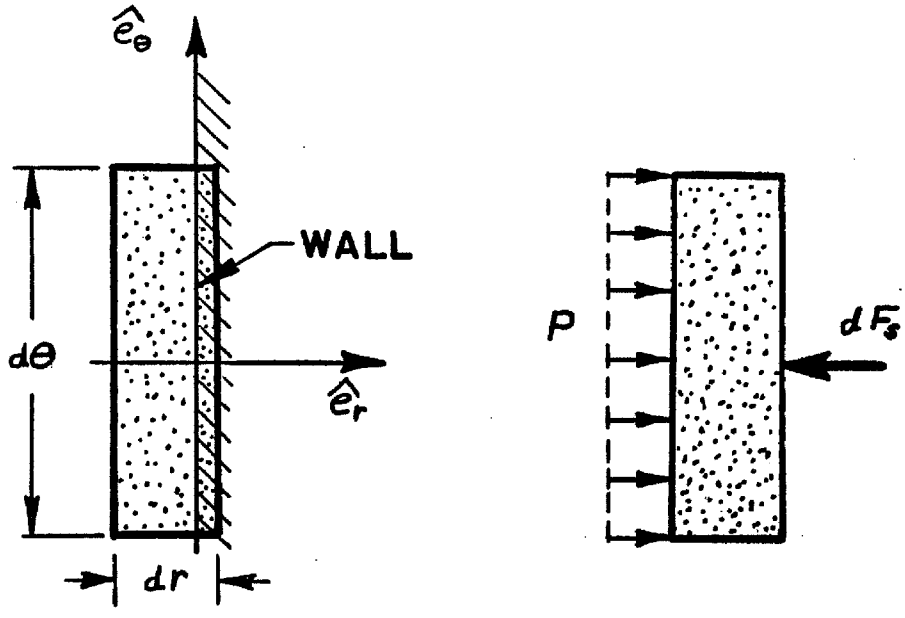

Fig. 8. Volume Element at Burning Surface.

$$\underline{dF}_{total} = \frac{\partial}{\partial t}\int_V (\underline{u}\rho)dV + \int_S (\underline{u}\rho)\underline{u}\cdot\hat{n}dS$$

where $\underline{dF}_{total}$ represents the vector sum of all forces acting on the element. Thus,

$$\underline{dF}_{total} = P(d\theta dr)\hat{e}_r + \underline{dF}_s$$

where $\underline{dF}_s$ is the reaction force on the surface. The volume element is defined such that

$$dr \ll 1\, d\theta$$

and

$$dz \sim 1\, d\theta$$

Also, the pressure, density, and velocity variations within the element may be taken as negligible due to its small size; thus,

$$P\hat{e}_r + d\underline{F}_s = \frac{\partial}{\partial t}[\underline{u}\rho]_{wall}dr + [(\underline{u}\rho)(\underline{u}\cdot\hat{n})]_{wall}$$

where momentum flux through the sides of the element has also been neglected. Taking $d\underline{F}_s$ to be the force per unit area, and neglecting the volume integral term which may be regarded as of differential order, we may write

$$d\underline{F}_s = -P\hat{e}_r + [(\underline{u}\rho)(\underline{u}\cdot\hat{n})]_{wall} .$$

Expanding P, ρ, and $\underline{u}$ as before, and noting that $\underline{U} = -\hat{e}_r$ and $\underline{u} = -\nu p^{(1)}Ae^{iKt}\hat{e}_r$ on the boundary, the force per unit surface area acting on the wall is

$$d\underline{F} = -d\underline{F}_s = \{1 + \epsilon[\gamma p^{(1)}e^{iKt} + O(\nu^2)] + O(\epsilon^2)\}_{r=1} .$$

The momentum force due to mass efflux is seen to be of order ν^2, and is thus a negligible contribution to the driving force.

Integrating $d\underline{F}$ over the inner surface of the combustion chamber results in the driving force vector

$$\underline{F} = \epsilon\left(\frac{\gamma L}{R}\right)\int_0^{2\pi} \Re[p^{(1)}e^{iKt}]_{r=1}\cdot[\hat{i}\cos\theta + \hat{j}\sin\theta]\,d\theta \qquad (7.1)$$

where i and j are unit vectors in the x- and y-directions, respectively. Adopting notation compatible with that introduced in preceding sections,

$$\underline{F} = \epsilon\{\underline{F}^{(10)} + \nu\underline{F}^{(11)} + \ldots\}$$

where

$$\underline{F}^{(10)} = \left(\frac{\gamma L}{R}\right)\int_0^{2\pi} \Re[p^{(10)}e^{iKt}]_{r=1}\cdot[\hat{i}\cos\theta + \hat{j}\sin\theta]\,d\theta \qquad (7.2)$$

and so on. The last expression is readily evaluated for transverse modes, and the result is zero for $m \neq 1$; thus, for traveling waves*

$$\underline{F}^{(10)} = \begin{cases} \left(\frac{\gamma \pi L}{R}\right) J_1(k_{10}) e^{-\nu \Lambda^{(1)} t} [\hat{i} \cos(k_{10} t) \mp \hat{j} \sin(k_{10} t)] & m = 1 \\ 0 & m \neq 1 \end{cases} \tag{7.3}$$

Therefore, no motion of the chamber (taken as a rigid body) results unless the first transverse mode ($m = 1$) is present.

Motion of the Combustion Chamber. Using equation (7.3), the motion of the rocket can be computed to first order in ϵ and zeroth order in ν. From this result, the body force on the gas can be established to the same level of approximation. Each of the representative cases discussed above is considered separately.

Case 1 - Freely Moving Chamber.

In this case, $\underline{Q} = \underline{F}$, and the acceleration is simply

$$\frac{d^2 \underline{s}}{dt^2} = \lambda \underline{F} . \tag{7.4}$$

Thus, for the first traveling tangential mode, the axis of the combustion chamber orbits the inertial axis system as depicted in Figure 9. The shaded areas in the drawing depict the high density regions of the acoustic wave as the nodes traverse the chamber wall. The Cartesian components of velocity and displacement of the chamber axis are

---

* Wall forces due to a standing wave pattern are governed by the same expression, with one or the other of the components deleted depending on the orientation of the pressure nodes. Motion of the chamber in this case takes place in the direction of the line of nodes.

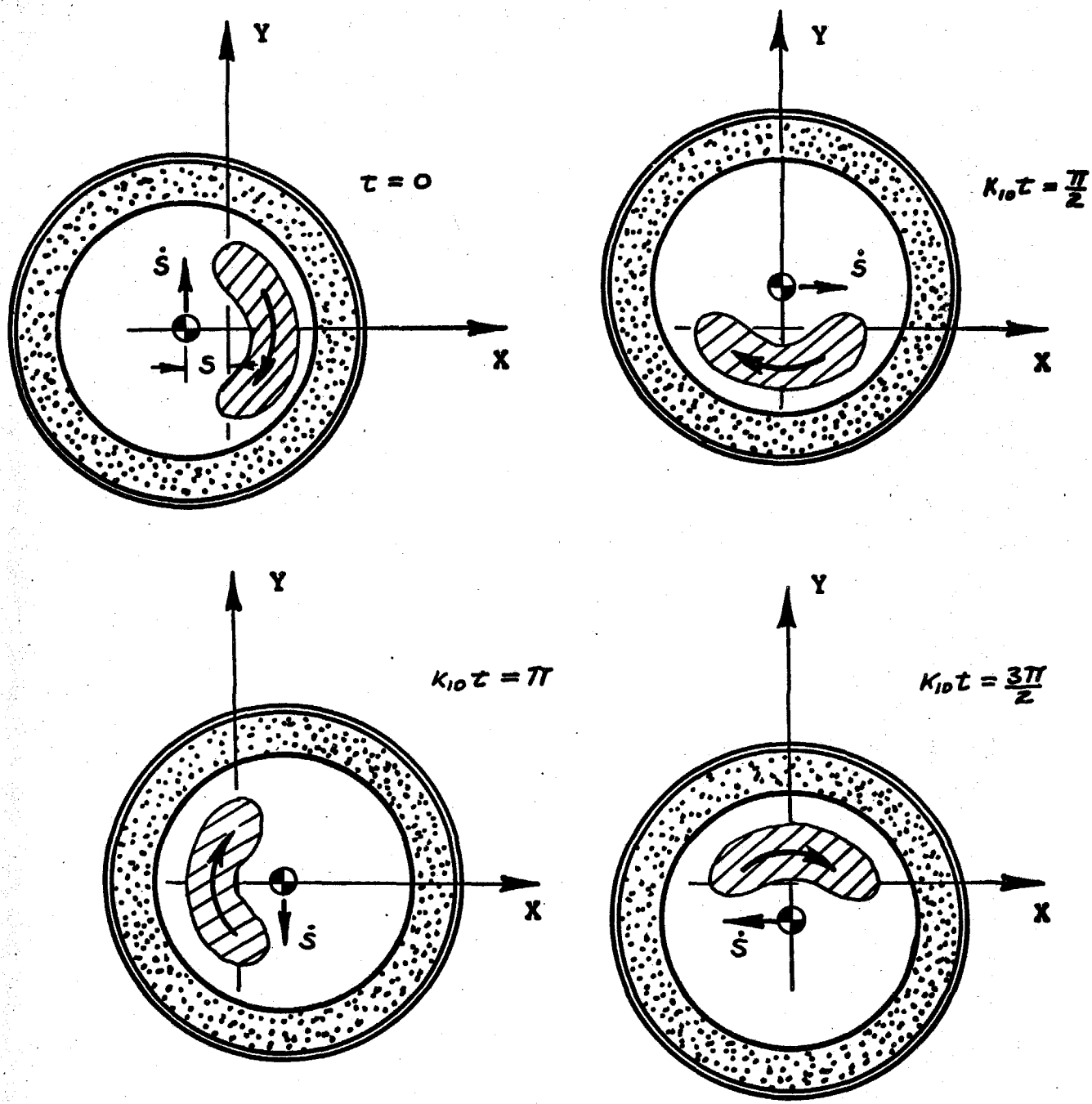

Fig. 9. Motion of Combustion Chamber in Response to Clockwise Traveling Wave.

$$\frac{d\underline{s}}{dt} = \lambda\varepsilon\left(\frac{\gamma\pi L}{R}\right)\frac{J_1(k_{10})}{k_{10}}e^{-\nu\Lambda^{(11)}t}[\hat{i}\sin(k_{10}t)\pm\hat{j}\cos(k_{10}t)] + O(\nu)$$

$$\underline{s} = -\lambda\varepsilon\left(\frac{\gamma\pi L}{R}\right)\frac{J_1(k_{10})}{k_{10}^2}e^{-\nu\Lambda^{(11)}t}[\hat{i}\cos(k_{10}t)\mp\hat{j}\sin(k_{10}t)] + O(\nu)$$

and the displacement amplitude increases at the same rate as the acoustic wave amplitude, as one would expect.

Using (7.4), the body force on the gas corresponding to free motion of the combustion chamber can be established. Expanding as usual,

$$\begin{aligned}\underline{\mathfrak{F}} &= \varepsilon\underline{\mathfrak{F}}^{(1)} + \varepsilon\underline{\mathfrak{F}}^{(2)} + \dots \\ &= \varepsilon[\underline{\mathfrak{F}}^{(10)} + \nu\underline{\mathfrak{F}}^{(11)} + \dots] + \varepsilon^2[\underline{\mathfrak{F}}^{(20)} + \nu\underline{\mathfrak{F}}^{(21)} + \dots] \\ &= -(1 + \varepsilon\rho^{(1)} + \dots)\lambda\varepsilon(\underline{F}^{(10)} + \nu\underline{F}^{(11)})\end{aligned}$$

and noting that

$$\rho^{(1)} = p^{(1)}e^{iKt} = e^{iKt}[p^{(10)} + \nu p^{(11)} + \dots] ,$$

the body force to various levels of approximation is given by

$$\begin{aligned}\underline{\mathfrak{F}}^{(1)} &= -\lambda[\underline{F}^{(10)} + \nu\underline{F}^{(11)} + \dots] \\ \underline{\mathfrak{F}}^{(2)} &= -\lambda[p^{(10)}\underline{F}^{(10)} + \nu(p^{(10)}\underline{F}^{(11)} + p^{(11)}\underline{F}^{(10)}) + \dots]e^{iKt}\end{aligned} \qquad (7.5)$$

and so on. Writing $\underline{F}$ in complex form, and putting $\underline{\mathfrak{F}}^{(1)}$ in notation compatible with the equations of the last section,

$$\underline{\mathfrak{F}}^{(1)} = \lambda\underline{f}^{(1)}e^{iKt}$$

where

$$\underline{f}^{(1)} = \underline{f}^{(10)} + \nu\underline{f}^{(11)} + \dots \ .$$

Evaluating for the traveling tangential mode, and expressing the result in polar coordinates:

$$\underline{f}^{(10)} = -\left(\frac{\gamma\pi L}{R}\right)J_1(k_{10})e^{\pm i\theta}[\hat{e}_r \pm i\hat{e}_\theta] \ . \qquad (7.6)$$

and so on to higher order in ν.

The term $\underline{\mathfrak{F}}^{(2)}$ will be required later when second-order solutions of the gas motion are considered. It is appropriate at this point to note a few characteristics of this forcing term. $\underline{\mathfrak{F}}^{(2)}$ is readily evaluated to zeroth order in ν using the solution already obtained. Thus

$$\underline{\mathfrak{F}}^{(20)} = -\lambda[p^{(10)}e^{iKt}]\underline{F}^{(10)}$$

which displays several characteristics of the second-order terms which will occur frequently in later considerations. In particular, it is necessary to take the real parts of physical quantities which are multiplied together as for $p^{(10)}$ and $\underline{F}^{(10)}$ in the above expression. Thus, for the (0, 1, 0) mode,

$$\mathfrak{F}^{(20)} = -\lambda\Re\left[J_1(k_{10}r)e^{-\nu\Lambda^{(11)}t}e^{i(k_{10}t\pm\theta)}\right]\underline{F}^{(10)}$$

where $\underline{F}^{(10)}$ is given in polar coordinates by

$$\underline{F}^{(10)} = \left(\frac{\gamma\pi L}{R}\right)J_1(k_{10})\,e^{-\nu\Lambda^{(10)}t}[\hat{e}_r\cos(k_{10}t\pm\theta)\mp\hat{e}_\theta\sin(k_{10}\pm\theta)]\,. \tag{7.7}$$

Thus,

$$\underline{\mathfrak{F}}^{(20)} = -\lambda\left(\frac{\gamma\pi L}{R}\right)J_1(k_{10})J_1(k_{10}r)e^{-2\nu\Lambda^{(11)}t}\,.$$

$$\cdot\left\{\begin{array}{l}\hat{e}_r\,[1+\cos 2(k_{10}t\pm\theta)]\\ \hat{e}_\theta\,[\sin 2(k_{10}t\pm\theta)]\end{array}\right\}\,. \tag{7.8}$$

Note the appearance of a steady radial force component on the gas, the forcing in the tangential direction remaining harmonic to this order.

Case 2 - Flexibly Mounted Chamber.

For this case, the function $\underline{Q}$ is given by

$$\underline{Q} = \hat{i}\left[F_x - c_x \frac{ds_x}{dt} - \varkappa_x s_x\right] + \hat{j}\left[F_y - c_y \frac{ds_y}{dt} - \varkappa_y s_y\right]$$

where subscripts x and y denote quantities corresponding to the x- and y-directions, respectively. Thus, c_x and $\varkappa_x$ are the effective damping and spring constants for motion in the x-direction. The motion is analyzed in two dimensions for simplicity, but in actuality three-dimensional motions would be expected if the flexibility of the mounting system were to vary longitudinally. It is reasonable to expect that the important elements of the situation can be gleaned from the two-dimensional model. As a further simplification, it is convenient to take

$$c_x = c_y = c$$

and

$$\varkappa_x = \varkappa_y = \varkappa$$

where, again, the important features of the motion can be extracted in spite of the idealizations.

The displacement of the combustion chamber is easily computed, and the result for the first traveling tangential mode of acoustic oscillation is, neglecting higher order terms,

$$\underline{s} = \frac{\epsilon\lambda}{I}\left(\frac{\gamma\pi L}{R}\right) J_1(k_{10}) e^{-\nu\Lambda^{(11)}t}\left[\hat{i}\cos(k_{10}t-\alpha) \mp \hat{j}\sin(k_{10}t-\alpha)\right] ,$$

where I is the impedance

$$I = \lambda\varkappa\left[\left(1 - \frac{k_{10}^2}{\lambda\varkappa}\right)^2 + k_{10}^2\left(\frac{c}{\varkappa}\right)^2\right]^{\frac{1}{2}}$$

and α is the phase angle

$$\alpha = \tan^{-1}\left[\frac{\lambda k_{10} c}{(\lambda\kappa - k_{10}^2)}\right]$$

which measures the lag of the combustion chamber response to the traveling pressure disturbance. The acceleration is readily determined to be

$$\frac{d^2\underline{s}}{dt^2} = -\frac{\varepsilon\lambda}{I}\left(\frac{\gamma\pi L}{R}\right)k_{10}^2 J_1(k_{10})e^{-\nu\Lambda^{(11)}t}[\hat{i}\cos(k_{10}t-\alpha)\mp\hat{j}\sin(k_{10}t-\alpha)] \tag{7.9}$$

in Cartesian coordinates.

The body force on the gas can now be found. Using the usual notation, the result is

$$\underline{\mathfrak{F}}^{(1)} = \lambda\underline{f}^{(1)}e^{ikt} = \lambda[\underline{f}^{(10)} + \nu\underline{f}^{(11)} + \dots]e^{ikt}$$

where

$$\underline{f}^{(10)} = \frac{1}{I}\left(\frac{\gamma\pi L}{R}\right)k_{10}^2 J_1(k_{10})e^{\pm i(\theta\mp\alpha)}[\hat{e}_r \pm i\hat{e}_\theta] \tag{7.10}$$

and so on. The order ε^2 body force is (to zeroth order in ν)

$$\underline{\mathfrak{F}}^{(20)} = \frac{\lambda}{I}\left(\frac{\gamma\pi L}{2R}\right)k_{10}^2 J_1(k_{10})J_1(k_{10}r)e^{-2\nu\Lambda^{(11)}t}\cdot$$

$$\cdot\left\{\begin{array}{l}\hat{e}_r[\cos\alpha\left(1+\cos 2(k_{10}t\pm\theta)\right) + \sin\alpha\sin 2(k_{10}t\pm\theta)] \\ \pm\hat{e}_\theta[-\cos\alpha\sin 2(k_{10}t\pm\theta) + \sin\alpha\left(1+\cos 2(k_{10}t\pm\theta)\right)]\end{array}\right\}. \tag{7.11}$$

Thus, when the rocket is constrained by a flexible supporting system, there is, in addition to a steady radial force as in the free moving case, a steady tangential body force:

$$\left\langle \mathfrak{F}_\theta^{(20)} \right\rangle = \pm\frac{\lambda}{I}\left(\frac{\gamma\pi L}{2R}\right)k_{10}^2 J_1(k_{10})J_1(k_{10}r)e^{-2\nu\Lambda^{(11)}t}\sin\alpha \tag{7.12}$$

which acts in a direction opposite to the traveling pressure disturbance.

The role of the phase angle α is clearly seen in equation (7.11). For a stiffly mounted rocket (say, in a static test stand) with a natural frequency which is large compared to the frequency of gas oscillations,

$$\alpha \to 0$$

and no tangential force would appear. Similarly, for a motor mounted in a very flexible system,

$$\alpha \to \pi$$

and again, no important tangential force would be present. If, however, the natural frequency of the mounting system is rather close to that of the gas oscillations, then

$$\alpha \to \pi/2$$

and I^{-1} can become large. Thus, the most pronounced effect on the gas due to chamber motion should be experienced under these conditions.

Case 3 -

For the case of a rigidly mounted rocket motor, no motion relative to the inertial coordinates obtains. Thus, the body force term vanishes from the equations of motion and no further comment is necessary.

8. Stability of Traveling Waves

We are now in a position to prove that the traveling tangential acoustic modes in a cylindrical, internal burning solid propellant charge can be driven by combustion and mean-flow interactions. The influence of the chamber motions discussed in the last section will be included. We have already found an expression for the growth rate

constant Λ, and have shown that for conditions near the stability boundary (that is, for very weak disturbances) the amplification rate is of first order in the wall Mach number:

$$\Lambda = \nu\Lambda^{(11)} = \frac{\nu}{2K_N E_N^2}\,\vartheta\left[\int_V g^{(10)}p^{(10)*}dV + \int_S h^{(10)}p^{(10)*}dS\right] . \quad (8.1)$$

The integral terms are now readily evaluated:

$$I_1 \equiv \int_V g^{(10)}p^{(10)*}dV = \int_V iK_N(p^{(10)})^*\,\underline{U}\cdot\nabla p^{(10)}dV$$

$$-\int_V \frac{i}{K_N}(p^{(10)})^*\nabla^2(\underline{U}\cdot\nabla p^{(10)})dV + \left(\frac{\lambda}{\nu}\right)\int_V (p^{(10)})^*\nabla\cdot\underline{f}^{(10)}dV \quad . \quad (8.2)$$

Using Green's theorem, the second term can be expanded to the form

$$\int_V \frac{i}{K_N}(p^{(10)})^*\nabla^2(\underline{U}\cdot\nabla p^{(10)})dV = \int_V \frac{i}{K_N}\,\underline{U}\cdot\nabla p^{(10)}\nabla^2(p^{(10)})^*dV$$

$$+\int_S \frac{i}{K_N}\left\{(p^{(10)})^*\nabla(\underline{U}\cdot\nabla p^{(10)}) - (\underline{U}\cdot\nabla p^{(10)})\nabla(p^{(10)})^*\right\}\cdot\hat{n}dS \quad .$$

Now, using (5.29):

$$\nabla^2 p^{(10)} = -K_N^2 p^{(10)}$$

and

$$(\nabla p^{(10)})\cdot\hat{n} = 0 \qquad \text{at} \qquad r = 1 \quad .$$

Therefore,

$$I_1 = 2iK_N\int_V (p^{(10)})^*\,\underline{U}\cdot\nabla p^{(10)}dV - \frac{i}{K_N}\int_S[(p^{(10)})^*\nabla(\underline{U}\cdot\nabla p^{(10)})]\cdot\hat{n}dS$$

$$+\left(\frac{\lambda}{\nu}\right)\int_V (p^{(10)})^*\nabla\cdot\underline{f}^{(10)}dV \quad . \quad (8.3)$$

Manipulating the surface integral

$$I_2 \equiv \int_S h^{(10)}(p^{(10)})^* dS$$

in a similar fashion,

$$I_2 = \int_S -iK_N A p^{(10)}(p^{(10)})^* dS + \int_S \frac{i}{K_N} \hat{n}\cdot\nabla(\underline{U}\cdot\nabla p^{(10)})(p^{(10)})^* dS$$

$$- \left(\frac{\lambda}{\nu}\right)\int_S \underline{f}^{(10)}(p^{(10)})^* \cdot \hat{n}\, dS \quad . \tag{8.4}$$

Gathering the results and again using Green's theorem:

$$\Lambda = \frac{\nu}{E_N^2}\, \mathcal{J} \begin{cases} i\int_V (p^{(10)})^* \underline{U}\cdot\nabla p^{(10)} dV \\ -i\,(A^{(r)} + iA^{(i)})\int_S \frac{p^{(10)}p^{(10)*}}{2}\, dS \\ -\left(\frac{\lambda}{\nu}\right)\frac{1}{2K_N}\int_V \underline{f}^{(10)}\cdot\nabla p^{(10)*} dV \end{cases} \tag{8.5}$$

Culick has discussed the physical significance of the integral terms (16). The first term represents the average convection of energy into the system by the mean flow, since

$$\mathcal{J}\left\{i\int_V (p^{(10)})^* \underline{U}\cdot\nabla p^{(10)} dV\right\} = \int_V \underline{U}\cdot\nabla \frac{(p^{(10)})^*(p^{(10)})}{2}\, dV$$

$$= \int_S \left[\frac{(p^{(10)})^*(p^{(10)})}{2}\right] \underline{U}\cdot\hat{n}\, dS$$

and

$$\left[\frac{(p^{(10)})^*(p^{(10)})}{2}\right]$$

is a measure of the energy per unit volume. The second term

$$\mathcal{I}\left\{-i(A^{(r)}+iA^{(i)})\int_S\left[\frac{(p^{(10)})^*p^{(10)}}{2}\right]dS\right\} = -A^{(r)}\int_S\frac{(p^{(10)})^*p^{(10)}}{2}\,dS$$

represents work input associated with the oscillatory combustion, and the last reflects work done on the system by body forces or other additional forces.

We can now evaluate (8.5) in detail for the first traveling tangential mode. Thus,

$$\Lambda = -\frac{\nu}{(k_{10}^2-1)}\left[1+k_{10}^2A^{(r)}-\left(\frac{\lambda}{\nu}\right)k_{10}\left(\frac{\gamma\pi L}{R}\right)\beta^{(i)}\right] \qquad (8.6)$$

where we have included the effect of the moving combustion chamber, and

$$\beta \equiv \begin{cases} 1 & \text{freely moving motor} \\ -\frac{k_{10}^2}{I}e^{-i\alpha} & \text{flexibly mounted motor} \\ 0 & \text{rigidly mounted motor} \end{cases} \qquad (8.7)$$

Notice that the chamber motion does not affect the growth rate unless the motor is mounted flexibly. The correction is, of course, a stabilizing one, since maintenance of oscillations of the chamber requires that energy be extracted from the combustion gases to replace that dissipated in the damping of the supporting system. This also constitutes a crude model for the effect of visco-elastic motions of the propellant grain on the stability of the waves.

A discussion of the result (8.6) is now in order in the light of the angular momentum discussion. We note first that except for the term of order (λ/ν) the growth rate is identical to that found by Culick for the corresponding standing mode. Thus, neglecting other contributions to Λ, there is no reason, on the basis of stability of the sys-

tem, to expect standing waves to be amplified in preference to traveling ones or vice versa. In a given set of circumstances, it is likely that distortion of the grain shape, erosive burning effects, or the like could be the determining factor in whether traveling vis-á-vis standing waves are driven to high amplitude. Perhaps the most significant result is that except for the chamber-motion correction term, Λ is just that value which we have found would account completely for the steady angular momentum carried by the wave. Inserting (8. 6) into the equation (6. 13) for the steady moment acting on the gas, we find

$$\left\langle M_z^{(2)} \right\rangle = \left\langle \frac{\partial}{\partial t} \int_V r v^{(2)} dV + \nu \int_S (\underline{U} \cdot \hat{n}) r v^{(2)} dS \right\rangle$$

$$\pm \left(\frac{L\pi}{k_{10} R} \right) \frac{\lambda}{k_{10}} \left(\frac{\gamma \pi L}{R} \right) \left(\frac{k_{10}^2}{I} \sin \alpha \right) J_1^2 (k_{10}) \ ,$$

but the latter term is just the moment of the body force $\langle \mathfrak{F}_\theta^{(20)} \rangle$ integrated over the volume of the chamber. Thus, neglecting viscous effects or other body forces arising from external fields for example, the second-order circumferential velocity component must satisfy the angular momentum equation

$$\left\langle \frac{\partial}{\partial t} \int_V r v^{(2)} dV + \nu \int_S (\underline{U} \cdot \hat{n}) r v^{(2)} dS \right\rangle = 0 \qquad (8.8)$$

which is simply the integral form of the equation of motion for the steady second-order circumferential velocity component. This equation will be used later in differential form to find the characteristics of that flow.

For a discussion of the correspondence of the results (8. 6) to

the experimental data of Brownlee and Marble (28) for the standing mode of oscillation, see Culick (16).

It is convenient at this point to determine the corrections to the oscillation frequency; the calculations are similar to those just employed for the stability computations. The order ν frequency correction is, according to (5.36),

$$\Omega^{(11)} = \frac{1}{2K_N E_N^2} \Re \left[\int_V g^{(10)} (p^{(10)})^* \, dV + \int_S h^{(10)} (p^{(10)})^* \, dS \right]$$

$$= \frac{1}{2K_N E_N^2} \Re [I_1 + I_2] \tag{8.9}$$

or, using the previous results,

$$\Omega^{(11)} = \frac{1}{E_N^2} \Re \left\{ \begin{array}{l} i \int_V (p^{(10)})^* \, \underline{U} \cdot \nabla p^{(10)} dV \\ -i(A^{(r)} + iA^{(i)}) \int_S \frac{(p^{(10)})(p^{(10)})^*}{2} \, dS \\ -(\frac{\lambda}{\nu}) \frac{1}{2K_N} \int_V \underline{f}^{(10)} \cdot \nabla p^{(10)^*} dV \end{array} \right. \tag{8.10}$$

Thus, for the (0, 1, 0) mode, the frequency to order ν is:

$$\Omega = k_{10} + \frac{\nu k_{10}}{(k_{10}^2 - 1)} \left[k_{10} A^{(i)} + (\frac{\lambda}{\nu})(\frac{\gamma \pi L}{R}) \beta^{(r)} \right] + O(\nu^2)$$

where $\beta^{(r)}$ is the real part of β as defined in (8.7). The frequency of oscillation is little changed from the acoustic value by the effects of burning or by the freedom of motion of the rocket. This, again, is in accord with the corresponding finding from much experimental work.

9. Corrections to the Acoustic Solutions

The form of the set of terms involving the as yet undetermined second-order velocity $\underline{u}^{(2)}$ in the momentum balance equation (6.13) suggests that it will be necessary to extend the first-order solutions to order ν in order to solve for $\underline{u}^{(2)}$. From equations (5.31) and (5.32) it is evidently possible to write the order ν correction to $p^{(1)}$ in the form

$$p^{(11)} = \sum_{\alpha \neq N} \frac{\psi_\alpha}{E_\alpha^2(K^2-K_\alpha^2)} \left[\int_V g^{(10)}\psi_\alpha^* dV + \int_S h^{(10)}\psi_\alpha^* dS\right] \qquad (9.1)$$

where $g^{(10)}$ and $h^{(10)}$ are given by (5.12) and (5.14) with $p^{(1)}$ and $q^{(1)}$ replaced by the zeroth-order approximations $p^{(10)}$ and $q^{(10)}$. Higher-order corrections can be found in the same way. In general,

$$p^{(1n)} = \sum_{\alpha \neq N} \frac{\psi_\alpha}{E_\alpha^2(K^2-K_\alpha^2)} \left[\int_V g^{(1\,n-1)}\psi_\alpha^* dV + \int_S h^{(1\,n-1)}\psi_\alpha^* dS\right] \qquad (9.2)$$

where n is the order, in ν, of the correction, i.e., $n = 1, 2, 3, \ldots$.

It is a consequence of orthogonality that the integral terms in (9.1) vanish for all values of ℓ and m not equal to the corresponding ones in the three-tuple N. Thus, the triple summation

$$\sum_{\alpha \neq N} \equiv \sum_{\ell \neq \ell'} \sum_{m \neq m'} \sum_{n=n'}$$

is reduced to a single summation

$$\sum_{n \neq n'}$$

where the primes denote the values of ℓ, m, and n corresponding to mode N. Therefore, (9.1) can be written for transverse modes as

$$p^{(11)} = \sum_{n\neq n'} \frac{e^{\pm im'\theta} J_{m'}(k_{m'n}r)}{E^2_{\alpha'}(K_N^2 - K^2_{\alpha'})} [I_1 + I_2] \qquad (9.3)$$

where

$$I_1 = \int_V g^{(10)} e^{\mp m'\theta} J_{m'}(k_{m'n}r)dV \qquad n \neq n'$$

$$I_2 = \int_S h^{(10)} e^{\mp m'\theta} J_{m'}(k_{m'n}r)dS \qquad n = n'$$

and $\alpha' = (0, m', n)$.

From (5.12) and (5.13),

$$\begin{cases} g^{(10)} = iK_N(\underline{U}\cdot\nabla p^{(10)} - \nabla\cdot(\underline{U}\cdot\nabla\underline{q}^{(10)} + \underline{q}^{(10)}\cdot\nabla U) + (\frac{\lambda}{\nu})\nabla\cdot\underline{f}^{(10)} \\ h^{(10)} = \left\{-iK_N A p^{(10)} + \hat{n}\cdot[\underline{U}\cdot\nabla\underline{q}^{(10)} + \underline{q}^{(10)}\cdot\nabla\underline{U} - (\frac{\lambda}{\nu})\underline{f}^{(10)}]\right\}_{r=1} \end{cases} \qquad (9.4)$$

Due to the importance of the mode N = (0, 1, 0) as demonstrated previously, it is appropriate to specialize the detailed calculation of the correction to this mode. Integrals I_1 and I_2 for the first traveling tangential mode are*

$$\begin{cases} I_1 = i(\frac{2\pi L}{R}) J_1(k_{10}) J_1(k_{1n}) \left[\frac{2k_{10}(k_{10}^2 - 1)}{(k_{1n} - k_{10})}\right] \\ I_2 = i(\frac{2\pi L}{R}) J_1(k_{10}) J_1(k_{1n}) \left\{(\frac{k_{10}^2 - 1}{k_{10}}) - k_{10}A - i(\frac{\lambda}{\nu})(\frac{\pi L}{R})\gamma\beta\right\} \end{cases} \qquad (9.5)$$

where the effects of the moving chamber have been included.

Noting that for the (0, 1, n) mode,

$$E^2_{\alpha'} = \frac{L\pi}{R} J_1^2(k_{1n})(\frac{k_{1n}^2 - 1}{k_{1n}^2})$$

---

* The detailed calculations leading to these results are included in the appendix.

(9. 3) can be written in the form

$$p^{(11)} = - J_1(k_{10})e^{\pm i\theta}f(r) \tag{9.6}$$

where

$$f(r) \equiv \sum_{n=1}^{\infty} J_1(k_{1n}r)[c_n^{(r)}+ic_n^{(i)}] \tag{9.7}$$

with

$$\begin{cases} c_n^{(r)} = \dfrac{\varkappa_n}{J_1(k_{1n})}\left[k_{10}A^{(i)}+\dfrac{\lambda}{\nu}\left(\dfrac{\gamma\pi L}{R}\right)\beta\right] \\ \\ c_n^{(i)} = \dfrac{\varkappa_n}{J_1(k_{1n})}\left[\dfrac{2k_{10}(k_{10}^2-1)}{(k_{1n}-k_{10})}+\dfrac{(k_{10}^2-1)}{k_{10}}-k_{10}A^{(r)}\right] \end{cases} \tag{9.8}$$

and

$$\varkappa_n = \frac{2k_{1n}^2}{(k_{1n}^2-1)(k_{1n}^2-k_{10}^2)} \quad .$$

The representation (9. 7) is in the form of a Dini - Bessel series expansion for a function closely resembling in behavior the imaginary part of the modified Bessel function with parameter $\pm\sqrt{i}$, usually referred to as the bei function in the literature.

The order ν velocity corrections are now obtained by substitution of (9. 6) into expression (5. 41). Thus, the amplitude of the correction is, for transverse modes,

$$\underline{q}^{(11)} = \frac{i}{k_{mn}}\left\{\nabla p^{(11)} - \frac{\nabla p^{(10)}}{k_{mn}}[\Omega^{(11)}+i\Lambda^{(11)}] + [\nabla(\underline{U}\cdot\underline{q}^{(10)})-(\tfrac{\lambda}{\nu})\underline{f}^{(10)}]\right\} \tag{9.9}$$

Evaluating this expression for the (0, 1, 0) mode,

$$\underline{q}^{(11)} = \frac{J_1(k_{10})}{k_{10}} e^{\pm i\theta}\left[-i\frac{d}{dr} f(r)\hat{e}_r + \frac{f(r)}{r}\hat{e}_\theta\right]$$

$$+ \frac{\underline{q}^{(10)}}{(k_{10}^2-1)}\left[\frac{i}{k_{10}} - k_{10}A^* - \left(\frac{\lambda}{\nu}\right)\left(\frac{\gamma\pi L}{R}\right)\beta\right]$$

$$+ \frac{e^{\pm i\theta}}{k_{10}^2}\left[\left(\frac{1-r}{r}\right)J_1(k_{10}r)\hat{e}_r \pm i\frac{d}{dr} J_1(k_{10}r)\hat{e}_\theta\right]$$

$$+ \frac{i}{k_{10}} J_1(k_{10})e^{\pm i\theta}\left(\frac{\lambda}{\nu}\right)\left(\frac{\gamma\pi L}{R}\right)\beta(\hat{e}_r \pm i\hat{e}_\theta) \qquad (9.10)$$

where A^* is the complex conjugate of the admittance function

$$A^* = A^{(r)} - iA^{(i)} .$$

Setting

$$\begin{cases} \Re f(r) = f^{(r)} \equiv \sum_{n=1}^{\infty} c_n^{(r)} J_1(k_{1n}r) \\ \Im f(r) = f^{(i)} \equiv \sum_{n=1}^{\infty} c_n^{(i)} J_1(k_{1n}r) \end{cases} \qquad (9.11)$$

the velocity vector correct to first order in ν can be written

$$\underline{u}^{(1)} = \left\{ \begin{array}{l} -\frac{1}{k_{10}} \frac{dJ_1(k_{10}r)}{dr} \sin(k_{10}t \pm \theta) \\ \\ +\nu[A(r)\cos(k_{10}t \pm \theta) + B(r)\sin(k_{10}t \pm \theta)] \end{array} \right\} e^{-\nu\Lambda^{(11)}t}\hat{e}_r$$

$$\mp \left\{ \begin{array}{l} \frac{J_1(k_{10}r)}{k_{10}r} \cos(k_{10}t \pm \theta) \\ \\ +\nu[c(r)\cos(k_{10}t \pm \theta) + D(r)\sin(k_{10}t \pm \theta)] \end{array} \right\} e^{-\nu\Lambda^{(11)}t}\hat{e}_\theta \qquad (9.12)$$

where

$$A(r) = \frac{(1-r)}{k_{10}^2 r} J_1(k_{10}r) + \frac{J_1(k_{10})}{k_{10}} \left(\frac{df^{(i)}}{dr}\right) - \frac{(1 + k_{10}^2 A^{(i)})}{k_{10}^2(k_{10}^2-1)} \frac{dJ_1(k_{10}r)}{dr} + \left(\frac{\lambda}{\nu}\right)\beta^{(i)}\left(\frac{\gamma\pi L}{R}\right)\left[\frac{1}{k_{10}(k_{10}^2-1)} \frac{dJ_1(k_{10}r)}{dr} - \frac{J_1(k_{10})}{k_{10}}\right] \quad (9.13)$$

$$B(r) = \frac{J_1(k_{10})}{k_{10}} \left(\frac{df^{(r)}}{dr}\right) + \frac{A^{(r)}}{(k_{10}^2-1)} \frac{dJ_1(k_{10}r)}{dr} + \left(\frac{\lambda}{\nu}\right)\beta^{(r)}\left(\frac{\gamma\pi L}{R}\right)\left[\frac{1}{k_{10}(k_{10}^2-1)} \frac{dJ_1(k_{10}r)}{dr} - \frac{J_1(k_{10})}{k_{10}}\right] \quad (9.14)$$

$$C(r) = -\frac{J_1(k_{10})}{k_{10}} \left(\frac{f^{(r)}}{r}\right) - \frac{A^{(r)}}{(k_{10}^2-1)} \frac{J_1(k_{10}r)}{r} + \left(\frac{\lambda}{\nu}\right)\beta^{(r)}\left(\frac{\gamma\pi L}{R}\right)\left[\frac{J_1(k_{10})}{k_{10}} - \frac{J_1(k_{10}r)}{k_{10}(k_{10}^2-1)r}\right] \quad (9.15)$$

and

$$D(r) = \frac{J_1(k_{10})}{k_{10}} \left(\frac{f^{(i)}}{r}\right) + \frac{1}{k_{10}^2} \frac{dJ_1(k_{10}r)}{dr} - \frac{(1+k_{10}^2 A^{(i)})}{k_{10}^2(k_{10}^2-1)} \frac{J_1(k_{10}r)}{r} + \left(\frac{\lambda}{\nu}\right)\beta^{(i)}\left(\frac{\gamma\pi L}{R}\right)\left[\frac{J_1(k_{10}r)}{k_{10}(k_{10}^2-1)r} - \frac{J_1(k_{10})}{k_{10}}\right] . \quad (9.16)$$

Equation (9. 12) shows that the effects of mean flow, combustion, and body force due to chamber motion are to produce an order ν correction which is out of phase with the first-order velocity vector.

10. The Second-Order Flow Field

It was implied in the discussion on the angular momentum

question (Section 6) that the second-order (in the amplitude parameter ϵ) corrections might play an important role. We have already demonstrated the existence of a steady moment on the gas due to motion of the chamber as indicated by the steady circumferential body force (7.12):

$$\left\langle \mathfrak{F}_\theta^{(20)} \right\rangle = \pm \frac{\lambda}{I} \left(\frac{\gamma \pi L}{2R}\right) k_{10}^2 J_1(k_{10}) J_1(k_{10} r) e^{-2\nu \Lambda^{(11)} t} \sin\alpha \quad .$$

Thus

$$\left\langle M_z^{(2)} \right\rangle = \pm \frac{\lambda}{I} \left(\frac{\pi L}{R}\right)^2 \gamma \sin\alpha \, J_1^2(k_{10})$$

but, as we have already found, this was balanced exactly by a term in the momentum equation resulting from the effect of chamber motion on the growth constant Λ. Thus, in the absence of other body forces it was concluded in equation (8.8) that

$$\left\langle \frac{\partial}{\partial t} \int_V r v^2 dV + \nu \int_S (\underline{U} \cdot \hat{n}) r v^{(2)} dS \right\rangle = 0 \quad .$$

Let us explore this question in greater detail by reverting to the formal second-order momentum equation (5.6) written in the form:

$$\frac{\partial \underline{u}^{(2)}}{\partial t} + \nu[\nabla(\underline{u}^{(2)} \cdot \underline{U}) - \underline{U} \times (\nabla \times \underline{u}^{(2)}] = \underline{\mathfrak{F}}^{(2)} - \rho^{(1)} \frac{\partial \underline{u}^{(1)}}{\partial t} - \underline{u}^{(1)} \cdot \nabla \underline{u}^{(1)}$$
$$- \nu[\rho^{(1)} \nabla(\underline{u}^{(1)} \cdot \underline{U})] \qquad (10.1)$$

where cognizance has been taken of the irrotationality of $\underline{U}$ and $\underline{u}^{(1)}$ as used here.

In anticipation of steady terms, $\underline{u}^{(2)}$ can be written in the form of a linear combination of oscillatory and non-oscillating components

$$\underline{u}^{(2)} = \tilde{\underline{u}}^{(2)} + \langle \underline{u}^{(2)} \rangle$$

where it is clear from the formulation that $\tilde{\underline{u}}^{(2)}$ will oscillate in time

and angle with argument $2(k_{mn}t \pm n\theta)$, and $\langle \underline{u}^{(2)} \rangle$ must have only exponential time dependence. Thus, one can write

$$\left\langle \underline{u}^{(2)} \right\rangle = [R(\underline{r})\hat{e}_r + \Theta(\underline{r})\hat{e}_\theta + Z(\underline{r})\hat{e}_z]\, e^{-2\Lambda t} \tag{10.2}$$

where R, Θ, Z are functions of position and remain to be determined. The boundary conditions are:

$$\begin{cases} R(1, \theta, z) = 0 \\ Z(r, \theta, 0) = 0 \end{cases} \tag{10.3}$$

and no boundary condition on $\Theta(\underline{r})$ can be specified within the confines of the inviscid theory. All we can say about the second-order flow near the wall is that it is parallel to the wall. A conservation of momentum argument will be used subsequently as a necessary condition on the azimuthal velocity.

The non-homogeneous terms in (10.1) are readily evaluated by inserting the first-order solutions. From the form of (10.1), it can be seen that terms of order ν must be carried through. Fortunately, most of the terms which have been left in series form cancel identically, and we find:

$$\left\langle \rho^{(1)} \frac{\partial v^{(1)}}{\partial t} \right\rangle = \mp \frac{\nu}{2} e^{-2\nu\Lambda^{(11)}t} \left[- \frac{\Lambda^{(11)} J_1^2(k_{10}r)}{k_{10}r} + k_{10} D(r) J_1(k_{10}r) \right.$$
$$\left. - \frac{J_1(k_{10}r)}{r} J_1(k_{10}) f^{(i)} \right]$$
$$+ O(\nu^2)$$
$$= \mp \nu e^{-2\nu\Lambda^{(11)}t} \left[\frac{1}{4k_{10}} \frac{d}{dr} J_1^2(k_{10}r) \right.$$
$$\left. - \beta^{(i)} \left(\frac{\lambda}{\nu}\right) \left(\frac{\gamma\pi L}{2R}\right) J_1(k_{10}) J_1(k_{10}r) \right]$$
$$+ O(\nu^2) \tag{10.4}$$

also,

$$\left\langle \underline{u}^{(1)} \cdot \nabla \underline{u}^{(1)} \right\rangle = \frac{e^{-2\nu\Lambda^{(11)}t}}{2k_{10}^2} \left\{ \begin{array}{l} \dfrac{dJ_1(k_{10}r)}{dr}\left(\dfrac{d^2J_1(k_{10}r)}{dr^2}\right) - \dfrac{J_1^2(k_{10}r)}{r^3} \\ \qquad + \dfrac{J_1(k_{10}r)}{r^2}\dfrac{dJ_1(k_{10}r)}{dr} \\ \nu k_{10}\left[-\dfrac{d^2J_1(k_{10}r)}{dr^2}B(r) - \dfrac{dB}{dr}\dfrac{dJ_1(k_{10}r)}{dr} \right. \\ \qquad + \dfrac{J_1(k_{10}r)}{r}\dfrac{dC}{dr} - \dfrac{J_1(k_{10}r)}{r^2}C(r) \\ \left. \qquad + \dfrac{C(r)}{r}\dfrac{dJ_1(k_{10}r)}{dr} \right] \end{array} \right\} \hat{e}_r$$

$$+ O(\nu^2) \qquad (10.5)$$

and

$$\left\langle \rho^{(1)} \nabla (\underline{u}^{(1)} \cdot \underline{U}) \right\rangle = \pm e^{-2\nu\Lambda^{(11)}t}\left[\frac{1}{4k_{10}}\frac{d}{dr}J_1^2(k_{10}r)\right]\hat{e}_\theta + O(\nu) \ . \qquad (10.6)$$

Focusing attention on the circumferential component, and noting

$$\frac{\partial \underline{u}^{(2)}}{\partial t} = -2\nu\Lambda^{(11)}[R(\underline{r})\hat{e}_r + \Theta(\underline{r})\hat{e}_\theta + Z(\underline{r})\hat{e}_z]\, e^{-2\nu\Lambda^{(11)}t} + O(\nu^2) \ ,$$

we find to order ν:

$$-2\Lambda^{(11)}\Theta(\underline{r}) + \left\{-\Theta(\underline{r}) - r\frac{\partial\Theta}{\partial r} + 2z\frac{\partial\Theta}{\partial z}\right\} = \frac{\left\langle \mathfrak{F}_\theta^{(20)} \right\rangle}{\nu e^{-2\nu\Lambda^{(11)}}}$$

$$\pm \left\{\frac{1}{4k_{10}}\frac{d}{dr}J_1^2(k_{10}r) - \beta^{(i)}\left(\frac{\lambda}{\nu}\right)\left(\frac{\gamma\pi L}{2R}\right)J_1(k_{10})J_1(k_{10}r)\right\}$$

$$\mp \left\{\frac{1}{4k_{10}}\frac{d}{dr}J_1^2(k_{10}r)\right\}$$

Rearranging, and remembering from (8.7) that

$$\beta^{(i)} = \frac{k_{10}^2}{I}\sin\alpha \ ,$$

the governing equation for circumferential second-order velocity is, regardless of the nature of the motion of the chamber,

$$r\frac{\partial\Theta}{\partial r} + (2\Lambda^{(11)}+1)\Theta - 2z\frac{\partial\Theta}{\partial z} = 0 \quad . \tag{10.7}$$

Note that $r\Theta$ is proportional to the axial angular momentum component for a fluid element, and that vorticity of second order may be thought of as being propagated along the mean-flow characteristics (29). Thus, the angular momentum must be constant along streamlines in the absence of a disturbance. Writing (10.7) for flow along a streamline, noting that for the mean flow,

$$U = -r \qquad \text{and} \qquad W = 2z \ ,$$

we have

$$\left(U\frac{\partial}{\partial r} + W\frac{\partial}{\partial z}\right)(r\Theta) = 2\Lambda^{(11)}(r\Theta) \ , \tag{10.8}$$

or

$$V\frac{d}{ds}(r\Theta) = 2\Lambda^{(11)}(r\Theta)$$

where V = velocity along the streamline. Now, in the absence of wave amplification or other disturbances, $r\Theta$ must be constant along a characteristic, since

$$\frac{d}{ds}(r\Theta) = 0 \ .$$

Thus,

$$r\Theta = \text{const.} \ ,$$

or

$$\Theta = \frac{\Gamma}{2\pi r} \tag{10.9}$$

along streamlines for $\Lambda^{(11)} = 0$. In the event that $\Lambda^{(11)}$ is non-zero,

$$\frac{d(r\Theta)}{r\Theta} = \left(\frac{2\Lambda^{(11)}}{V}\right)dS \ .$$

Therefore,

$$\Theta = \frac{\Gamma}{2\pi r} \exp\left[2\Lambda^{(11)} \int_{\psi=\text{const.}}^{r,z} \frac{dS}{V} \right] \qquad (10.10)$$

for $\Lambda^{(11)} \neq 0$. Where the integral is taken from a point on the transversal (in this case, the cylindrical wall of the motor) along a streamline to the point (r, z) in question. We must know the distribution of Θ along the transversal in order to complete the solution, at least to within a constant. A momentum argument will be introduced in the next section for determination of the constant Γ insofar as this is possible in the frictionless case. Later, satisfaction of the no-slip condition in the viscous computations will determine Γ exactly.

For later use, let us determine the form of the solution for the case that Θ is not a function of axial position along the wall. Then we can write

$$U \frac{\partial}{\partial r} (r\Theta) = 2\Lambda^{(11)}(r\Theta)$$

and

$$\Theta = \frac{\Gamma}{2\pi\left(r^{1+2\Lambda^{(11)}}\right)} \qquad (10.11)$$

anywhere in the chamber. Finally,

$$\left\langle v^{(2)} \right\rangle = \frac{\Gamma e^{-2\nu\Lambda^{(11)}t}}{2\pi r^{(1+2\Lambda^{(11)})}} \; . \qquad (10.12)$$

Note that for $\Lambda^{(11)} \equiv 0$, $\langle v^{(2)} \rangle$ has the form of a potential vortex of strength Γ, and that there is no direct dependence on any first-order quantities. It is important to note that no other circumferential secondary flow satisfies the second-order momentum equation.

The axial vorticity is

$$\zeta^{(2)} = \frac{\partial v^{(2)}}{\partial r} + \frac{v^{(2)}}{r} \tag{10.13}$$

Thus the steady part is

$$\left\langle \zeta^{(2)} \right\rangle = -\frac{\Lambda^{(11)} T}{\pi} r^{-2(\Lambda^{(11)}+1)} e^{-2\nu\Lambda^{(11)}t} \tag{10.14}$$

and, when motion is not being amplified, $\Lambda^{(11)} = 0$ and

$$\left\langle \zeta^{(2)} \right\rangle = 0 .$$

That is, the motion is irrotational (assuming, of course, an irrotational mean flow) when the growth rate of the wave motion is zero. When the waves are being amplified, $\Lambda^{(11)} < 0$, and the axial vorticity is given by (10.14). Thus, vorticity is generated at the wall and transported by the mean flow under these conditions. Figure 10 shows the effect of wave amplification on the radial distribution of $\langle v^{(2)} \rangle$.

11. Recapitulation

Before making computations with real fluid effects included, it seems appropriate to summarize what has been learned thus far.

It is not surprising in the light of two decades of experimental evidence to find that the wave motion, at least at low amplitudes, closely resembles the classical acoustic waves in form and frequency. For the same reasons, it is not surprising to find that the often observed traveling transverse (0, 1, 0) mode is subject to amplification in a cylindrically perforated, internally burning, solid propellant charge. The traveling mode is as susceptible to amplification as the corresponding standing mode, and on the basis of the first-order theory there is no way to determine for a given set of circumstances which form is more likely to appear.

The influence of freedom of movement of the combustion

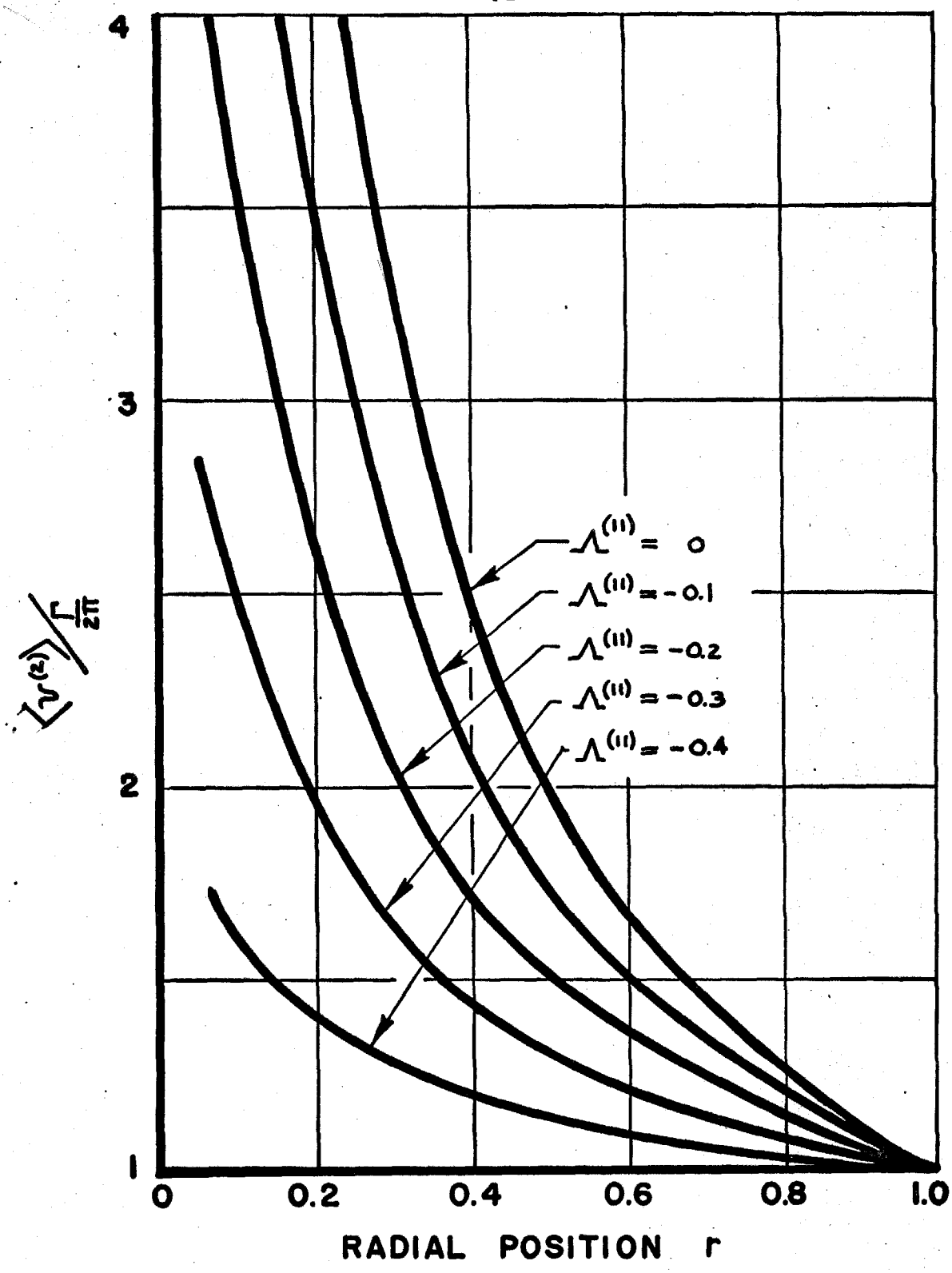

Fig. 10. Effect of Wave Amplification on Steady Second-Order Velocity Distribution.

chamber is a stabilizing one. A steady circumferential moment relative to the moving chamber axis acts on the gas in a direction opposite to the first-order wave motion. This moment only appears when the chamber is mounted flexibly, and the reduction of amplification rate corresponds to dissipation of energy in the supporting system. Similar effects no doubt arise as a result of flexibility of the propellant grain. The frequency of oscillation is slightly decreased in the case of a freely moving rocket or one which is constrained in a flexible mounting. Since the chamber motion effects are proportional to (λ/ν), where λ is the ratio of the mass of gas in the chamber to the overall mass of the rocket and ν is the mean-flow Mach number at the wall, none of the effects mentioned are really important in most cases of interest.

It is easily shown that for most rockets, regardless of size,

$$\lambda \approx 10^{-5}$$

while ν is usually in the range

$$10^{-3} < \nu < 10^{-2} .$$

Thus, $10^{-3} < \lambda/\nu < 10^{-2}$, and the above statement is justified. Only in special circumstances then, say, for a very light motor casing near the end of the motor run, would the influence of the moving system be of importance.

Culick (16) has already shown that the growth rate predicted by the present theory is quite representative of experimental data if damping mechanisms are taken into account. He suggests that in some cases, viscous shear at the head-end is an important contributor to the damping, while energy dissipation due to solid particles in

the flow is the dominant effect in others.

Perhaps the most significant finding is that angular momentum is introduced into the combustion products by the combination of mass influx and combustion at the wall. The second-order steady flow was found to consist of a superposition of the circumferential mass flux illustrated in Figure 7, which is in the direction of the wave motion and a potential vortex with magnitude and sense which cannot be specified without further argument. The reader has perhaps formed the mental image of a control volume surrounding the rocket motor with angular momentum emerging through the surface with the exhaust gases as the above calculations imply. This gives rise to questions regarding moments acting on the motor itself. The inviscid analysis cannot fully answer such questions since no information is given on the viscous stresses at the wall. The situation is analogous to that arising from application of inviscid flow theory to simple wing problems as we have already discussed in detail in the Introduction.

In that application, to secure results which correspond to reality, certain auxiliary conditions must be introduced. The presence of viscosity must be admitted and the Kutta condition must be imposed to place the rear stagnation point in the proper position. The result is a model which predicts, within certain limitations, the correct lift and moment on the airfoil. In the present problem, what sort of an analog to the Kutta condition to apply is not particularly clear.

To simplify the situation, one can <u>define</u> the inviscid approximation to mean that no tangential forces act at the walls of the chamber and therefore no moments act on the motor. Using the mechanism

postulated in the Introduction, we can easily demonstrate that this must be regarded as a definition only. Recalling that the vortex flow in the chamber may be thought of as resulting from a distribution of vortex filaments bound in the chamber walls parallel to the longitudinal axis, there is evidently implied the presence of a distributed force on the wall which is parallel at any point to the wall. The force may be estimated by the familiar Kutta-Joukowsky law if it is assumed that the mean flow originates from sources far from the chamber and flows radially through porous walls, past the bound vortices, and into the region of interest inside the rocket motor. The tangential force on the wall per unit area due to the presence of the bound vorticity has a direction opposite the concentrated axial vortex as illustrated in the sketch of an element of the wall.

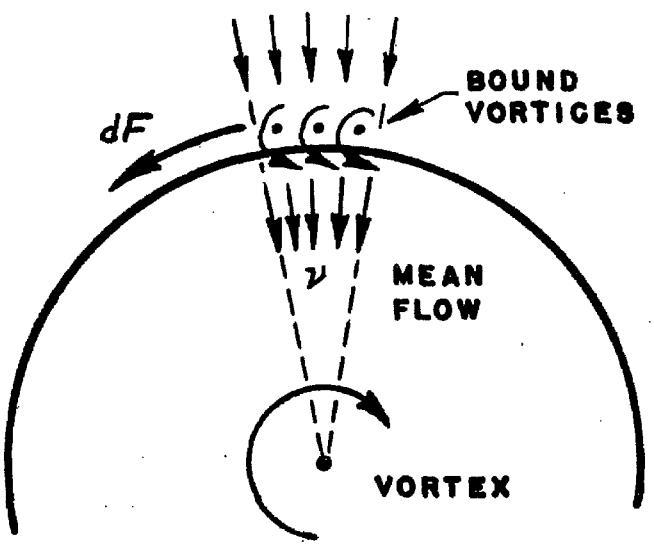

The circulation about a unit area element of the wall is

$$d\Gamma = \frac{\Gamma}{2\pi}$$

and the force per unit area is

$$dF = \frac{\nu\Gamma}{2\pi} \quad .$$

Thus, the roll torque about the axis of symmetry is

$$M_z = \frac{\nu\Gamma L}{R} \tag{11.1}$$

Remembering that Γ is of order ε^2, then the roll moment is of order $\nu\varepsilon^2$. We cannot calculate the actual moment from these results since Γ remains unknown, and forces due to dissipation at the wall are not accounted for. It will, however, be of interest later to compare the result (11.1) to the viscous calculations.

Proceeding with the assumption that the tangential forces are zero for the inviscid case (that is, the moment M from (11.1) is exactly balanced by the viscous forces at the wall), an angular momentum balance can be used to estimate the vortex strength Γ. Choosing a control volume enclosing the propellant grain such that the only efflux is through the nozzle entrance plane, and focusing attention on the steady second-order part of the axial component of the momentum balance, we obtain

$$\langle M_z^{(2)} \rangle = 0 = \frac{\partial}{\partial t} \int_V r \left[\langle \rho^{(1)} v^{(1)} \rangle + \langle v^{(2)} \rangle \right] dV +$$

$$+ \nu \int_S (\underline{U} \cdot \hat{n}) r \left[\langle \rho^{(1)} v^{(1)} \rangle + \langle v^{(2)} \rangle \right] dS \, . \tag{11.2}$$

Effects due to motor motion have been dealt with already, and are therefore neglected. We also assume $v^{(2)}$ to be constant along the

transversal. Inserting the expressions for $v^{(1)}$, $\rho^{(1)}$, and $v^{(2)}$ corresponding to the first traveling tangential mode, we find

$$\nu\left(\frac{4\pi L}{R}\right)(1-\Lambda^{(11)})e^{-2\nu\Lambda^{(11)}t}\int_0^1\left[\frac{\Gamma}{2\pi}\,r^{(1-2\Lambda^{(11)})}\mp\frac{rJ_1^2(k_{10}r)}{2k_{10}}\right]dr = 0$$

which sets the value of Γ required to satisfy the angular momentum balance. Thus,

$$\Gamma = \pm\frac{\int_0^1 rJ_1^2(k_{10}r)dr}{\frac{k_{10}}{\pi}\int_0^1 r^{(1-2\Lambda^{(11)})}dr}$$

in order that $<M_z^{(2)}> = 0$, and

$$\Gamma = \pm\frac{\pi(k_{10}^2-1)}{k_{10}^3}(1-\Lambda^{(11)})J_1^2(k_{10}) \quad . \tag{11.3}$$

Note that the sense of the vortex is opposite that of the wave, as expected, and that the vortex strength increases during amplification of the waves. It is now possible to discuss the features of the net steady second-order mass flow consisting of the mass flux carried by the wave and the superimposed vortex flow. Writing

$$<\mathbb{m}_z^{(2)}> = <\rho^{(1)}v^{(1)}> + <v^{(2)}> \quad , \tag{11.4}$$

we find for the (0, 1, 0) mode,

$$<\mathbb{m}_z^{(2)}> = \mp\frac{e^{-2\nu\Lambda^{(11)}t}}{2k_{10}}\left\{\frac{J_1^2(k_{10}r)}{r} + \right.$$
$$\left. - \frac{(k_{10}^2-1)(1-\Lambda^{(11)})J_1^2(k_{10})}{k_{10}^2\,r^{(1+2\Lambda^{(11)})}}\right\} \tag{11.5}$$

This relation is plotted in Figure 11 for the neutrally stable case

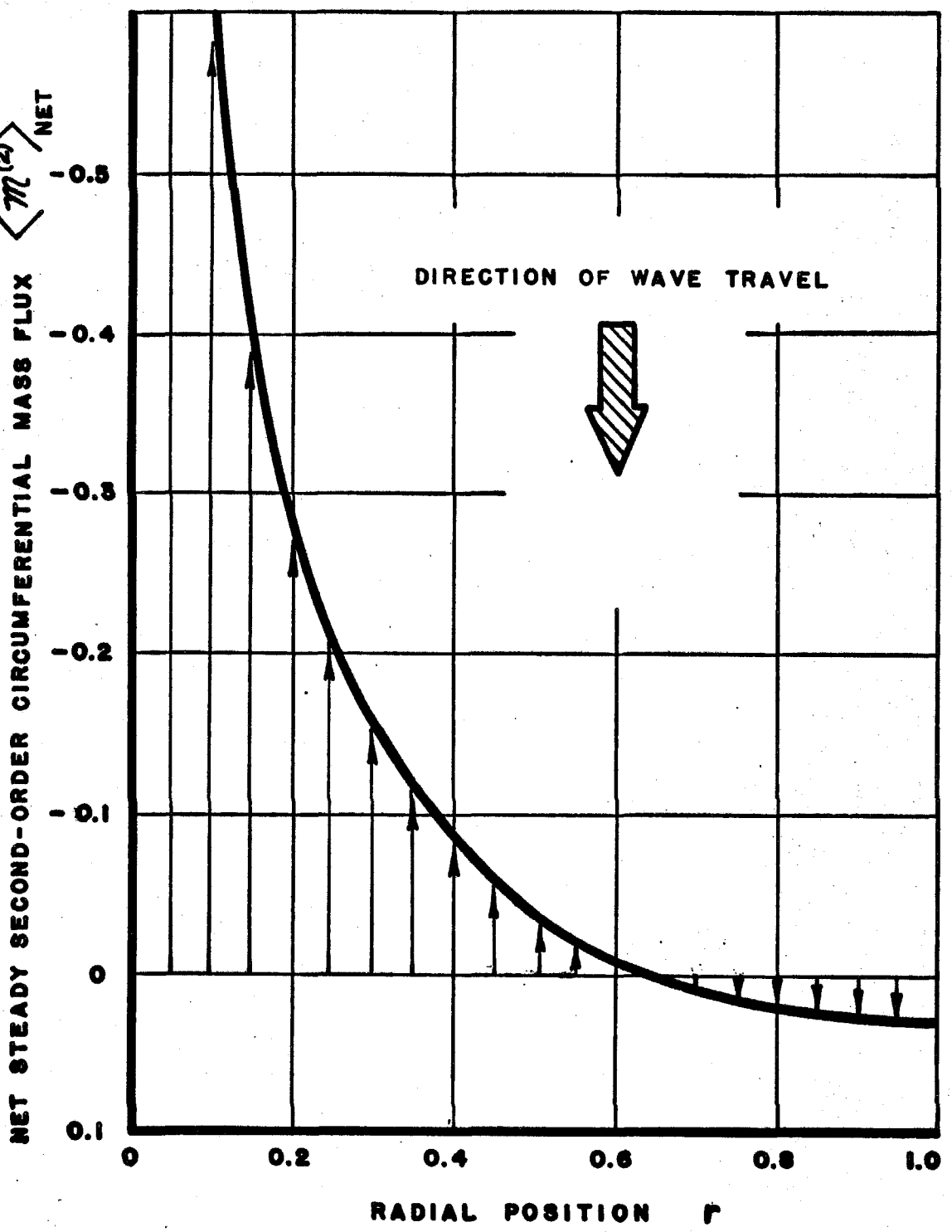

Fig. 11. Net Steady Second-Order Circumferential Momentum Flux (First Traveling Transverse Mode) $\Lambda = 0$.

($\Lambda = 0$). Note that the wave generated mass flux dominates near the wall. The superimposed vortex dominates the flow over most of the region, and in an experimental situation is certain to be the most apparent manifestation of the second-order flow field.

IV. VISCOUS THEORY

The potential importance of a more realistic representation of the fluid, particularly in regard to the tangential boundary condition at the wall and its influence on the second-order vortex flow, was brought out in the last section. Before proceeding, it seems advisable to emphasize again what will and what will not be simulated.

The attempt will be made to represent the following physical aspects of the real gas motion in an unstable rocket: 1) convective effects due to mean flow; 2) response of the combustion layer to pressure fluctuations; 3) variation of viscosity with temperature; 4) heat conduction in the gas, 5) compressibility; and 6) the no-slip boundary condition on the tangential velocity component at the wall.

No attempt will be made to represent the following: 1) a detailed model of the combustion process and flame structure; 2) turbulent flow effects; 3) diffusion of chemical species; 4) liquification or fizz zones at the gas - solid interface; 5) heat transfer to and from the wall; 6) complex geometrical features; 7) nozzle effects; and 8) flexibility of the propellant grain. The effects of combustion are represented by forcing the solutions to match the observed behavior at the outer edge of the combustion layer, and by including the effects of normal mass transport through the combustion layer. Although one can hardly expect the numerical results from such an idealized model to match experimental data, it can surely be hoped that some insight into the nature of the flow might be gained.

It is apparent from the mathematical formulation discussed in Part II that careful consideration must be given to the several simi-

larity parameters involved in planning an attack on the viscous aspects of the flow. Obviously, an important simplification results if the viscous effects can be considered to be confined in some sense to a thin layer in the vicinity of the wall. Let us first inquire as to the condition under which a boundary layer approach might be rewarding and determine if these conditions are met in the situation of interest. The existence of a "boundary layer" solution depends mainly on the magnitude of the parameter δ:

$$\delta = \left[\frac{\mu_o}{\rho_o a_o R}\right]^{\frac{1}{2}} .$$

From equations (2. 2) and (2. 3), it is seen that the boundary layer approximations can be justified only if

$$\delta^2 << 1 .$$

Physical meaning can be attached to this requirement if it is noted that the frequency of oscillation is

$$\omega \sim \frac{a_o}{R} .$$

Thus

$$\delta^2 = \frac{\nu_o}{R^2 \omega} ,$$

where ν_o is the average kinematic viscosity in the chamber. Taking ω^{-1} to be proportional to a characteristic time t_o,

$$\delta^2 = \frac{\nu_o t_o}{R^2} ;$$

δ may be interpreted as a dimensionless boundary layer thickness. Thus,

$$\delta^* = \sqrt{\nu_o t_o} = \sqrt{\nu_o / \omega} .$$

is the actual boundary layer thickness. t_o may be interpreted as the time for vorticity to diffuse through the distance δ^*, and it is clear that boundary layer approximations are justified only if the kinematic viscosity is very small and the frequency of oscillation is high. Note that

$$\frac{\nu_o t_o}{R^2} = \frac{\nu_o/R^2}{\nu_o/(\delta^*)^2} = \frac{\text{rate of diffusion through distance } R}{\text{rate of diffusion through boundary layer}}$$

and that this ratio of diffusion rates must be small [cf. reference (30), pp. 350-356].

Another parameter of importance is

$$\frac{\omega R}{a_o \epsilon} \approx 1/\epsilon$$

where $a_o\epsilon$ is the (dimensional) speed characteristic of the velocity fluctuations, and

$$\frac{\omega R}{a_o \epsilon} = \frac{1/t_o}{a_o\epsilon/R} = \frac{\nu/(\delta^*)^2}{a_o\epsilon/R} =$$

$$= \frac{\text{rate of diffusion through boundary layer}}{\text{rate of convection by speed } a_o\epsilon \text{ through distance } R} .$$

If this parameter is large, that is, if $\epsilon \to 0$, then a series expansion in ϵ is also justified. These ideas have been discussed in full detail by J. T. Stuart (30).

Finally, a comment on the effect of the "blowing" by the mean flow on the boundary layer is called for. It will be shown as the development unfolds that the mean flow contributes terms proportional to (ν/δ) in the governing equations in expanded form. Note ν is the mean-flow Mach number in what follows, and should not be confused with the average kinematic viscosity ν_o. The method of solution

will be based on the assumption

$$\nu/\delta = O(1)$$

which, fortunately, is actually the case in an average rocket. A few numbers are in order at this point to justify the above statements. For a typical rocket, say, $r = .5$ ft, $a_o = 3500$ ft/sec, $P_o = 600$ lb/in^2, and $\mu_o \approx 2 \cdot 10^{-6}$ lb-sec/ft, the corresponding boundary layer thickness is

$$\delta \approx 1 \cdot 10^{-3} .$$

As already mentioned, the wall Mach number is ordinarily approximately

$$\nu \approx 1 \cdot 10^{-3}$$

and all of the above assertions are justified if the wave amplitude ϵ is also small.

12. First-Order Boundary Layer Solutions

In light of the above discussions, it seems reasonable to expand equations (2.1) - (2.4) in a power series in ϵ and to apply the usual boundary layer approximations. Stuart (30) points out that this procedure is a safe one as long as only the periodic first-order solutions and the steady part of the second-order solutions are of interest; neglected terms may be of importance in higher order corrections. To first order in ϵ, the equations of motion are

$$\frac{\partial \rho^{(1)}}{\partial t} + \nabla \cdot (\underline{u}^{(1)} + \nu \rho^{(1)} \underline{U}) = 0 \qquad (12.1)$$

$$\frac{\partial \underline{u}^{(1)}}{\partial t} + \frac{\nabla P^{(1)}}{\gamma} = -\nu[\underline{U} \cdot \nabla \underline{u}^{(1)} + \underline{u}^{(1)} \cdot \nabla \underline{U}] + \delta^2 \{\nabla^2 \underline{u}^{(1)} + \frac{1}{3} \nabla(\nabla \cdot \underline{u}^{(1)}) +$$
$$+ \nu[\mu^{(1)}(\nabla\nabla \cdot \underline{U} + \nabla^2 \underline{U}) + \nu \nabla[\underline{U} \cdot \nabla \mu^{(1)} - \frac{2}{3} \mu^{(1)} \nabla \cdot \underline{U}) +$$
$$+ \nu[(\nabla \mu^{(1)} \cdot \nabla)\underline{U} - (\underline{U} \cdot \nabla) \nabla \mu^{(1)}]\} \qquad (12.2)$$

$$\frac{\partial T^{(1)}}{\partial t} + \nu \underline{U} \cdot \nabla T^{(1)} - \left(\frac{\gamma-1}{\gamma}\right) \frac{\partial P^{(1)}}{\partial t} = \left(\frac{\delta^2}{\sigma}\right) \nabla \cdot \nabla T^{(1)} \qquad (12.3)$$

$$P^{(1)} = \rho^{(1)} + T^{(1)} \qquad (12.4)$$

Introducing the boundary layer coordinate,

$$\eta \equiv \frac{1-r}{\delta} \qquad (12.5)$$

and applying the boundary layer approximations (retaining only terms of zeroth order in δ in the region near the wall), equations (12.2) and (12.3) become:

$$\frac{\partial v^{(1)}}{\partial t} + \frac{1}{\gamma} \frac{\partial P^{(1)}}{\partial \theta} = \frac{\partial^2 v^{(1)}}{\partial \eta^2} - \left(\frac{\nu}{\delta}\right) \frac{\partial v^{(1)}}{\partial \eta} \qquad (12.6)$$

and

$$\frac{\partial T^{(1)}}{\partial t} - \frac{(\gamma-1)}{\gamma} \frac{\partial P^{(1)}}{\partial t} = \left(\frac{1}{\sigma}\right) \frac{\partial^2 T^{(1)}}{\partial \eta^2} - \left(\frac{\nu}{\delta}\right) \frac{\partial T^{(1)}}{\partial \eta} \qquad (12.7)$$

where the momentum equation has been written for the tangential component only. Note the presence of the "blowing" terms proportional to (ν/δ). An additional assumption based on classical boundary layer theory is that the pressure distribution is only slightly affected by the presence of the layer. Thus, we may take $P^{(1)}$ to be that solution already found for the inviscid flow. Equations (12.6) and (12.7) are readily solved using standard procedures. The results are, for the (0, 1, 0) mode,

$$T^{(1)} = -(\gamma-1)J_1(k_{10})e^{-\Lambda t}e^{-c\eta}\cos(k_{10}t \pm \theta - d\eta) + $$

$$+(\gamma-1)J_1(k_{10}r)e^{-\Lambda t}\cos(k_{10}t \pm \theta) \qquad (12.8)$$

and

$$v^{(1)} = \pm \frac{J_1(k_{10})}{k_{10}} e^{-\Lambda t}e^{-a\eta}\cos(k_{10}t \pm \theta - b\eta) \mp \frac{J_1(k_{10}r)}{k_{10}r} e^{-\Lambda t}\cos(k_{10}t \pm \theta) \qquad (12.9)$$

where

$$\begin{cases} a = \left\{ \dfrac{\left[\left(\frac{\nu}{2\delta}\right)^4 + (k_{10})^2\right]^{\frac{1}{2}} + \left(\frac{\nu}{2\delta}\right)^2}{2} \right\}^{\frac{1}{2}} - \left(\frac{\nu}{2\delta}\right) & (12.10) \\ b = \left\{ \dfrac{\left[\left(\frac{\nu}{2\delta}\right)^4 + (k_{10})^2\right]^{\frac{1}{2}} - \left(\frac{\nu}{2\delta}\right)^2}{2} \right\}^{\frac{1}{2}} & \\ c = \left\{ \dfrac{\left[\left(\frac{\sigma\nu}{2\delta}\right)^4 + (\sigma k_{10})^2\right]^{\frac{1}{2}} + \left(\frac{\sigma\nu}{2\delta}\right)^2}{2} \right\}^{\frac{1}{2}} - \left(\frac{\sigma\nu}{2\delta}\right) & (12.12) \\ d = \left\{ \dfrac{\left[\left(\frac{\sigma\nu}{2\delta}\right)^4 + (\sigma k_{10})^2\right]^{\frac{1}{2}} - \left(\frac{\sigma\nu}{2\delta}\right)^2}{2} \right\}^{\frac{1}{2}} & (12.13) \end{cases}$$

Note the first term in the solution for $v^{(1)}$ represents an exponentially decaying shear wave traveling away from the wall with Mach number

$$u_s = \left[\frac{k_{10}\delta}{b}\right] . \qquad (12.14)$$

Note also that b diminishes as the blowing becomes stronger; thus the rate of travel of the shear waves grows rapidly with increasing mean-flow Mach number ν, as expected. Plots of the variation of functions a, b, c, and d with (ν/δ) are shown in Figures 12 and 13. The second term in (12.9) is required for continuity, and of course represents the tangential velocity in the wave motion outside the boundary layer.

Figure 14 shows the boundary layer profiles at $\theta = 0$ with no blowing $(\nu/\delta = 0)$ for a half-cycle of wave motion. The influence of blowing is illustrated in Figure 15, for argument $(k_{10}t \pm \theta) = 0$. Note in particular the thickening effect brought about by the mass flux through the layer. This implies that the theory breaks down for (ν/δ) too large.

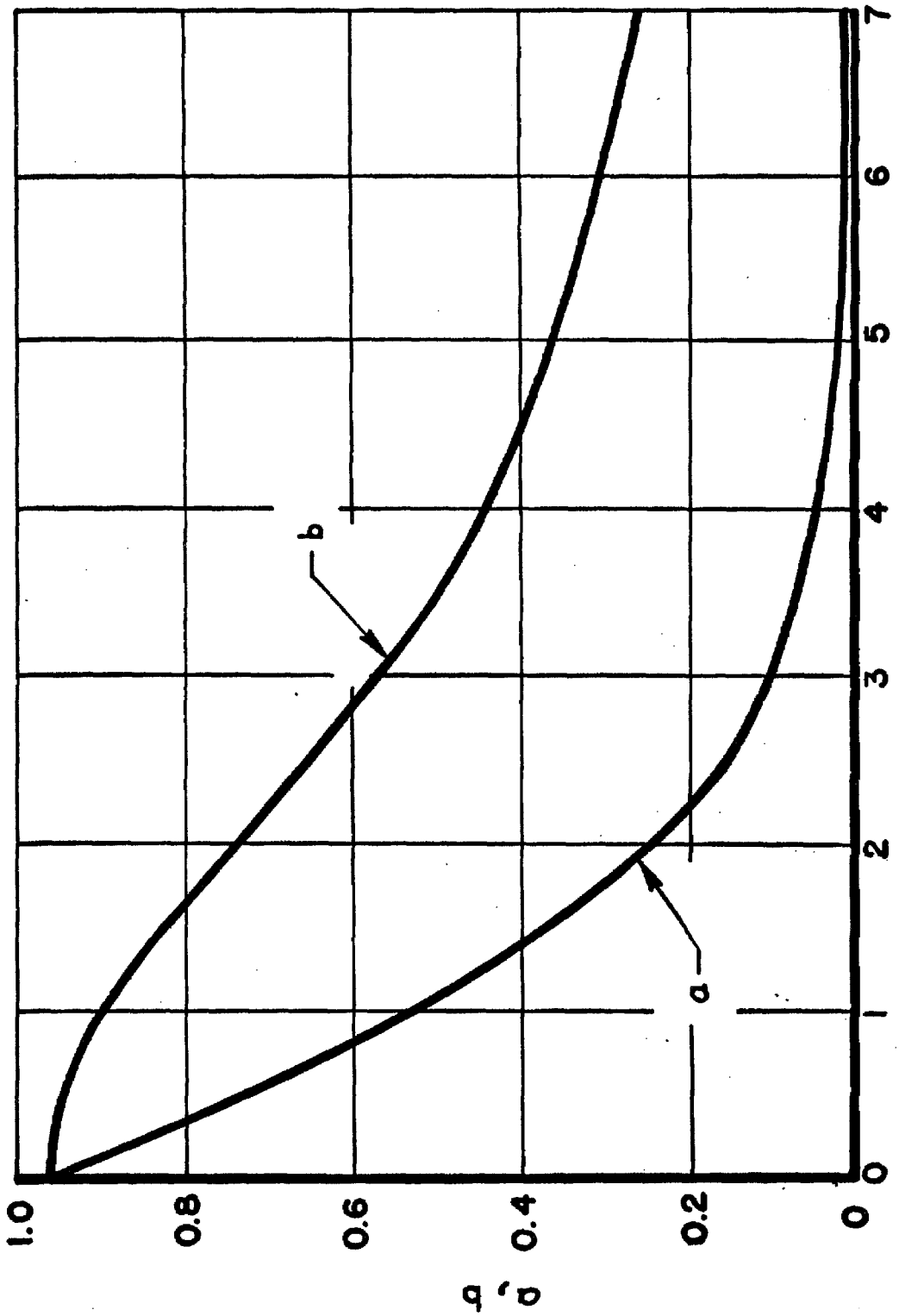

Fig. 12. Functions a and b vs (ν/δ) for (0,1,0) Mode.

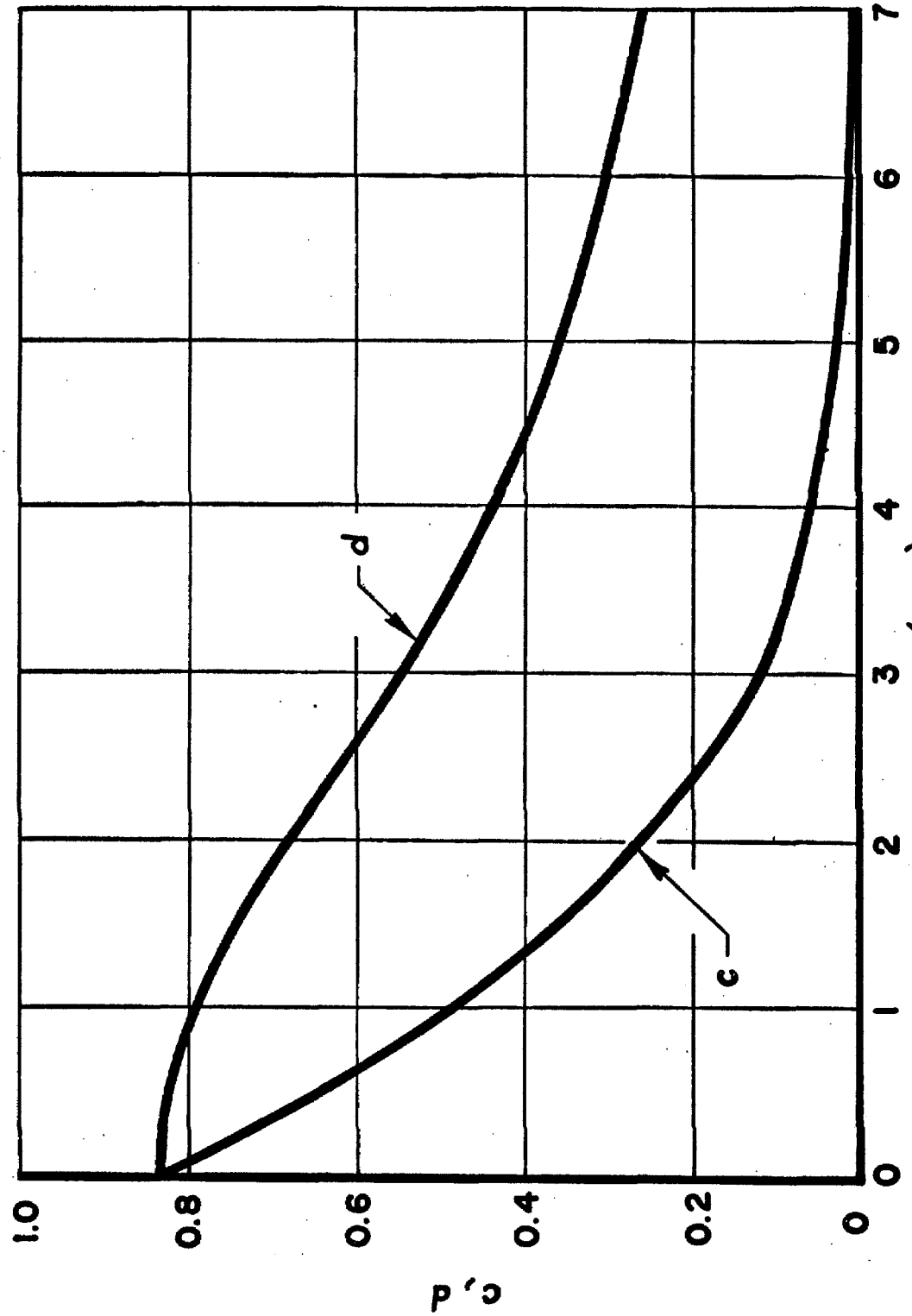

Fig. 13. Functions c and d vs (y/δ) for (0,1,0) Mode.

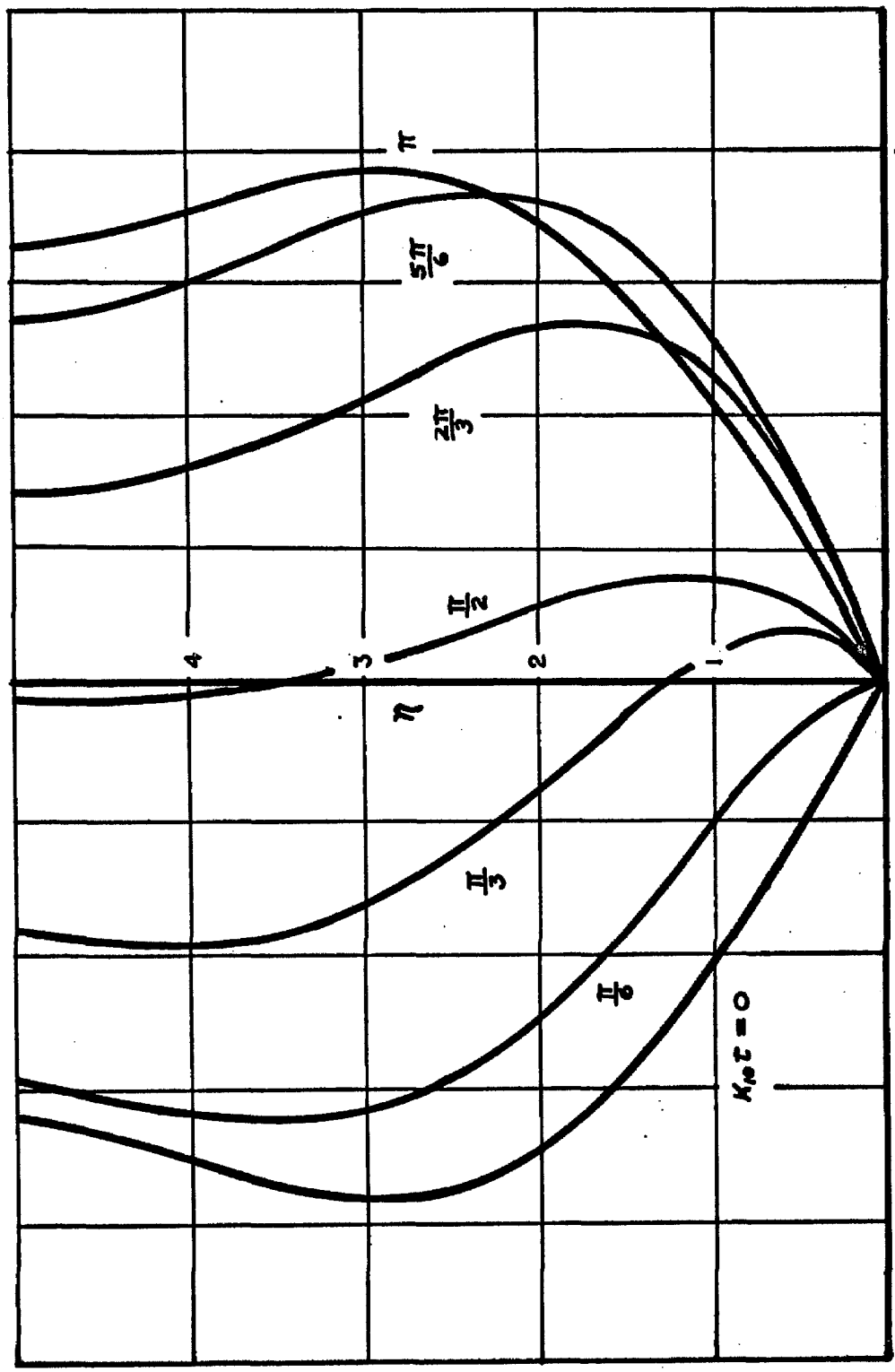

Fig. 14. First-Order Periodic Boundary Layer Profiles

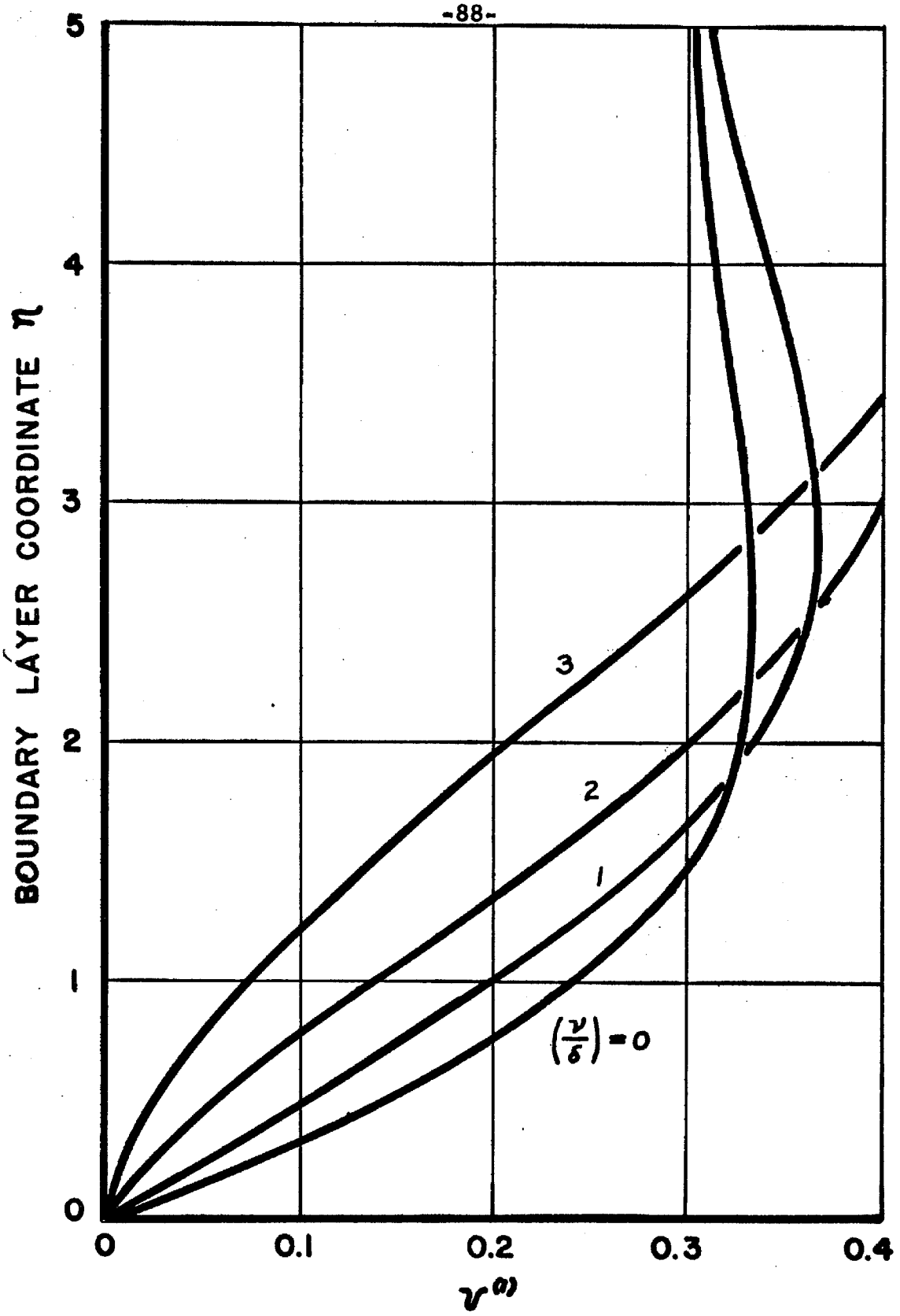

Fig. 15. Effect of Mean Flow on First-Order Boundary Layer Profiles.

The density distribution in the oscillating boundary layer is easily found by substituting the result (12.8) for the temperature fluctuation into the equation of state (12.4). Thus

$$\rho^{(1)} = (\gamma-1)J_1(k_{10})e^{-\Lambda t}e^{-c\eta}\cos(k_{10}t\pm\theta-d\eta)+J_1(k_{10}r)e^{-\Lambda t}\cos(k_{10}t\pm\theta)\,. \tag{12.15}$$

The radial velocity component is most easily found from the continuity equation written in the form

$$\frac{\partial\rho^{(1)}}{\partial t}+\frac{1}{r}\left(u^{(1)}+r\frac{\partial u^{(1)}}{\partial r}\right)+\frac{1}{r}\frac{\partial v^{(1)}}{\partial\theta}-\nu r\frac{\partial\rho^{(1)}}{\partial r} = 0\,. \tag{12.16}$$

In terms of the boundary layer coordinate this becomes

$$\frac{\partial u^{(1)}}{\partial\eta}-\delta u^{(1)} = \delta\left[\frac{\partial\rho^{(1)}}{\partial t}+\frac{\partial v^{(1)}}{\partial\theta}+\left(\frac{\nu}{\delta}\right)\frac{\partial\rho^{(1)}}{\partial\eta}\right]\,. \tag{12.17}$$

Note the correction term due to mass efflux. The boundary condition to be satisfied is that the behavior of the layer far from the wall ($\eta\to\infty$) matches that exhibited experimentally. Thus

$$u^{(1)} = -\nu J_1(k_{10}r)e^{-\Lambda t}[A^{(r)}\cos(k_{10}t\pm\theta)-A^{(i)}\sin(k_{10}t\pm\theta)] \tag{12.18}$$

far from the wall in accordance with equation (4.1). The solution is

$$u^{(1)} = \delta e^{-\Lambda t}\left\{\begin{array}{l}(\nu/\delta)J_1(k_{10}r)[A^{(i)}\sin(k_{10}t\pm\theta)-A^{(r)}\cos(k_{10}t\pm\theta)] \\ +\dfrac{J_1(k_{10})}{k_{10}(a^2+b^2)}e^{-a\eta}[a\sin(k_{10}t\pm\theta-b\eta)-b\cos(k_{10}t\pm\theta 0b\eta)] \\ +\dfrac{(\gamma-1)J_1(k_{10})}{(c^2+d^2)}e^{-c\eta}\left\{\begin{array}{l}k_{10}c\sin(k_{10}t\pm\theta-d\eta)+ \\ +[(\frac{\nu}{\delta})(c^2+d^2)-k_{10}d]\cos(k_{10}t\pm\theta-d\eta)\end{array}\right\}\end{array}\right\}$$

$$-\frac{1}{k_{10}}\frac{d}{dr}J_1(k_{10}r)e^{-\Lambda t}\sin(k_{10}t\pm\theta) \tag{12.19}$$

13. Viscous Damping of Wave Motion

The effect of the first-order wall shear stresses on the wave growth constant can now be assessed by using the results of the last section in the stability arguments set forth in Section 8. Culick (16) has already investigated the damping due to shear at the head-end closure and to presence of small particles in the flow.

According to equation (8.5), the part of the growth constant affected by body or shear forces may be written as

$$\Lambda_d = \frac{\nu}{2K_N E_N^2} \mathcal{J} \begin{cases} \left(\frac{\lambda}{\nu}\right) \int_V (p^{(10)})^* \nabla \cdot \underline{f}^{(10)} dV \\ - \left(\frac{\lambda}{\nu}\right) \int_S (p^{(10)})^* \underline{f}^{(10)} \cdot \hat{n} dS \end{cases} \tag{13.1}$$

Since the shear stress is parallel to the wall,

$$\underline{f}^{(10)} \cdot \hat{n} = 0$$

and

$$\Lambda_d = \frac{\lambda}{2K_N E_N^2} \mathcal{J} \int_V (p^{(10)})^* \nabla \cdot \underline{f}^{(10)} dV \ . \tag{13.2}$$

Now, the shear force per unit volume is

$$\underline{\mathcal{F}}_s^{(10)} = \delta^2 \left(\frac{\partial^2 v^{(10)}}{\partial r^2} \right) = \frac{\partial^2 v^{(10)}}{\partial \eta^2} \tag{13.3}$$

where η is the boundary layer coordinate as before. Thus, writing

$$\underline{\mathcal{F}}_s^{(10)} = \lambda \underline{f}^{(10)} e^{ikt} \tag{13.4}$$

in accordance with equations (5.9) and using (12.9), we find

$$\frac{\partial^2 v^{(10)}}{\partial \eta^2} = \pm \frac{J_1(k_{10})}{k_{10}} \left[(a+ib)^2 e^{\pm i\theta} e^{-(a+ib)\eta} \right] e^{ikt}$$

in complex form, and identify

$$\lambda \underline{f}^{(10)} = \pm \frac{J_1(k_{10})}{k_{10}} \left[(a+ib)^2 e^{\pm i\theta_e - (a+ib)\eta} \right] \hat{e}_\theta \ . \qquad (13.5)$$

Thus, for the (0, 1, 0) mode,

$$\Lambda_d = \frac{\left(\frac{2\pi L}{R}\right) J_1^2(k_{10})}{2k_{10}^2 \left(\frac{L\pi}{R}\right) J_1^2(k_{10}) \left(1 - \frac{1}{k_{10}^2}\right)} \delta \int_0^\infty \delta i (a+ib)^2 e^{-(a+ib)\eta} d\eta$$

$$= \frac{\delta a}{(k_{10}^2 - 1)} \ . \qquad (13.6)$$

Thus, the growth rate including wall dissipation is

$$\Lambda = - \frac{\nu}{(k_{10}^2 - 1)} \left[1 + k_{10}^2 A^{(r)} - \left(\frac{\delta}{\nu}\right) a \right] \qquad (13.7)$$

where a is given by (12. 10). Note that dissipation due to friction at the wall decreases as the mean flow Mach number at the wall increases. Λ_d is plotted in Figure 16 versus the blowing parameter (ν/δ). For $\nu \sim \delta$, the dissipative effect due to viscous shear is roughly half the amplification due to mean flow; for $\nu \sim 10\,\delta$, the dissipation is negligible in comparison to the amplification.

14. Second-Order Solutions

We now turn our attention to the second-order approximation to the boundary layer flow with the object of learning something about the proper boundary condition to apply to the inviscid second-order vortex flow whose existence has been proven in prior calculations. Again, it is clear that a steady flow component will appear due to combinations of the form

$$\rho^{(1)} \underline{u}^{(1)}$$

which have been discussed already. Also, we have demonstrated the presence of a steady, second-order mass transport in the inviscid

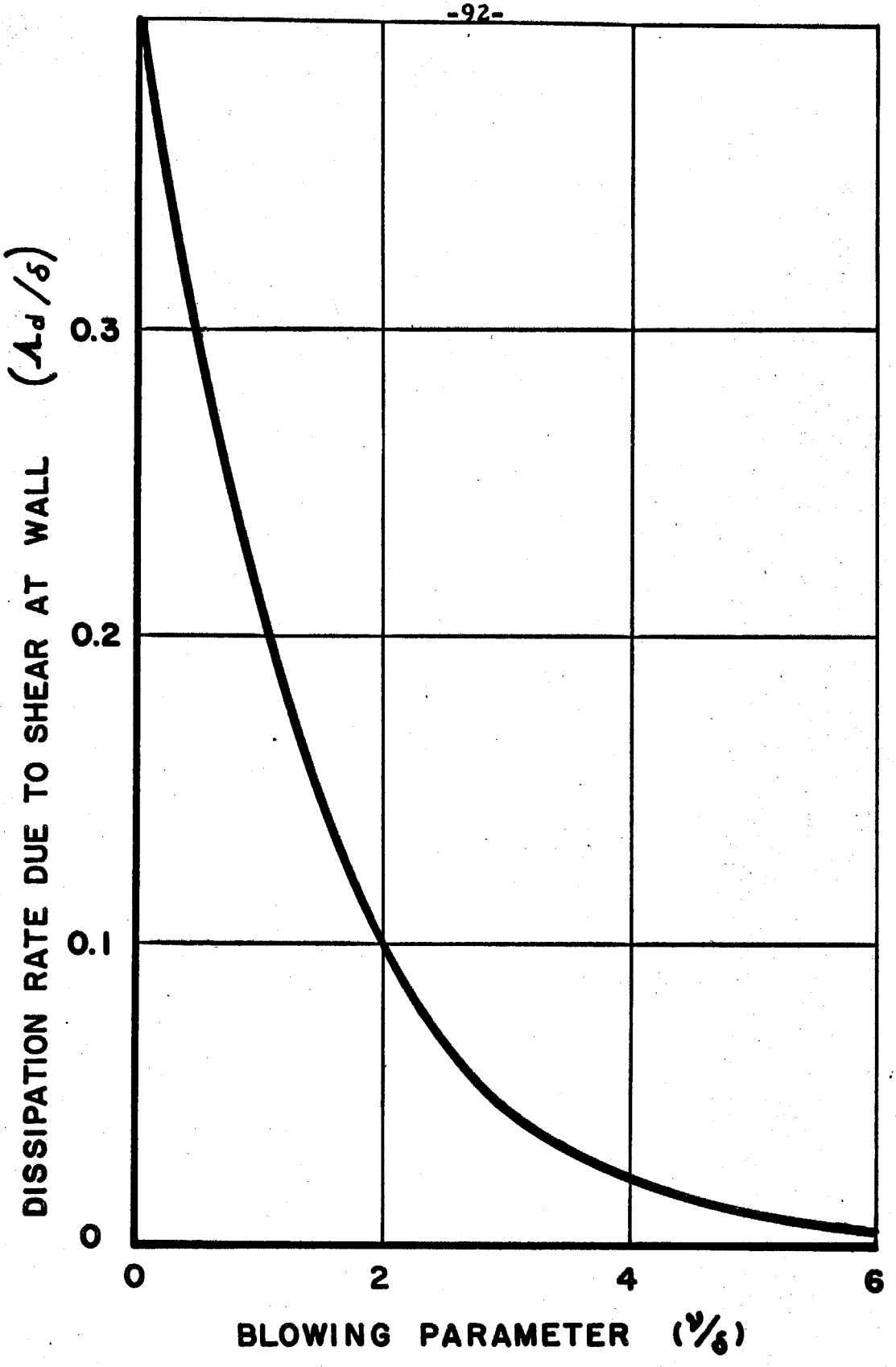

Fig. 16. Effect of Mean Flow on Viscous Dissipation of Waves

flow. This flow has been often referred to in the literature dealing with acoustic streaming theory as the "mass transport velocity," or "velocity transform" (21, 31, 32, 33, 34), and represents the effects of non-linear Reynolds stresses in traveling wave motions (30). It must be carefully distinguished from the "acoustic streaming" itself which is another steady part of the second-order mass flow. The "net mass transport velocity" is the vector sum of the mass transport velocity and the acoustic streaming, and represents the actual steady flow which could be measured in an experimental situation. Additional comments on acoustic streaming and the like will follow the calculation of $\langle v^{(2)} \rangle$ itself in the region of non-uniformity close to the chamber wall.

Expanding the momentum equation and collecting terms of order ϵ^2, we find

$$\frac{\partial \underline{u}^{(2)}}{\partial t} + \rho^{(1)} \frac{\partial \underline{u}^{(1)}}{\partial t} + \nabla \frac{\underline{u}^{(1)} \cdot \underline{u}^{(1)}}{2} - \underline{u}^{(1)} \times \nabla \times \underline{u}^{(1)}$$

$$+ \nu \{ \rho^{(1)} [\nabla \underline{U} \cdot \underline{u}^{(1)} - \underline{U} \times \nabla \times \underline{u}^{(1)}] + [\nabla \underline{U} \cdot \underline{u}^{(2)} - \underline{U} \times \nabla \times \underline{u}^{(2)}] \} =$$

$$= \delta^2 \left\{ \begin{array}{l} \nabla^2 \underline{u}^{(2)} + \frac{\partial \mu}{\partial T} T^{(1)} \nabla^2 \underline{u}^{(1)} + \nabla (\nabla \cdot \underline{u}^{(2)}) + \frac{\partial \mu}{\partial T} T^{(1)} \nabla (\nabla \cdot \underline{u}^{(1)}) \\ + \frac{\partial \mu}{\partial T} \nabla (\underline{u}^{(1)} \cdot \nabla T^{(1)}) - \frac{2}{3} \nabla (\nabla \cdot \underline{u}^{(2)}) - \frac{2}{3} \frac{\partial \mu}{\partial T} \nabla (T^{(1)} \nabla \cdot \underline{u}^{(1)}) \\ + \frac{\partial \mu}{\partial T} [\nabla T^{(1)} \cdot \nabla] \underline{u}^{(1)} - \frac{\partial \mu}{\partial T} (\underline{u}^{(1)} \cdot \nabla) \nabla T^{(1)} + O(\nu) \end{array} \right\} \qquad (14.1)$$

where terms of order $\delta^2 \nu$ are not written out in detail, since they will vanish when use is made of the boundary layer approximations. Focusing attention on the azimuthal component of the momentum equation, we find:

$$\frac{\partial v^{(2)}}{\partial t} + \rho^{(1)}\frac{\partial v^{(1)}}{\partial t} + \frac{1}{r}\left(u^{(1)}\frac{\partial u^{(1)}}{\partial \theta} + v^{(1)}\frac{\partial v^{(1)}}{\partial \theta}\right) + \left[\frac{u^{(1)}}{r}\left(v^{(1)} + r\frac{\partial v^{(1)}}{\partial r} - \frac{\partial u^{(1)}}{\partial \theta}\right)\right] +$$

$$+ \nu\left\{\begin{array}{l}\rho^{(1)}\left[\frac{1}{r}\frac{\partial}{\partial\theta}\left(u^{(1)}U + w^{(1)}W\right) - W\left(\frac{1}{r}\frac{\partial w^{(1)}}{\partial\theta} - \frac{\partial v^{(1)}}{\partial z}\right) + U\left(\frac{\partial v^{(1)}}{\partial r} + \frac{v^{(1)}}{r} - \frac{1}{r}\frac{\partial u^{(1)}}{\partial\theta}\right)\right] \\ + \left[\frac{1}{r}\frac{\partial}{\partial\theta}\left(u^{(2)}U + w^{(2)}W\right) - W\left(\frac{1}{r}\frac{\partial w^{(2)}}{\partial\theta} - \frac{\partial v^{(2)}}{\partial z}\right) + U\left(\frac{\partial v^{(2)}}{\partial r} + \frac{v^{(2)}}{r} - \frac{1}{r}\frac{\partial u^{(2)}}{\partial\theta}\right)\right]\end{array}\right\} =$$

$$= \delta^2\left\{\begin{array}{l}\left[\frac{2}{r^2}\frac{\partial u^{(2)}}{\partial\theta} + \frac{\partial^2 v^{(2)}}{\partial r^2} + \frac{1}{r^2}\frac{\partial^2 v^{(2)}}{\partial\theta^2} + \frac{1}{r}\frac{\partial v^{(2)}}{\partial r} - \frac{v^{(2)}}{r^2} + \frac{\partial^2 v^{(2)}}{\partial z^2}\right] \\ + \frac{\partial\mu}{\partial T}T^{(1)}\left[\frac{2}{r^2}\frac{\partial u^{(1)}}{\partial\theta} + \frac{\partial^2 v^{(1)}}{\partial r^2} + \frac{1}{r^2}\frac{\partial^2 v^{(1)}}{\partial\theta^2} + \frac{1}{r}\frac{\partial v^{(1)}}{\partial r} - \frac{v^{(1)}}{r^2} + \frac{\partial^2 v^{(1)}}{\partial z^2}\right] \\ + \frac{1}{3}\left[\frac{1}{r^2}\frac{\partial^2 u^{(2)}}{\partial\theta} + \frac{1}{r}\frac{\partial^2 u^{(2)}}{\partial\theta\partial r} + \frac{1}{r^2}\frac{\partial^2 v^{(2)}}{\partial\theta^2} + \frac{1}{r}\frac{\partial^2 w^{(2)}}{\partial\theta\partial z}\right] \\ + \frac{1}{3}\frac{\partial\mu}{\partial T}T^{(1)}\left[\frac{1}{r^2}\frac{\partial u^{(1)}}{\partial\theta} + \frac{1}{r}\frac{\partial^2 u^{(1)}}{\partial\theta\partial r} + \frac{1}{r^2}\frac{\partial^2 v^{(1)}}{\partial\theta^2} + \frac{1}{r}\frac{\partial^2 w^{(1)}}{\partial\theta\partial z}\right] \\ + \frac{\partial\mu}{\partial T}\frac{1}{r}\frac{\partial}{\partial\theta}\left[u^{(1)}\frac{\partial T^{(1)}}{\partial r} + \frac{v^{(1)}}{r}\frac{\partial T^{(1)}}{\partial\theta} + w^{(1)}\frac{\partial T^{(1)}}{\partial z}\right] \\ - \frac{2}{3}\frac{\partial\mu}{\partial T}\left[u^{(1)^2} + v^{(1)^2} + w^{(1)^2}\right]\frac{1}{r}\frac{\partial T^{(1)}}{\partial\theta} \\ + \frac{\partial\mu}{\partial T}\left[\frac{\partial}{\partial r}\left(v^{(1)}\frac{\partial T^{(1)}}{\partial r} - \frac{u^{(1)}}{r}\frac{\partial T^{(1)}}{\partial\theta}\right) + \frac{\partial}{\partial z}\left(\frac{w^{(1)}}{r}\frac{\partial T^{(1)}}{\partial\theta} - v^{(1)}\frac{\partial T^{(1)}}{\partial z}\right)\right] \\ + \frac{\partial\mu}{\partial T}\left[\frac{1}{r}\frac{\partial T^{(1)}}{\partial\theta}\left(\frac{u^{(1)}}{r} + \frac{\partial u^{(1)}}{\partial r} + \frac{1}{r}\frac{\partial v^{(1)}}{\partial\theta} + \frac{\partial w^{(1)}}{\partial z}\right)\right] \\ - \frac{\partial\mu}{\partial T}v^{(1)}\left[\frac{1}{r}\frac{\partial T^{(1)}}{\partial r} + \frac{\partial^2 T^{(1)}}{\partial r^2} + \frac{1}{r^2}\frac{\partial^2 T^{(1)}}{\partial\theta^2} + \frac{\partial^2 T^{(1)}}{\partial z^2}\right] + O(\nu)\end{array}\right\} \quad (14.2)$$

Applying the boundary layer approximations,

$$\frac{\partial v^{(2)}}{\partial t} - \left(\frac{\nu}{\delta}\right)U\frac{\partial v^{(2)}}{\partial\eta} - \frac{\partial^2 v^{(2)}}{\partial\eta^2} = -\rho^{(1)}\frac{\partial v^{(1)}}{\partial t} - \frac{v^{(1)}}{r}\frac{\partial v^{(1)}}{\partial\theta} - \frac{u^{(1)}v^{(1)}}{r}$$

$$+ \frac{u^{(1)}}{\delta}\frac{\partial v^{(1)}}{\partial\eta} + \left(\frac{\nu}{\delta}\right)\rho^{(1)}U\frac{\partial v^{(1)}}{\partial\eta} + \frac{\partial\mu}{\partial T}\frac{\partial}{\partial\eta}\left(T^{(1)}\frac{\partial v^{(1)}}{\partial\eta}\right) \quad (14.3)$$

which represents a considerable simplification. Note the presence of the terms proportional to (ν/δ) which reflect the influence of the mass efflux from the wall on the boundary layer flow.

In anticipation of steady terms, put

$$v^{(2)} = e^{-2\Lambda t}[\tilde{v}^{(2)} + \langle v^{(2)} \rangle] \quad . \tag{14.4}$$

The non-oscillatory part is governed by

$$\frac{d^2}{d\eta^2}\langle v^{(2)}\rangle - \left(\frac{\nu}{\delta}\right)\frac{d}{d\eta}\langle v^{(2)}\rangle + 2\Lambda\langle v^{(2)}\rangle =$$

$$= e^{2\Lambda t}\langle \text{inhomogeneous terms} \rangle \quad . \tag{14.5}$$

A complementary function for this second-order ordinary equation is

$$\langle v^{(2)}\rangle_c = B e^{\xi\eta} \tag{14.6}$$

where

$$\xi = \left(\frac{\nu}{2\delta}\right) \pm \left[\left(\frac{\nu}{2\delta}\right)^2 - 2\Lambda\right]^{\frac{1}{2}} = \left(\frac{\nu}{2\delta}\right)\left\{1 \pm \left[1 - \nu\,\frac{2\Lambda^{(11)}}{\left(\frac{\nu}{2\delta}\right)^2}\right]^{\frac{1}{2}}\right\}$$

$$\approx \left\{\nu\,\frac{\Lambda^{(11)}}{\left(\frac{\nu}{2\delta}\right)}\right\} = 2\delta\Lambda^{(11)} \tag{14.7}$$

for cases of interest*. Note ξ is negative since $\Lambda^{(11)}$ is negative in an unstable rocket. The constant B will be used later in satisfying the no-slip condition at the wall. We must now find a particular integral. In working with the terms on the right of (14.5), it is convenient to put all input quantities in the form

---

* The complementary function (14.6) would in general be

$$\langle v^{(2)}\rangle_c = B_1 e^{(\nu/\delta - 2\delta\Lambda^{(11)})\eta} + B_2 e^{2\delta\Lambda^{(11)}\eta}$$

but the first term vanishes in the process of asymptotic matching to the outer solution represented by equation (10.12).

$$Q_n(\eta, \theta, t) = \alpha_n \sin(k_{10}t \pm \theta) + \beta_n \cos(k_{10}t \pm \theta) \quad .$$

Then for the correlation $Q_n Q_m$, the steady part is

$$\langle Q_n Q_m \rangle = \tfrac{1}{2}(\alpha_m \alpha_n + \beta_m \beta_n) \quad .$$

Thus, the particular integral must satisfy

$$\frac{d^2}{d\eta^2}\langle v^{(2)}\rangle_p - \left(\frac{\nu}{\delta}\right)\frac{d}{d\eta}\langle v^{(2)}\rangle_p + 2\Lambda\langle v^{(2)}\rangle_p =$$

$$= \pm \frac{J_1^2(k_{10})}{2} \left\{ \begin{array}{l} C_1 e^{-2a\eta} + C_2 e^{-a\eta}\sin b\eta \\ + C_3 e^{-a\eta}\cos b\eta + C_4 e^{-c\eta}\sin d\eta \\ + C_5 e^{-(a+c)\eta}\sin(b-d)\eta \\ + C_6 e^{-(a+c)\eta}\cos(b-d)\eta \end{array} \right\} \qquad (14.8)$$

where

$$\left\{ \begin{array}{l} C_1 = -\dfrac{2ab}{k_{10}^2(a^2+b^2)} \qquad (14.9) \\ C_2 = 1 - \dfrac{1}{k_{10}}\left(\dfrac{\nu}{\delta}\right)\left[b(A^{(r)}+1) - aA^{(i)}\right] - \dfrac{2(\gamma-1)ab}{k_{10}}\dfrac{\partial\mu}{\partial T} \qquad (14.10) \\ C_3 = -\dfrac{1}{k_{10}}\left(\dfrac{\nu}{\delta}\right)\left[a(A^{(r)}+1) + bA^{(i)}\right] - \dfrac{(\gamma-1)(a^2-b^2)}{k_{10}}\dfrac{\partial\mu}{\partial T} \qquad (14.11) \\ C_4 = (\gamma-1) \qquad (14.12) \\ C_5 = (\gamma-1)\left\{1 + \left[\dfrac{ac-bd}{(c^2+d^2)}\right] + \left[\dfrac{b(a+c)+a(b-d)}{k_{10}}\right]\dfrac{\partial\mu}{\partial T}\right\} \qquad (14.13) \\ C_6 = (\gamma-1)\left\{-\left[\dfrac{bc+ad}{(c^2+d^2)}\right] + \left[\dfrac{a(a+c)-b(b-d)}{k_{10}}\right]\dfrac{\partial\mu}{\partial T}\right\} \qquad (14.14) \end{array} \right.$$

and a, b, c, and d have been defined previously. The particular integral is easily found by standard techniques, and the complete solution is

$$\langle v^{(2)} \rangle = \langle v^{(2)} \rangle_c + \langle v^{(2)} \rangle_p = B\left(1 + 2\delta\Lambda^{(11)}\eta + O(\delta^2)\right) +$$

$$\pm \frac{J_1^2(k_{10})}{2} \left\{ \begin{array}{l} \dfrac{C_1}{F_1} e^{-2a\eta} - \dfrac{C_3}{k_{10}} e^{-a\eta} \sin b\eta + \dfrac{C_2}{k_{10}} e^{-a\eta} \cos b\eta \\ + (\gamma-1)\left[F_3 e^{-c\eta} \sin d\eta + G_3 e^{-c\eta} \cos d\eta\right] \\ + (F_4 C_5 - G_4 C_6) e^{-(a+c)\eta} \sin(b-d)\eta \\ + (G_4 C_5 + F_4 C_6) e^{-(a+c)\eta} \cos(b-d)\eta \end{array} \right. \tag{14.15}$$

where a Taylor series expansion has been inserted for the complementary function and

$$\left\{ \begin{array}{l} F_1 = 2a[2a + (\nu/\delta)] \qquad (14.16) \\ F_3 = \dfrac{[(c^2-d^2) + c(\nu/\delta)]}{\{[(c^2-d^2)+c(\nu/\delta)]^2 + d^2[2c+(\nu/\delta)]^2\}} \qquad (14.17) \\ G_3 = \dfrac{d[2c + (\nu/\delta)]}{\{[(c^2-d^2)+c(\nu/\delta)]^2 + d^2[2c+(\nu/\delta)]^2\}} \qquad (14.18) \\ F_4 = \dfrac{[(a+c)^2-(b-d)^2+(\nu/\delta)(a+c)]}{\{[(a+c)^2-(b-d)^2+(\frac{\nu}{\delta})(a+c)]^2+(b-d)^2[2(a+c)+(\frac{\nu}{\delta})]^2\}} \qquad (14.19) \\ G_4 = \dfrac{(b-d)[2(a+c)+(\nu/\delta)]}{\{[a+c)^2-(b-d)^2+(\frac{\nu}{\delta})(a+c)]^2+(b-d)^2[2(a+c)+(\frac{\nu}{\delta})]^2\}} \qquad (14.20) \end{array} \right.$$

and to satisfy the no-slip condition,

$$B = \mp \frac{J_1^2(k_{10})}{2} \left\{ \begin{array}{l} \dfrac{C_1}{F_1} + \dfrac{C_2}{k_{10}} + (\gamma-1)G_3 \\ + G_4 C_5 + F_4 C_6 \end{array} \right\} \tag{14.21}$$

It is important to note from (14.15) that the complementary function contributes a term

$$\langle v^{(2)} \rangle_{\eta \to \infty} = B \qquad (14.22)$$

which does not diminish with distance η from the wall to the zeroth order in δ. This is the classical "acoustic streaming" effect, and in the present case, it must be interpreted with great care. First, it is of interest to compare (14.22) with the results of other investigators. In particular, it can be compared to the work of Maslen and Moore (12) who solved for the streaming flow in a circular cylinder for the case of zero mean flow ($v/\delta = 0$) and no unsteady combustion effects ($A = 0$). Their result for the (0, 1, 0) mode in the present notation is

$$\langle v^{(2)} \rangle_{\eta \to \infty} = \pm \frac{J_1^2(k_{10})}{2k_{10}} \left[1 - \frac{3}{2k_{10}^2} - \frac{(\gamma-1)}{(1+\sigma)} \left(\frac{1}{\sigma} - \sigma \frac{\partial \mu}{\partial T} \right) \right] \qquad (14.23)$$

which indicates the streaming flow to be in the direction <u>opposite</u> to the direction of nodal travel of the wave. From (14.22), we find, for the case $(v/\delta) = 0$, $A = 0$, that

$$\langle v^{(2)} \rangle_{\eta \to \infty} = \pm \frac{J_1^2(k_{10})}{2k_{10}} \left[-1 + \frac{1}{2k_{10}^2} - \frac{(\gamma-1)}{(1+\sigma)} \left(\frac{1}{\sigma} - \sigma \frac{\partial \mu}{\partial T} \right) \right] \qquad (14.24)$$

which differs in several respects. Most importantly, (14.24) indicates that the streaming is in the direction of wave travel, a result more in line with other calculations involving no wall efflux (cf. 30, 31, 32). The reversed signs on the first two terms and the three in the second term on the right of (14.23) appear to be typographical errors. Unfortunately, these errors affect the validity of later investigations (4, 9, 10, 11) which utilized the Maslen and Moore results. It is also important to note that the presence of unsteady combustion and the generation of gases at the burning surface affect both the magni-

tude and direction of the streaming flow. Thus, the Maslen and Moore theory is not applicable to the unstable solid propellant rocket problem in any case.

The effects of mass efflux through the boundary layer on the acoustic streaming are shown in Figure 17. The calculations are for $\gamma = 1.25$, $\sigma = 0.75$, $\partial\mu/\partial T = 1$, and $A^{(i)} = 0$. Note that $\langle v^{(2)} \rangle_{\eta\to\infty}$ is opposite in sense to the wave under conditions representative of an unstable rocket ($\nu/\delta = O(1)$, $A^{(r)} > 0$), and the value of $A^{(i)}$ is of little consequence since its effect on $\langle v^{(2)} \rangle$ is proportional to $a(\nu/\delta)$ which is always small. For $(\nu/\delta) > 5$, the value of $\langle v^{(2)} \rangle_{\eta\to\infty}$ changes little with increasing (ν/δ). Figure 18 illustrates the effect of blowing on the steady second-order boundary layer for $A^{(r)} = 0.25$. These velocity profiles represent the mean about which the first-order circumferential flow oscillates. Note the strong effect of mass flux on the direction of steady flow near the wall.

It is now possible to match the inner expansion represented by equation (14.15) to the outer expansion represented by the steady second-order vortex solution found for theinviscid flow outside the boundary layer. Thus, the acoustic streaming correction gives the boundary condition necessary to specify completely the flow through the chamber to second order. The appropriate form of the outer solution is (cf. eqn. 10.12),

$$\langle v^{(2)} \rangle = \frac{\Gamma e^{-2\nu\Lambda^{(11)}t}}{2\pi r^{(1+2\Lambda^{(11)})}} \qquad (14.25)$$

and the correct value of Γ can now be found using (14.22). The result is

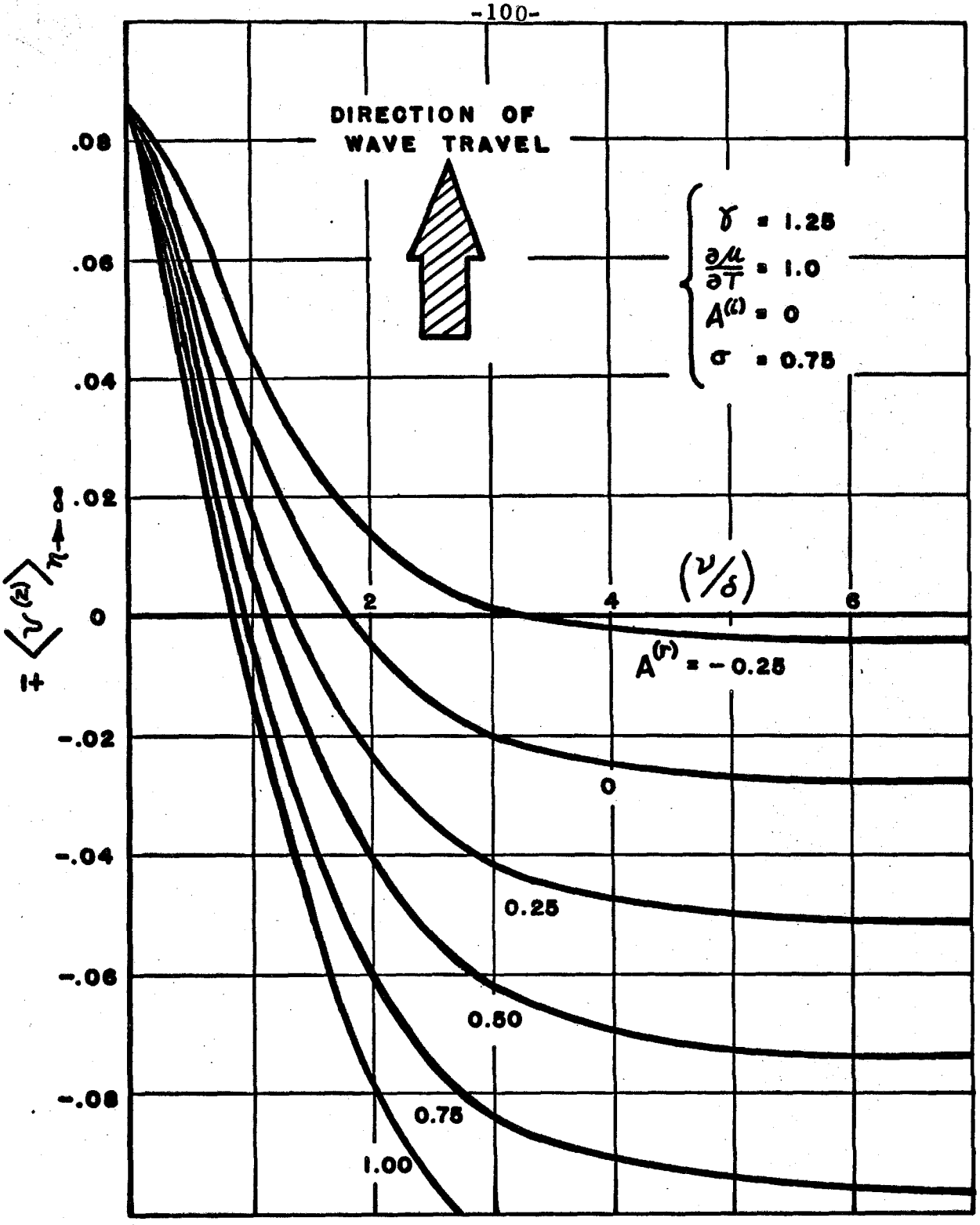

Fig. 17. Effect of Mean Flow and Oscillatory Combustion on Acoustic Streaming Velocity Near Wall.

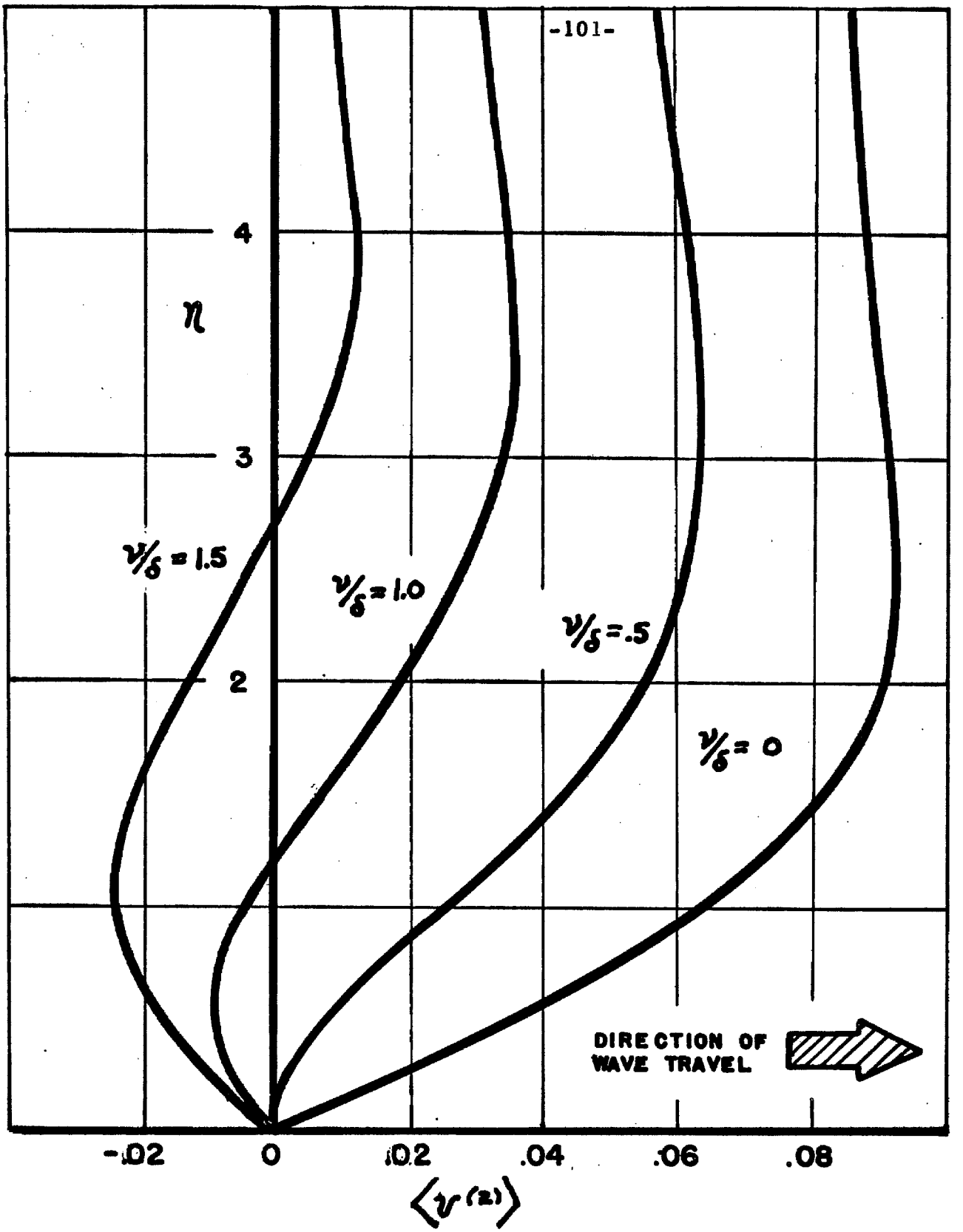

Fig. 18. Effect of Blowing on Second-Order Steady Boundary Layer Profile.

$$\Gamma = \mp \pi J_1^2(k_{10})\left[\frac{C_1}{F_1} + \frac{C_2}{k_{10}} + (\gamma-1)G_3+G_4C_5+F_4C_6\right] \qquad (14.26)$$

and we have established the presence of a vortex-like circumferential flow. Note from Figure 17 that this flow is opposite to the wave direction for a given set of conditions and for values of ν/δ above some critical value. The critical value of ν/δ corresponds to the transition from decaying to amplifying conditions, and can be estimated from the results of equation (13.7). Thus, neglecting damping from other sources, the waves are amplified for values of ν/δ greater than the value given by

$$(\nu/\delta)_{critical} = k_{10}^{\frac{1}{2}}\left\{\left[2(3/2+k_{10}^2A^{(r)})^2 - 1/4\right]^2 - 1/16\right\}^{-1/4}, \qquad (14.27)$$

and under these condition, the vortex is opposite in sense to the direction of wave travel.

Torque on the Rocket Motor. One of the manifestations of traveling mode combustion instability which is of great practical importance is the appearance of a torque on the rocket motor about the longitudinal axis during periods of intense oscillations. This must be due to a steady component of shear stress at the chamber wall due to viscous dissipation of the gas motions. The shear stress vector is given by

$$\underline{\tau} = \delta\mu \frac{\partial v}{\partial \eta}\hat{e}_\theta \qquad (14.28)$$

where

$$|\underline{\tau}| = \frac{\tau'}{\gamma P_o} \qquad (14.29)$$

and τ' is the dimensional shear stress. Expanding in the usual fashion, and writing τ for the magnitude of $\underline{\tau}$, the shear in the gas to

various orders is

$$\begin{cases} \tau^{(1)} = \delta \dfrac{\partial v^{(1)}}{\partial \eta} & (14.30) \\ \tau^{(2)} = \delta \left(\dfrac{\partial v^{(2)}}{\partial \eta} + \dfrac{\partial \mu}{\partial T} T^{(1)} \dfrac{\partial v^{(1)}}{\partial \eta} \right) & (14.31) \end{cases}$$

and so on. The second-order correction exhibits a steady component:

$$\langle \tau^{(2)} \rangle = \pm \frac{\delta J_1^2(k_{10})}{2} \left\{ \begin{aligned} & - 2a \frac{C_1}{F_1} e^{-2a\eta} + \left(\frac{aC_3 - bC_2}{k_{10}} \right) e^{-a\eta} \sin b\eta \\ & - \left(\frac{bC_3 + aC_2}{k_{10}} \right) e^{-a\eta} \cos b\eta \\ & - (\gamma - 1)(cF_3 + dG_3) e^{-c\eta} \sin d\eta \\ & + (\gamma - 1)(dF_3 - cG_3) e^{-c\eta} \cos d\eta \\ & - [(a+c)(F_4C_5 - G_4C_6) \\ & \quad + (b-d)(G_4C_5 + F_4C_6)] e^{-(a+c)\eta} \sin(b-d)\eta \\ & + [(b-d)(F_4C_5 - G_4C_6) - \\ & \quad - (a+c)(G_4C_5 + F_4C_6)] e^{-(a+c)\eta} \cos(b-d)\eta \end{aligned} \right.$$

$$+ \delta \left(\frac{\partial \mu}{\partial T} \right) \left\langle T^{(1)} \frac{\partial v^{(1)}}{\partial \eta} \right\rangle + O(\delta^2) \quad . \qquad (14.32)$$

Evaluating the shear stress at the wall, noting that the steady part of the temperature dependent term $\left\langle T^{(1)} \dfrac{\partial v^{(1)}}{\partial \eta} \right\rangle$ vanishes since the first order temperature fluctuations were assumed zero at the wall,

$$\langle \tau^{(2)} \rangle_{\eta=0} = \pm \frac{\delta J_1^2(k_{10})}{2} \left\{ \begin{aligned} & - 2a \frac{C_1}{F_1} - \left(\frac{bC_3 + aC_2}{k_{10}} \right) + (\gamma - 1)(dF_3 - cG_3) \\ & + (b-d)(F_4C_5 - G_4C_6) - (a+c)(G_4C_5 + F_4C_6) \end{aligned} \right\} \qquad (14.33)$$

Figure 19 shows the variation of shear stress on the wall with the

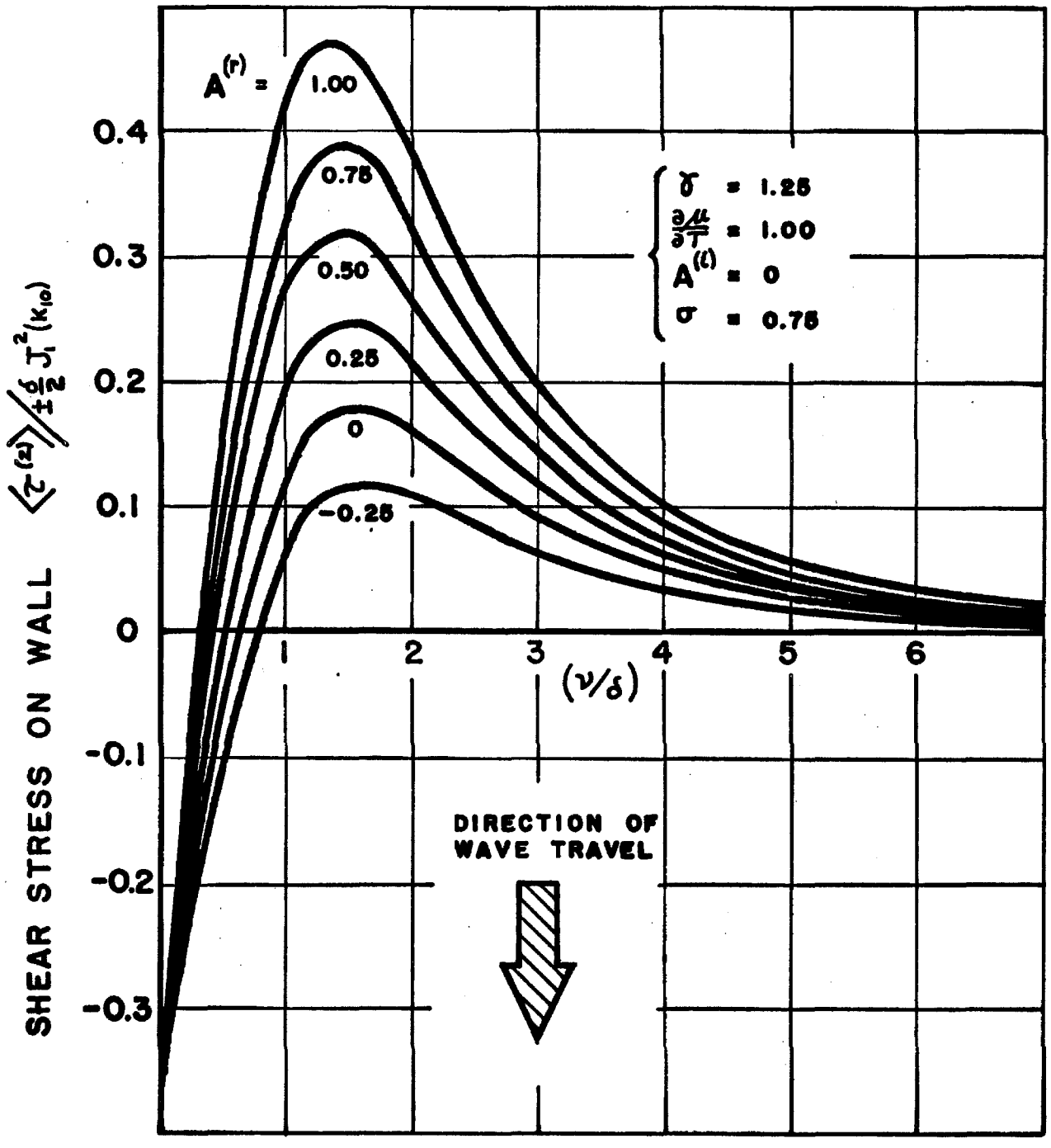

Fig. 19. Steady Second-Order Shear Stress at Wall vs. Mass Efflux Parameter ν/δ.

mass efflux parameter (ν/δ) for several values of the real part of the acoustic admittance of the burning surface $A^{(r)}$. Note that the stress is opposite in direction to the wave motion for conditions corresponding to wave amplification.

The roll moment acting on the motor is approximately

$$\langle M_z^{(2)} \rangle = \int_0^{L/R} \int_0^{2\pi} \langle \tau^{(2)} \rangle_{\eta=0} \, d\theta \, dz = \left(\frac{2\pi L}{R}\right) \langle \tau^{(2)} \rangle_{\eta=0} \, . \qquad (14.34)$$

This is a conservative estimate, since we have neglected the torque due to dissipation at the motor head-end and in the nozzle where the swirl is greatly intensified.

V. CONCLUSIONS

The detailed calculations support the simple conceptual model of vortex generation in acoustically unstable solid-propellant rockets introduced earlier. This simple mechanism is based on the observation that traveling transverse waves in the combustion chamber transport mass circumferentially in the direction of wave travel. This implies a layer of vorticity at the wall composed of axially oriented bound vortex filaments. Vorticity shed at the periphery of the nozzle exit is balanced by an oppositely spinning concentrated vortex emerging from the motor along the axis. The vortex system may be imagined to be composed of a series of horseshoe vortices arranged as illustrated in Figure 5. The presence of the mean flow and its interaction with the bound wall vortices implies a roll torque on the motor of order $\nu\varepsilon^2$, but the direction and numerical magnitude of the torque must be established by detailed calculations taking account of viscous dissipation of the circumferential wave motion near the wall.

The calculations show that traveling tangential waves are amplified under conditions typical of those in a solid propellant rocket. The response of the combustion process to the pressure fluctuations in combination with the mean flow act to drive the wave motion to higher amplitude. The presence of a second-order circumferential mean flow in the direction of the wave indicates an axial angular momentum component in the gas. This swirling flow is introduced into the fluid by the same processes that drive the first-order wave motion. The effect of motion of the rocket in response to the oscillating transverse pressure forces is to damp the wave motions through the action of a

steady second-order body moment on the gas relative to the moving chamber-fixed coordinate system. In addition to the steady mass flux carried by the wave, the inviscid theory predicts a steady second-order flow which takes the form of a potential vortex in the absence of amplification. With amplification, the radial velocity distribution is altered by vorticity driven into the flow in the amplification process. A simple angular momentum argument shows that the vortex is always opposite in sense to the direction of wave travel during amplification of the oscillations, but may have the same sense as the nodal travel during decay ($\Lambda^{(11)} > 1$).

The magnitude of the vortex strength, and the direction and amplitude of the axial torque due to circumferential shear stress, were estimated by application of laminar boundary-layer theory to the region near the wall. The validity of a boundary layer approach to the viscous calculations was established on the grounds that the frequency of the oscillations is high and that the ratio of wall Mach number ν to the Reynolds number δ is of order unity in a typical situation. The first-order boundary layer is purely oscillatory and consists of exponentially damped shear waves propagating into the outer flow. The damping rate decreases with wall Mach number, and therefore, the boundary layer approach breaks down when ν/δ reaches some critical value. The first-order oscillations are about a non-zero mean represented by a steady part of the second-order boundary layer flow which is identifiable with the "acoustic streaming" effect.

The magnitude of the acoustic streaming just outside the influence of the shear layer sets the strength and direction of the vortex

predicted by the inviscid theory. The vortex strength depends on the mean flow Mach number ν and on the acoustic admittance of the combustion layer at the wall. The net steady circumferential flow in the chamber is the superposition of the vortex on the mass flux transported by the wave itself. The vortex is, however, the dominating feature under a typical set of conditions. This is mainly due to the presence of the radial mean-flow component typical of an internally-burning solid-propellant rocket configuration. Effects similar to those just described are known to accompany transverse mode instability in some liquid propellant rockets, but since the mean flow is nearly axial, and since combustion takes place in a region normal to the motor axis, the vortex flow fails to appear. However, a swirling flow with complicated radial distribution is undoubtedly present in such cases.

Figure 20 summarizes some of the key findings of the study. Shown are the relative directions of the swirling flow emerging from the motor and the torque on the motor case for clockwise and counterclockwise traveling waves. The illustration corresponds to conditions which would exist during amplification of the pressure fluctuations.

As has already been indicated, one cannot expect the numerical computations of the idealized theory to be a particularly good representation of reality, especially in the case of finite amplitude waves. Nevertheless, let us extrapolate the results to finite amplitudes ($\epsilon = O(1)$) to see what sort of torque effects can be predicted by the theory. Using equation (14. 34), and neglecting dissipation at the head-end and in the nozzle, we find, for the (dimensional) torque

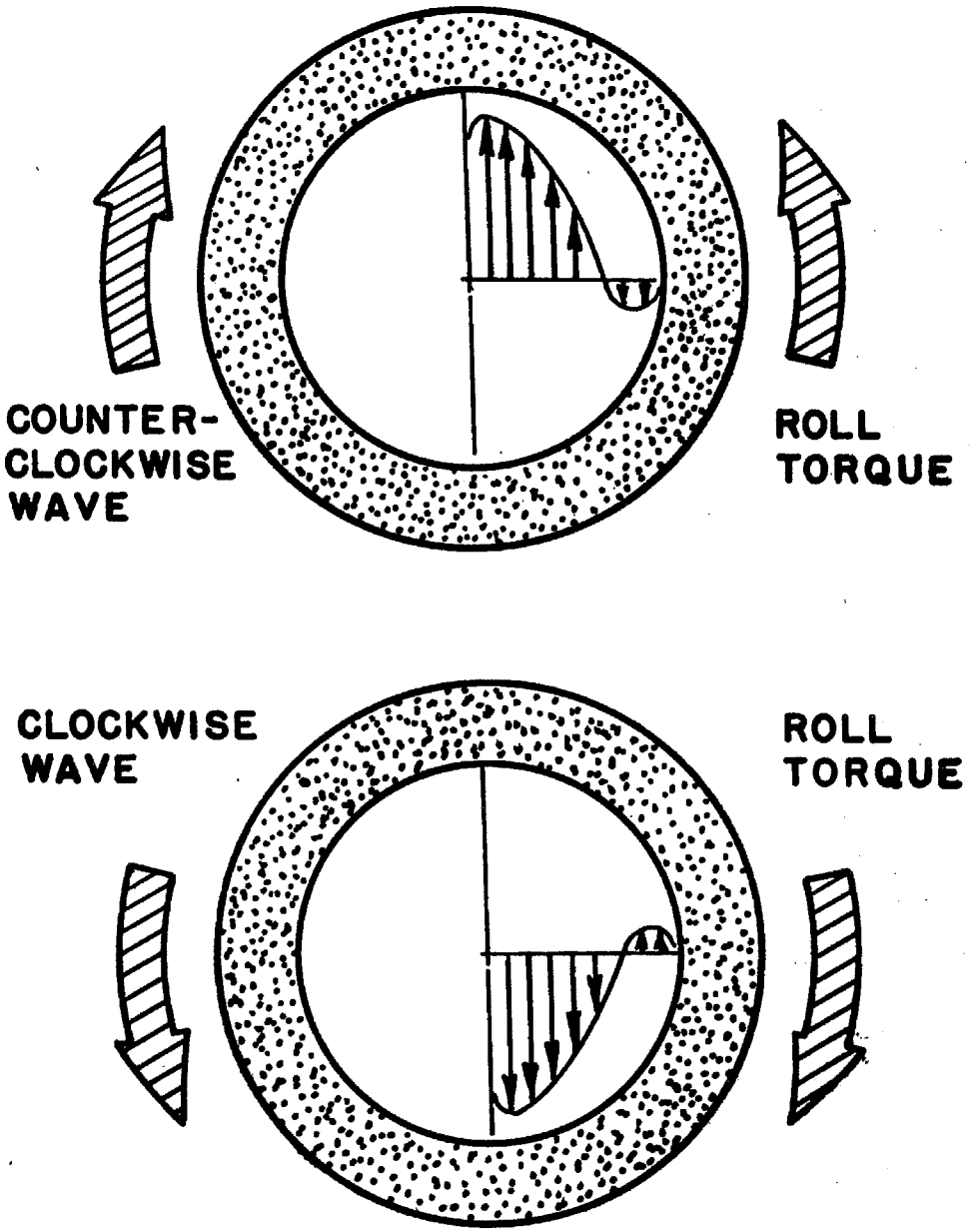

Fig. 20. Relative Directions of Traveling Wave, Roll Moment on the Motor, and Swirling Flow Emerging from the Nozzle.

about the motor axis of symmetry,

$$\langle M_z' \rangle = 2\pi R^2 L \tau' = 2\pi \epsilon^2 R^2 L \gamma P_o \delta^2 \langle \tau^{(2)} \rangle_{\eta=0} \ .$$

For $(\nu/\delta) = 1.5$, $R = .5$ ft, $L = 6$ ft, $P_o = 600$ lb/in^2, $\delta = 1 \cdot 10^{-3}$, which are numbers representative of a typical small rocket, we find

$$\langle M_z' \rangle = \epsilon^2 (53.5) \qquad \text{ft lb} \ .$$

Thus, for $\epsilon \approx .5$, $\langle M_z' \rangle \approx 10$ ft lb, which is in close correspondence to torques actually measured in the presence of finite amplitude waves.

Additional contributions to the roll moment are produced by viscous dissipation of the steady flow at the head-end of the motor and within the nozzle. The latter may be the dominating effect in an actual case due to intensification of the swirling flow through the nozzle throat due to angular momentum conservation. These considerations, coupled with the fact that laminar theory was used to estimate shear stresses in an unquestionably turbulent situation, implies that the numerical results just given represent in fact an underestimate of the actual torque acting on the system. The latter may thus be taken as a lower bound on the actual roll moment. Finally, it has been suggested by Swithenbank and Sotter (9) that the interaction of the spinning flow with the nozzle flow may be responsible for the pressure peaks ("irregular combustion") which often accompany combustion instability involving the traveling transverse acoustic modes.

VI. APPENDICES

APPENDIX 1 - Calculation of I_1 for the (0, 1, 0) Mode

It is desired to evaluate the integral

$$I_1 = \int_V g^{(10)} e^{\mp im'\theta} J_{m'}(k_{m'n'} r) dV \qquad \text{(A. 1)}$$

where $n \neq n'$ and

$$g^{(1)} = iK_N(\underline{U}\cdot\nabla p^{(10)}) - \nabla\cdot(\underline{U}\cdot\nabla\underline{q}^{(10)} + \underline{q}^{(10)}\cdot\nabla\underline{U}) \ . \qquad \text{(A. 2)}$$

For the (0, 1, 0) mode,

$$\begin{cases} p^{(10)} = e^{\pm i\theta} J_1(k_{10} r) \\ \underline{q}^{(10)} = \dfrac{i}{k_{10}} \left[e^{\pm i\theta} \dfrac{d}{dr} J_1(k_{10} r)\hat{e}_r \pm i e^{\pm i\theta} \dfrac{J_1(k_{10} r)}{r} \hat{e}_\theta \right] \\ \underline{U} = -r\hat{e}_r + 2Z\hat{e}_z \end{cases}$$

It is easily shown that $\underline{U}$ and $\underline{q}^{(10)}$ are each irrotational flow fields.

Thus, (A. 2) simplifies to

$$g^{(10)} = iK_N(\underline{U}\cdot\nabla p^{(10)}) - \nabla\cdot\nabla(\underline{U}\cdot\underline{q}^{(10)}) , \qquad \text{(A. 3)}$$

and evaluating for the (0, 1, 0) mode,

$$g^{(10)} = \frac{i}{k_{10}} \left[r\frac{d^3}{dr^3} + 3\frac{d^2}{dr^2} - k_{10}^2 r \frac{d}{dr} \right] J_1(k_{10} r) e^{\pm i\theta} \ .$$

Put $x = k_{10} r$ and $d/dr = k_{10} \dfrac{d}{dx}$ and denote derivatives W. R. T. x by primes. Then

$$g^{(10)} = ik_{10} e^{\pm i\theta} [x J_1'''(x) + 3J_1''(x) - x J_1'(x)] \ .$$

Noting

$$J_1'(x) = J_o(x) - \frac{J_1(x)}{x}$$

$$J_1''(x) = \left(\frac{2}{x^2} - 1\right) J_1(x) - \frac{J_o(x)}{x}$$

$$J_1'''(x) = \left(\frac{3}{x^2} - 1\right)J_o(x) + \left(\frac{2}{x} - \frac{6}{x^3}\right)J_1(x)$$

Substituting the Bessel function derivatives and simplifying:

$$g^{(10)} = -2ik_{10}xJ_o(x)e^{\pm i\theta} = -2ik_{10}^2 rJ_o(k_{10}r)e^{\pm i\theta} \quad . \qquad \text{(A. 4)}$$

Thus, integral I_1 is

$$I_1 = \int_0^{L/R}\int_0^{2\pi}\int_0^{1}(dzd\theta dr)r[-2ik_{10}^2 rJ_o(k_{10}r)e^{\pm i\theta}]e^{\mp\theta}J_1(k_{1n}r)$$

$$= -4\pi i\left(\frac{L}{R}\right)k_{10}^2\int_0^1 r^2J_o(k_{10}r)J_1(k_{1n}r)dr \quad . \qquad \text{(A. 5)}$$

The latter integral is readily evaluated by recourse to the Bessel equations defining the two Bessel components of the integral.

Consider the following pair:

$$\begin{cases} x^2\dfrac{d^2J_1(x)}{dx^2} + x\dfrac{dJ_1(x)}{dx} + (x^2-1)J_1(x) = 0 \\[2ex] x^2\dfrac{d^2J_1(\xi x)}{dx^2} + x\dfrac{dJ_1(\xi x)}{dx} + (\xi^2x^2-1)J_1(\xi x) = 0 \end{cases}$$

where $x = k_{10}r$ and $\xi = k_{1n}/k_{10}$. Differentiating the first equation, multiplying by $J_1(\xi x)$, and subtracting the second multiplied by $[dJ_1(x)]/dx$ yields

$$(\xi-1)x^2\frac{dJ_1(x)}{dx}J_1(\xi x) = 2xJ_1(x)J_1(\xi x) +$$

$$+\frac{d}{dx}\left\{x^2J_1(\xi x)\frac{d^2J_1(x)}{dx^2} - x^2\frac{dJ_1(x)}{dx}\frac{dJ_1(\xi x)}{dx} + xJ_1(\xi x)\frac{dJ_1(x)}{dx}\right\} \quad .$$

Integrating:

$$(\xi-1)\int_0^{k_{10}} x^2 J_1'(x)J_1(\xi x)dx = 2\int_0^{k_{10}} xJ_1(x)J_1(\xi x)dx$$

$$+\left[x^2 J_1(\xi x)\frac{d^2J_1(x)}{dx^2} - x^2\frac{dJ_1(x)}{dx}\frac{dJ_1(\xi x)}{dx} + xJ_1(\xi x)\frac{dJ_1(x)}{dx}\right]_0^{k_{10}} .$$

Using the boundary conditions

$$\frac{d}{dr}J_1(k_{1n}r)\Big]_{r=1} = 0 ,$$

$$\int_0^{k_{10}} x^2 J_1'(x)J_1(\xi x)dx = \frac{2}{(\xi-1)}\int_0^{k_{10}} xJ_1(x)J_1(\xi x)dx + \frac{k_{10}^2}{(\xi-1)}J_1(k_{1n})\frac{d^2J_1(k_{10})}{dx^2} .$$

Using this result, the integral in (A. 5) can be evaluated as follows:*

$$\int_0^{k_{10}} r^2 J_o(k_{10}r)J_1(k_{1n}r)dr = \frac{1}{k_{10}^3}\int_0^{k_{10}} x^2 J_o(x)J_1(\xi x)dx$$

$$= \frac{1}{k_{10}^3}\int_0^{k_{10}} xJ_1(x)J_1(\xi x)dx + \frac{1}{k_{10}^3}\int_0^{k_{10}} x^2 J_1'(x)J_1(\xi x)dx .$$

The first integral on the right is a tabulated one; the second has been evaluated above. Thus,

$$\int_0^1 r^2 J_o(k_{10}r)J_1(k_{1n}r)dr = \frac{1}{k_{10}^3}\left[1+\frac{2}{\xi-1}\right]\int_0^{k_{10}} xJ_1(x)J_1(\xi x)dx$$

$$+\frac{J_1(k_{1n})}{k_{10}(\xi-1)}\frac{d^2J_1(k_{10})}{dx^2}$$

$$= -\frac{(k_{10}^2-1)}{k_{10}(k_{1n}-k_{10})}J_1(k_{10})J_1(k_{1n})$$

and finally

$$I_1 = 4\pi i\left(\frac{L}{R}\right)\frac{k_{10}(k_{10}^2-1)}{(k_{1n}-k_{10})}J_1(k_{10})J_1(k_{1n}) . \qquad \text{(A. 6)}$$

---

* noting $J_o(x) = J_1'(x) + \frac{1}{x}J_1(x)$

APPENDIX 2. Calculation of I_2 for the (0, 1, 0) Mode

Integral I_2 is defined as

$$I_2 = \int_S h^{(10)} e^{\mp im'\theta} J_{m'}(k_{m'n} r) dS \qquad \text{(A. 7)}$$

where

$$h^{(10)} = \left\{ -iK_N A p^{(10)} + n \cdot \left[\underline{U} \cdot \nabla \underline{q}^{(10)} + \underline{q}^{(10)} \cdot \nabla \underline{U} - \left(\frac{\lambda}{\nu}\right) \underline{f}^{(10)} \right] \right\}_{r=1} .$$

For the first tangential mode,

$$h^{(10)} = -ik_{10} A J_1(k_{10}) e^{\pm i\theta} - \frac{i}{k_{10}} \left[r \frac{d^2 J_1(k_{10} r)}{dr^2} + \frac{dJ_1(k_{10} r)}{dr} \right]_{r=1} e^{\pm i\theta} - \left(\frac{\lambda}{\nu}\right) n \cdot \underline{f}^{(10)}$$

where $\underline{f}^{(10)}$ is given by equation (7. 6) for a rocket in free motion, by (7. 10) for a rocket motor in a flexible mounting, and is zero for a rigidly fixed motor. Noting

$$\left[\frac{dJ_1(k_{10} r)}{dr^2} \right]_{r=1} = 0$$

and

$$\frac{d^2 J_1(k_{10} r)}{dr^2} = k_{10}^2 \left\{ \left(\frac{2}{k_{10}^2 r^2} - 1 \right) J_1(k_{10} r) - \frac{J_o(k_{10} r)}{k_{10} r} \right\}_{r=1}$$

$$= (1 - k_{10}^2) J_1(k_{10}) .$$

Also,

$$\hat{n} \cdot \underline{f}^{(10)} = \begin{cases} -\left(\frac{\gamma \pi L}{R}\right) J_1(k_{10}) e^{\pm i\theta} & \text{for case 1 (freely moving case)} \\ \frac{k_{10}^2}{I} \left(\frac{\gamma \pi L}{R}\right) J_1(k_{10}) e^{\pm i\theta} e^{-i\alpha} & \text{for case 2 (flexibly mounted motor)} \\ 0 & \text{for case 3 (rigidly mounted motor)} \end{cases}$$

where I and α are the mechanical impedance and lag angle resulting from the flexible mounting in case 2. The integral is now easily evaluated with the result

$$I_2 = i\left(\frac{2\pi L}{R}\right) J_1(k_{10}) J_1(k_{1n}) \left[\frac{k_{10}^2 - 1}{k_{10}} - k_{10} A\right] +$$

$$+ \left(\frac{\lambda}{\nu}\right) 2\gamma \left(\frac{\pi L}{R}\right)^2 J_1(k_{10}) J_1(k_{1n}) \begin{cases} 1 & \text{case 1} \\ -\frac{k_{10}^2}{I} e^{-i\alpha} & \text{case 2} \\ 0 & \text{case 3} \end{cases} \qquad \text{(A. 8)}$$

VII. NOTATION

a_o	average speed of sound
A	acoustic admittance of burning surface
c	damping constant
E_α	normalization constant for mode α
$\underline{f}$	amplitude of body force on gas
$\underline{\mathfrak{F}}$	body force vector
$\underline{F}$	integrated pressure force on chamber wall
g	function defined by equation (5.12)
h	function defined by equation (5.14)
$\mathfrak{I}$	refers to imaginary part
J_m	Bessel function of first kind of order m
k	thermal conductivity
k_{mn}	root of $d/dr\ J_m(k_{mn}r) = 0$ at $r = 1$
K	complex frequency = $\Omega + i\Lambda$
L	chamber length (dimensional)
m	dimensionless motor mass
$\underline{M}$	moment vector
$\underline{\mathfrak{m}}$	mass flux vector
$\hat{n}$	outward pointing normal unit vector
N	refers to mode (ℓ, m, n)
p	amplitude of pressure
P	pressure
$\underline{q}$	amplitude of velocity
$\underline{Q}$	chamber constraint function
$\underline{r}$	position vector

R	chamber radius (dimensional)
$\Re$	refers to real part
$\underline{s}$	position of chamber axis relative to inertial system
t	time
T	temperature
$\underline{u}$	velocity vector
$\underline{U}$	geometrical part of mean-flow velocity vector
α	three-tuple defining mode, phase angle
β	function defined by equation (8.7)
γ	ratio of specific heats
Γ	vortex strength
δ	boundary layer parameter
$\delta(\underline{r}-\underline{r}_o)$	Dirac delta function
ϵ	amplitude parameter
η	boundary layer coordinate
θ	azimuthal position
$\varkappa$	spring constant
λ	magnitude of perturbing force
Λ	growth constant for wave amplification
μ	viscosity coefficient
ν	mean-flow Mach number
ρ	density
σ	Prandtl number
τ	shear stress
ψ	eigenfunction of unperturbed problem
ω	frequency

Ω frequency

Subscripts

o refers to average (dimensional) conditions in absence of wave

z refers to axial component

Superscripts

' refers to dimensional quantities

(i) refers to imaginary part

(r) refers to real part

(mn) refers to term of order m in ϵ and order n in ν

(m) refers to term of order m in ϵ

Triangular brackets $< >$ indicate the non-oscillatory part of the enclosed function.

VIII. REFERENCES

1. Boys, S. F. and Schofield, A., "Studies Accessory to the Development of Classified Rockets," Woolwich Arsenal (England) 1942.

2. Flandro, G. A., "Theoretical Investigations of the Sergeant Roll Transient Problem," Sperry Utah Engineering Laboratory, Rept. No. 211-SA-526C-61. 14, April 1961.

3. Flandro, G. A., "Roll Moment Generation by Solid Propellant Rocket Motors," Sperry Utah Company, Rept. No. 211-SA-526C-61. 51, August 1961.

4. Flandro, G. A., "Roll Torque and Normal Force Generation in Acoustically Unstable Rocket Motors," AIAA Journal, Vol. 2, No. 7, July 1964.

5. Mayhue, R. J., "NASA Scout ST-1 Flight Test Results and Analyses," NASA TN D-1240, pp. 37-38 and 69-71, 1962.

6. Landsbaum, E. M. and Spaid, F. W., "Experimental Studies of Unstable Combustion in Solid-Propellant Rocket Motors," Jet Propulsion Laboratory, TR 32-146, pp. 13-14, August 1961.

7. Green, L., "Some Effects of Charge Configuration in Solid Propellant Combustion," Jet Propulsion, Vol. 28, No. 7, July 1958.

8. Green, L., "Studies on the Reaction Stability of Solid Propellant Charges," Aerojet-General Corp., Rept. 1077, pp. 23-26, 1956.

9. Swithenbank, J. and Sotter, G., "Vortex Generation in Solid Propellant Rockets," AIAA Journal, Vol. 2, No. 7, July 1964.

10. Swithenbank, J. and Harris, D., "Intentional Combustion Oscillations in Propulsion Systems," Rept. No. H. I. C. 45, University of Sheffield (England), 1965.

11. Swithenbank, J., "Non-Linear Behavior of Solid Propellant Rocket Combustion Instability," Rept. No. H. I. C. 65, University of Sheffield (England), 1965.

12. Maslen, S. H. and Moore, F. K., "On Strong Transverse Waves Without Shocks in a Circular Cylinder," J. Aeronautical Sci., Vol. 23, pp. 583-593, 1956.

13. Denison, M. R. and Baum, E., "A Simplified Model of Unstable Burning in Solid Propellants," ARS Journal, Vol. 31, No. 8 pp. 1112-1122, August 1961.

14. Williams, F. A., "Response of a Burning Fuel Plate to Sound Vibrations," AIAA Journal, Vol. 3, No. 11, pp. 2112-2124, November 1965.

15. Van Dyke, M., Perturbation Methods in Fluid Mechanics, Academic Press, Inc., New York (1964), p. 21.

16. Culick, F. E. C., "Acoustic Oscillations in Solid Propellant Rocket Chambers," Astronautica Acta, Vol. 12, No. 2, pp. 113-136, March-April 1966.

17. Horton, M. D., "Acoustic Admittance of a Burning Solid Propellant Surface," ARS Journal, Vol. 32, pp. 644-646, April 1962.

18. Hart, R. W. and McClure, F. T., "Combustion Instability: Acoustic Interaction with a Burning Propellant Surface," J. of Chemical Physics, Vol. 30, p. 1501, June 1959.

19. Coates, R. L., et al., "The T-Burner Method of Determining the Acoustic Admittance of Burning Propellants," AIAA Journal, Vol. 2, No. 6, June 1964.

20. Culick, F. E. C., "Rotational Axisymmetric Mean Flow and Damping of Acoustic Waves in Solid Propellant Rockets," AIAA Journal, Vol. 4, No. 8, pp. 1462-1464, August 1966.

21. Longuet-Higgins, M. S., "Mass Transport in Water Waves," Phil. Trans. Roy. Soc. (London), A 245, pp. 535-581, 1953.

22. Rosenhead, L., Laminar Boundary Layers, Clarendon Press, Oxford (1963), pp. 387-388.

23. Crow, S. C., "The Shake-Up Problem," Unpublished paper, California Institute of Technology, 1965.

24. Berlot, R. R., "Production of Rotation in a Confined Liquid Through Translational Motion of the Boundaries," Journal of Applied Mechanics, Vol. 26, Series E, No. 4, pp. 513-516, December 1959.

25. Abramson, H. N., et al., "Some Studies of Liquid Rotation and Vortexing in Rocket Propellant Tanks," NASA TN D-1212, January 1962.

26. McClure, F. T., et al., "Solid Propellant Rocket Motors as Acoustic Oscillators," Solid Propellant Rocket Research, Progress in Astronautics and Rocketry, Vol. I, Academic Press, New York (1960), pp. 295-358.

27. Ryan, N. W. and Coates, R. L., "Acoustic Instability: Influence of and on the Solid Plant," AIAA Preprint No. 64-139, presented at Solid Propellant Rocket Conference, January 29-31, 1964.

28. Brownlee, W. G. and Marble, F. E., "An Experimental Investigation of Unstable Combustion in Solid Propellant Rocket Motors," Solid Propellant Rocket Research, Progress in Astronautics and Rocketry, Vol. 1, Academic Press, New York (1960), pp. 455-494.

29. Marble, F. E., "Some Problems Concerning the Rotational Motion of a Perfect Fluid," Ph. D. Thesis, California Institute of Technology, 1948.

30. Stuart, J. T., Laminar Boundary Layers (L. Rosenhead, Ed.) Part VII, "Unsteady Boundary Layers," Clarendon Press, Oxford (1963), pp. 349-356 and pp. 381-406.

31. Nyborg, W. L., Physical Acoustics (W. P. Mason, Ed.), Part 10, "Acoustic Streaming," Academic Press, New York (1965), pp. 265-280.

32. Schlichting, H., "Berechnung ebener Periodischer Grenzschichtströmungen," Physik. Zeit., Vol. 33, pp. 327-335, 1932.

33. Rayleigh, Lord, Theory of Sound, Vol. II, Dover Publications, New York (1945).

34. Nyborg, W. L., "Acoustic Streaming Due to Attenuated Plane Waves," J. Acoust. Soc. Am., Vol. 25, No. 1, pp. 68-75, January 1953.